Applied AdS/CFT:
From Hot Quarks to Condensed Matters

by

Christopher Andrew Rosen

B.A., University of Colorado, 2006

A thesis submitted to the

Faculty of the Graduate School of the

University of Colorado in partial fulfillment

of the requirements for the degree of

Doctor of Philosophy

Department of Physics

2012

This thesis entitled:
Applied AdS/CFT:
From Hot Quarks to Condensed Matters
written by Christopher Andrew Rosen
has been approved for the Department of Physics

Oliver DeWolfe

Assoc. Prof. Phil Armitage

Prof. Shanta de Alwis

Prof. Tom DeGrand

Prof. Anna Hasenfratz

Date

The final copy of this thesis has been examined by the signatories, and we find that both the content and the form meet acceptable presentation standards of scholarly work in the above mentioned discipline.

Rosen, Christopher Andrew (Ph.D., Physics)

Applied AdS/CFT:

From Hot Quarks to Condensed Matters

Thesis directed by Asst. Prof. Oliver DeWolfe

We apply the techniques of gauge/gravity duality to a variety of physical systems at very different energy scales. Gravitational duals of hot, strongly coupled plasmas qualitatively similar to the matter produced in collisions of heavy nuclei are considered first. These bulk theories are constructed from a "bottom-up" approach, in which the minimal field content relevant for phenomenology is considered. The effects of the inclusion of one such field, a conformal symmetry breaking bulk scalar, are studied in the context of the speed of sound and jet quenching parameter of the dual field theory. We find that the sound speed is robust to the manner in which conformal symmetry is broken, while the jet quenching parameter is less so.

Increasing the complexity of the bulk theory to include a $U(1)$ gauge field provides theoretical access to a strongly coupled gauge theory at finite temperature and chemical potential. We study the phase structure of this gauge theory by numerically constructing many black hole solutions to the bulk Einstein-Maxwell equations, and searching them for thermodynamic instabilities. This results in the identification of a line of first order phase transitions, terminating in a second order critical point. The divergence of susceptibilities in the vicinity of this critical point are examined, and the critical exponents are determined to be the mean field exponents of a theory in the universality class of the three dimensional Ising model. Fluctuations of bulk fields about these backgrounds are also considered, leading to calculations of transport properties such as conductivity and bulk viscosity in the gauge theory. From these quantities, dynamic critical exponents characterizing their behavior near the critical point are computed and the dual gauge theory is determined to be model B in the classification scheme of Hohenberg and Halperin.

We then turn to applying these duality techniques to condensed matter systems at very low energies. These systems include cold atomic realizations of fermions at unitarity, and non-Fermi liquids. The former are thought to be described by a non-relativistic field theory. We build "top-down" gravitational duals to such theories with finite density and/or rotation, by using a solution generating technique called the Null-Melvin Twist. The resulting bulk theories are consistent solutions to type IIB string theory. Finally, we construct holographic top-down realizations of Fermi surfaces in maximal gauged supergravity in four and five dimensions. These are dual to non-Fermi liquids in the ABJM and $\mathcal{N} = 4$ Super Yang-Mills theories in three and four dimensions respectively. We conclude with additional comments on the results and avenues for continued research.

Dedication

To alpine adventures and 3,000 days of sun.

Acknowledgements

I have thoroughly enjoyed the last decade I spent earning degrees in the physics department at CU. This is in large part due to the interactions I have had with an outstanding faculty. As my advisor, Oliver DeWolfe has been a perpetual source of motivation, inspiration, and technical expertise. Jamie Nagle has played an integral role in my advance through academia, providing friendship, direction, and a perfect example of scientific excellence. I will fondly remember early summer TASI treks with Tom DeGrand, and beautiful bike rides with Steve Pollock. Although not a Buff, I am also incredibly fortunate to have been able to spend many days with Steve Gubser, who graciously collaborated with me to solve problems both in string theory and on the rocks.

No calculation I accomplished as a graduate student would have materialized without the love, support, and oddly unwavering confidence of my girlfriend, Morgan Newberg. This dissertation is a testament to her patience and generousity. She is also beautiful.

Thanks to my parents, who never asked me to trade my dreams for any one elses, and fervently encourage all my passions and pursuits.

Finally, the work presented in this thesis has benefited greatly from the insights of others. I wish to thank M. Brown, A. Buchel, T. DeGrand, S. de Alwis, K. Givens, V. Gurarie, A. Hasenfratz, M. Hermele, G. Horowitz, P. Huovinen, D. Huse, S. Kachru, A. Karch, H. Liu, D. Marolf, B. Müller, L. Radzihovsky, P. Romatschke, K. Rajagopal, S. Sachdev, T. Schaefer, A. Sinha, M. Shultz, D. Son, J. Wang, A. Yarom, and W. A. Zajc for discussions that lead to the realization of this dissertation. This research has been funded in part by DOE grants DE-FG02-91-ER-40672 and DE-FG02-00-ER-41152.

Contents

Figures

Figure

Chapter 1

Preliminary Points

1.1 Introducing AdS/CFT

Not coincidentally, some of the most theoretically interesting problems in contemporary physics are centered on systems characterized by strong interactions. With no perturbative tools available to make progress, one must move beyond the diagrammatic techniques used to organize a perturbation series, and turn to other technologies. Historically, the most successful methods for investigating systems at strong coupling are either numerical or based on the powerful and beautiful concept of "duality". Numerical methods, such as Lattice Quantum Chromodynamics, often allow direct calculation in strongly coupled theories, involve large scale computing efforts, and will not play a prominent role in this dissertation. Instead we will focus our attention on dual descriptions of a variety of strongly interacting systems of interest.

Simply put, the fundamental property of a duality in theoretical physics is the existence of a dictionary that allows one to translate a question in one theory into the language of a different theory. Some of the most revered examples of duality share the useful ability to rephrase "difficult" problems in one theory into problems in another theory that are qualitatively easier to address. Many dualities of this type are generically termed "strong/weak dualities" because they map the coupling constant g in one theory to the coupling in the other g', like $g \to g' = 1/g$. Thus, non-perturbative physics on one side of the duality can be reformulated as a weakly coupled problem on the other.

A closely related duality, which emerged from string theory a little more than a decade ago, is the so-called "**A**nti-**d**e **S**itter/**C**onformal **F**ield **T**heory" (AdS/CFT) correspondence [1]. The amazing thing about this proposed duality is that it relates a consistent theory of gravity, type IIB string theory in Anti-de Sitter space, to a particular gauge theory in a lower dimensional spacetime without gravity. Furthermore, in a way that will be made somewhat more precise below, the AdS/CFT correspondence has all the important elements of a strong/weak duality. When the coupling in the gauge theory is large, the relevant dual description is classical supergravity in AdS space—a theory which is far more accessible computationally.

Broadly, the application of AdS/CFT techniques to physical systems can follow either a "top-down" or "bottom-up" approach. While both avenues of investigation are equally important and rather similar in spirit, they are technically distinct. Top-down models of gauge/gravity duality (of which AdS/CFT provides the canonical example) involve calculations in supergravity theories that are known to be low energy limits of consistent string theories. For such models, the field theory dual is in general a legitimate gauge theory and in many cases well known. For example, the conformal field theory dual to type IIB string theory on AdS space is known as $\mathcal{N} = 4$ super Yang-Mills with gauge group $SU(N)$.

By contrast, bottom-up models are built from gravitational theories that do not descend from any known consistent theory of quantum gravity. These models are in some sense "effective theories"—they contain the minimal ingredients to be considered for phenomenologically viable dual field theories. The implicit assumption is that the gravity theory in this case is dual to *some* gauge theory with properties such as field content and symmetry groups encoded in the bulk. What bottom-up models lose in rigour, they typically recover in accessibility and computational convenience. In the chapters that follow, examples of both top-down and bottom-up constructions will be considered.

The remainder of this introduction to gauge/gravity duality will be devoted to motivating some important features of this correspondance, and describing some broad-stroke considerations regarding their application to physical systems. We begin with a pedagogical argument for the existence of a gauge/gravity duality in section 1.1.1, and continue by highlighting aspects of the duality relevant to performing calculations in a strongly coupled gauge theory (section 1.1.2). We then turn our attentions to two strongly coupled systems particularly amenable to these techniques. In section 1.2, we work out the characteristics desirable for a gravity dual to the strongly coupled matter produced by colliding heavy nuclei at high energies. Section 1.3 develops the necessary requirements for a gravitational dual to condensed matter systems, including fermions at unitarity and non-Fermi liquids.

1.1.1 The way things work (part I)

String theory is a gravitationally complete framework that describes interactions between an assortment of interesting objects. There are the namesake strings, of course—objects extended along one spatial dimension, that trace two-dimensional "worldsheets" as they propagate in space and time. There are also an assortment of "branes", which are objects that can extend in as many as nine spatial dimensions. These branes can carry different types of charges, and provide a place for strings to begin and end.

From these branes, and the strings that stretch between them, it is already possible to heuristically describe the primary features of AdS/CFT duality. A cartoon of the correspondence appears in figure 1.1, with a rendering of branes and strings appearing at the top of the triangle. To motivate the correspondence, we consider a stack of N_c D3 branes (which have four dimensional world volumes), placed directly atop one another. For strings confined to this stack of branes, there are evidently N_c^2 ways in which the string endpoints can be arranged. Each of these N_c^2 strings has in its excitation spectrum a massless gauge boson, which is suggestive of a $U(N_c)$ gauge theory living in the worldvolume of the brane stack, a guess that is vindicated by careful calculation. If N_c is taken to be very large, $N_c^2 \sim N_c^2 - 1$, and we arrive at the 't Hooft limit of a $SU(N_c)$ gauge theory in four dimensions.

When the stack contains a very large number of branes, their backreaction on the (ten dimensional) space they live in becomes non-trivial. As per Einstein's equations, this stack's energy and momentum tensor sources the geometry, and consequently the stack curves spacetime

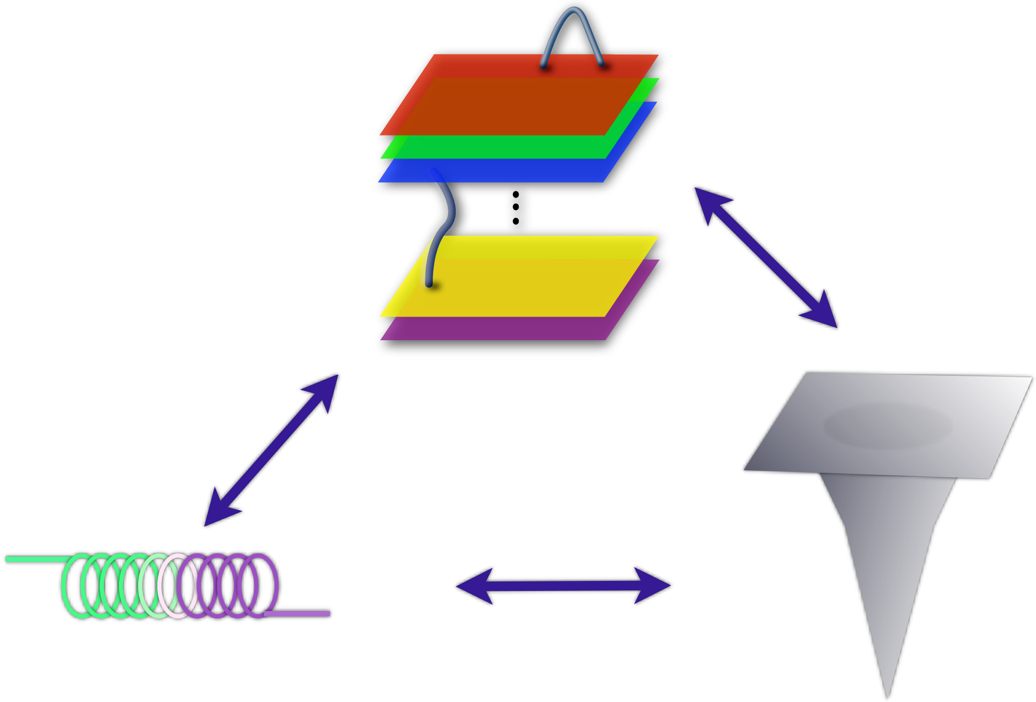

Figure 1.1: Illustration of the central idea of gauge/gravity duality. A stack of branes (12 o'clock) can be described either in terms of the gauge theory that lives on it (7 o'clock) or the geometric imprint it leaves on space time around it (5 o'clock). Thus, a dictionary should exist between the gauge theory, and the gravity theory.

in a characteristic way. This observation suggests an equivalent, but logically distinct description of the stack of branes—namely, a description in terms of the metric in the space around them.

The fact that **one** system, consisting of a pile of D3 branes placed atop one another, can be described either in the language of a gauge theory living on the pile's world volume *or* in the language of the gravitational imprint it leaves in the geometry of spacetime suggests that a dictionary ought to exist allowing one to translate one language to another. This dictionary is the primary result of the AdS/CFT duality.

Like the previously mentioned strong/weak dualities, the AdS/CFT dictionary relates strongly coupled physics to perturbative physics. This is a consequence of the dictionary entry

$$\frac{R^4}{l_s^4} \leftrightsquigarrow \lambda \tag{1.1}$$

where the left hand side refers to quantities in the gravitational language, and the right hand side pertains to gauge theory quantities. Specifically, R is the radius of curvature of the "imprint" spacetime, l_s is the string length, and λ is the 't Hooft coupling of the gauge theory. From this, we discover that when the coupling in the gauge theory is large, the dual gravity theory has no sharp curves or points. These are the circumstances necessary to neglect "stringy" effects, and is the regime of classical supergravity in curved space. Calculationally, classical supergravity is far more accessible than a strongly coupled gauge theory. In practice, physical problems in this regime can often be formulated in terms of finding solutions to classical equations of motion for vector, scalar or fermion fields in fairly simple spacetimes. In this way, gauge/gravity duality offers one exciting route to the exploration of strongly coupled systems.

An important aspect of the AdS/CFT duality is that the dictionary interprets between a *specific* gauge theory and its unique gravitational dual. In the canonical example, this map can take one from strongly coupled $\mathcal{N} = 4$ Super Yang-Mill (SYM) in four dimensions to classical supergravity on AdS_5 (the other five dimensions present on the gravity side are compactified into a five-sphere, S^5, and will not play a prominent role in this discussion). Perhaps not surprisingly, the symmetries of the gauge theory are intimately tied to the isometries of the bulk (gravity) theory. The $\mathcal{N} = 4$ SYM theory, for example, is a conformal field theory. This means, among other things, that the theory is scale invariant and thus the physics looks the same at all energies. To see how this manifests geometrically, it is useful to consider the metric of AdS_5:

$$\mathrm{d}s^2 = \frac{r^2}{R^2}\left(-\mathrm{d}t^2 + \mathrm{d}\vec{x}^2\right) + \frac{R^2}{r^2}\mathrm{d}r^2 \tag{1.2}$$

In this presentation, the radial variable r tracks position in the "throat" region of the geometry. With respect to figure 1.1, the location $r = 0$ would refer to the bottom of the AdS diagram, while the boundary is at $r = \infty$. It is not difficult to see that a rescaling of the form

$$t \to \Lambda\, t, \qquad \vec{x} \to \Lambda\, \vec{x}, \qquad r \to \frac{r}{\Lambda} \tag{1.3}$$

leaves the metric unchanged. If the gravitational theory is unchanged under such a scaling, it stands to reason that the dual gauge theory is indifferent to this action as well. Since this isometry forces r to scale as an inverse length, it is natural to associate the radial coordinate with an energy scale under duality, and we see that this isometry is the geometric realization of the conformal symmetry present in the $\mathcal{N} = 4$ theory. In later chapters, we will see that the temperature of the gauge theory is related to the radial location of an event horizon in the bulk, justifying our association of an energy scale to location in the throat.

1.1.2 The way things work (part II)

To actually exploit this duality computationally, it is of course necessary to move beyond the heuristic picture provided above. Mathematically, the fundamental assertion of gauge gravity duality is the equivalence of the partition function for the gauge and gravity theories. In the applications addressed in this dissertation, the relevant equivalence is that of the partition function of the strongly coupled gauge theory to the saddle point approximation of the string theory partition function (the large N_c classical limit):

$$\mathcal{Z}_{\text{bulk}}\left[\phi_0(t,\vec{x})\right] \approx e^{-N_c^2\, S_{\text{class.}}[\phi_0]} = \left\langle e^{\int \mathrm{d}^4x\, \phi_0(x)\mathcal{O}(x)} \right\rangle \tag{1.4}$$

From (1.4) it is clear that the boundary value of a field in the gravitational theory, ϕ_0, plays the role of a source for some gauge theory operator $\mathcal{O}$. Which gauge theory operator, exactly, can be deduced from an assortment of symmetry considerations in some special cases. In any case, computing the on-shell boundary action for the bulk theory immediately provides access to correlators in the dual gauge theory. Many examples of this relationship between bulk fields and gauge theory correlators will appear in this work.

With correlation functions in hand, many of the standard techniques of quantum field theory can be employed to develop a description of the strongly coupled physics. Playing a prominent role in applied gauge/gravity duality are the so-called Kubo formulas which relate Green's functions to transport coefficients in the boundary (gauge) theory. These sorts of techniques are particularly interesting theoretically, because they allow one to calculate where standard lattice gauge theory methods can not. More specifically, because these lattice theories are formulated in euclidean spacetimes, they in some sense trade thermodynamics for dynamical processes. We will see shortly that in AdS/CFT we need make no such concession. As an example of utility of Kubo formulas in the gauge/gravity correspondence, consider the computation of the shear viscosity in a strongly coupled gauge theory (figure 1.2). By way of the AdS/CFT dictionary, one discovers that the graviton in the bulk theory $h_{\mu\nu}$ is dual to the stress tensor of the boundary theory, $T_{\mu\nu}$. Thus, to compute the Green's function for the stress tensor, one simply needs to solve the linearized Einstein equations for fluctuations about the background spacetime (note that linear equations of motion correspond to terms quadratic in the graviton in the Lagrangian, which are the terms required for a two-point function as per (1.4)). The Kubo formula for the shear viscosity (η) does the rest of the work:

$$\eta = \lim_{\omega \to 0} = \frac{1}{2\omega} G^{R}{}_{x,y\,;\,x,y}(\omega) \tag{1.5}$$

In the above formula, ω refers to the frequency of the fluctuation, the R denotes a retarded (causal) propagator, and the x, y label the relevant components of the stress tensor.

As alluded to above, the ability to easily probe the thermodynamic behavior of the strongly coupled gauge theory is another nicety of AdS/CFT. Indeed, it's not hard to guess the gravity dual of a theory in some thermodynamic ensemble—as is well known in cosmology, geometries with black holes in their interior contain all the desired thermodynamic properties. Black holes are characterized by a Hawking temperature related to the thermal radiation they emit, and they carry entropy in an amount proportional to the area of their horizon. Conveniently, the duality dictionary identifies this temperature and entropy with that of the dual field theory. More thermodynamic properties of the gauge/gravity correspondence will be elucidated below.

Before focusing on aspects of AdS/CFT that are specific to physical systems studied in

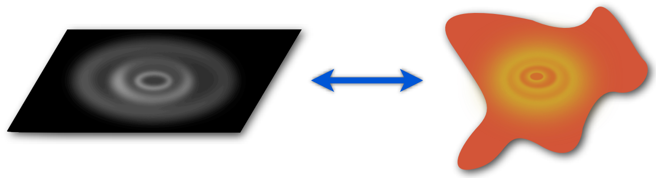

Figure 1.2: Dissipative phenomena in gauge theories are dual to objects falling into black holes

the lab, it is worth highlighting one breed of result likely applicable to *all* systems with gravity duals. These "universal" results are more or less the zenith of what one might hope to compute in gauge/gravity applications. They are largely impervious to the argument that the exact gravity dual of the relevant gauge theory may not be known, as they hold in all (or nearly all) AdS/CFT arrangements. The shining example of universality of AdS/CFT is the ratio of the viscosity to entropy density, η/s. This result is universal because both the viscosity and the entropy density of the gauge theory are related via duality to the horizon area of a black hole in the bulk. In taking their ratio, all information about the details of the black hole background divide out, and the resulting number ($1/4\pi$ in this case) is expected to be applicable to all gauge theories dual to two-derivative gravity theories. While this thesis contains no original examples of such universal quantities, attempts to quantify the universality of several gauge/gravity calculations are performed in chapter 2.

1.2 Remarks on AdS/QCD

The majority of this dissertation will be focused on applying the techniques of gauge/gravity duality to the strongly coupled matter produced in highly energetic collisions of heavy nuclei.

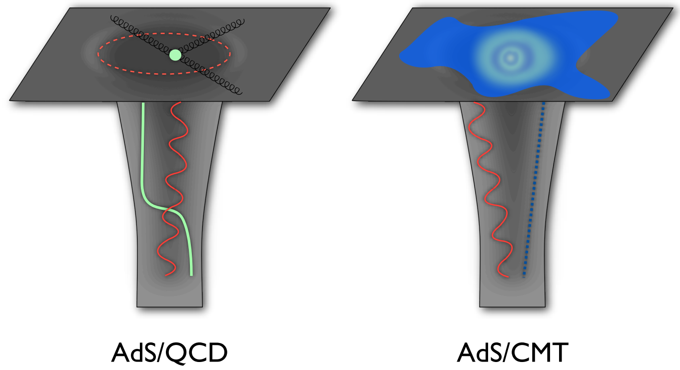

Figure 1.3: Sample gauge/gravity setups for bulk theories dual to Quantum Chromodynamics (QCD) like theories (left) and condensed matter theories (CMT) (right). Wavy lines are gauge fields, solid lines are scalars, and dashed lines in the bulk are fermions.

Characterizing this medium is central to the research program at the Relativistic Heavy Ion Collider (RHIC) at Brookhaven National Laboratory, and is a goal of the Large Hadron Collider at CERN as well. With this in mind, it will prove beneficial to briefly review some desirable ingredients one might attempt to incorporate in a gravitational dual of this phenomenologically rich system of strongly interacting quarks and gluons.

Certainly any viable dual to the matter produced at RHIC should include a temperature and entropy, and we are thus led to bulk theories with black hole backgrounds. Another fundamental property of this system is the absence of conformal symmetry. With a running coupling connecting the strongly coupled theory at relatively low energy to the asymptotically free theory at very high energies, QCD is very much not scale invariant. This can be incorporated into the gravitational theory by introducing a scalar field with a non-trivial bulk profile. This scalar is roughly dual to the Yang-Mills coupling, and by allowing it to vary in the radial direction, one introduces an energy dependence in the gauge theory. Finally, it would be useful to be able to study our dual gauge theory at finite density as well. Fortunately, introducing a chemical potential gravitationally is a simple matter of adding a $U(1)$ gauge field to the bulk. By the magic of duality, this gauge symmetry becomes a global symmetry on the boundary. Thus, charged black hole backgrounds correspond to finite temperature, finite density field theories (figure 1.3, left).

All of these features will be of central importance in this work. In chapter 2, the effects of consistently introducing a scalar field are examined in the context of the gauge theory's speed of sound and its ability to stop energetic partons from propagating through it. Following this, in chapters 3 and 4, the phase diagram of a QCD-like dual is explored. This involves non-conformal physics at finite temperature and density, and results in a theory with a second order phase transition and accompanying critical phenomena.

1.3 Remarks on AdS/CMT

The utility of gauge/gravity duality extends to energies far below those relevant to RHIC. Indeed, there are many condensed matter systems that are accessible in the laboratory and are good candidates for gravitational duals even at extremely low temperatures. These are often systems of strongly interacting electrons, or other fermions scattering in the unitarity regime. In the examples presented in this dissertation, the relevant field theory will be a conformal theory at finite density with fermionic operators.

All of the generic statements about developing a dual description of physics at finite temperature and density written in the preceding section apply equally well to duals of condensed matter systems. One interesting difference is that it will also be interesting to ask what happens at zero temperature. The gravitiational picture relevant to this scenario is now that of an "extremal" black hole, which is more or less a charged black hole with the minimal mass allowed given its charge. These charged black holes have a vanishing Hawking temperature, and thus their field theory dual has zero temperature but non-zero chemical potential. In addition to studying finite density theories at zero temperature, it will also be interesting to obtain duals to systems with angular momentum. An experimental example might arise in a cold atomic system rotating in an optical trap. This too is easily accommodated in AdS/CFT, namely by considering generalizations of the Kerr black hole, which spins.

An obvious puzzle in the study of strongly interacting electrons is whether or not a given system supports a Fermi surface. A field theoretic definition of a Fermi surface is a location in momentum space where the zero frequency fermion correlator diverges. Accordingly, the appropriate gravity dual should contain a fermionic field (figure 1.3) propagating in an extremal black hole. In a way that will be made more precise in a later chapter, the divergence in the correlator can be identified by studying the boundary behavior of the bulk fermion at different momenta.

These aspects of geometric duals to condensed matter systems play an important role in chapters 5 and 6. In the former, we construct consistent gravitational theories dual to non-relativistic conformal boundary theories. This is accomplished by modifying the asymptotic behaviour of the background metric by employing a solution generating technique called the Null-Melvin twist. This technique ensures that the bulk theory is a legitimate solution to type IIB string theory, which helps justify its utility in AdS/CFT. The resulting theories are at finite density and temperature, and can rotate as well. In chapter 6, we embed well worn models of Fermi surfaces in three and four dimensions into maximal gauged supergravity. This is an important and non-trivial task. It is important because it demonstrates that these Fermi surfaces and the non-Fermi liquids they reside in can be described by a consistent string theory. It is non-trivial because maximal gauged supergravity is a highly constrained theory whose underlying symmetries force very special interactions amongst its assorted fields. Thus, finding and isolating a sector of the theory capable of producing a Fermi surface is no easy task. In addition to performing the embedding and finding the Fermi surfaces, we study the properties of the “particle” and “hole” excitations about this surface.

Chapter 2

Robustness of Sound Speed and Jet Quenching for Gauge/Gravity Models of Hot QCD

2.1 Overview

The dual description of hot, strongly coupled gauge theories in terms of weakly coupled supergravity in a curved spacetime is one of the greatest surprises of the last dozen years. This correspondence is tantalizingly close to offering a theoretical framework by which one might hope to understand the dense matter produced at the Relativistic Heavy Ion Collider (RHIC) — after all, with collision energies around 40 TeV the produced plasma is certainly "hot" (on the order of a couple hundred MeV), and the quantifiable successes of hydrodynamic models applied to RHIC flow phenomena suggest that the matter may indeed be "strongly coupled".

Unfortunately, it is not yet known *what* curved spacetime we should study in order to calculate in quantum chromodynamics. The simplest examples of the gauge/gravity correspondence, like the one between $\mathcal{N} = 4$ Super Yang-Mills and $AdS_5 \times S^5$, often exhibit decidedly un-QCD like characteristics. These include supersymmetry, exact conformal symmetry and an absence of degrees of freedom transforming under the fundamental representation of the gauge group.

In light of this somewhat bothersome obstacle, there remain several options for applying these string theoretic techniques to hot QCD matter. First, one could continue calculating in $AdS_5 \times S^5$ and hope that the results obtained do not depend much on the details of the geometry. Such is the case for the ratio of the viscosity to entropy density obtained in [2], in which the specifics of the geometry (and hence the corresponding gauge theory) "divide out", leaving a result universal over a broad class of theories (for possible exceptions, see [3, 4, 5, 6]). Such results are probably rare, but highly desirable — their indifference to the details of the theory imply that if QCD has a gravitational dual, they hold there as well. However, since such universality can at best hold for some subset of all properties of hot QCD, it is useful to think about looking further.

Alternatively, one may attempt to incorporate more QCD-like features into the correspondence (see for example [7, 8, 9] and references therein). The ideal situation, of course, is to find an exact solution to string theory or supergravity with more realistic features, such as non-conformality, less supersymmetry or fundamental matter. (The **most** ideal situation would be to find an exact dual to QCD, but this seems at present too much too hope for.) A difficulty with this important path is that only a very small number of exact string or supergravity solutions at finite temperature with the appropriate features are known; for example, the $\mathcal{N} = 2^*$ model [10, 11, 12] and the Sakai-Sugimoto model [13, 14, 15, 16]. Much important work has been done in this direction.

Another possibility, however, is to sidestep the scarcity and complexity of exact solutions by simply postulating a spacetime geometry with the desired properties, preferably a simple one, without explicit knowledge of what matter content (if any) renders this background a solution of the supergravity equations. For example, the metric of Kajantie, Tahkokallio and Yee [17] breaks conformal symmetry by introducing a simple dimensionful parameter in a warp factor while simultaneously turning on a scalar field. This metric was then explored by Liu, Rajagopal and Shi [18], and its consequences for a number of dynamical properties in the QCD fireball were worked out. If such models can yield useful results, a great deal of effort obtaining exact solutions can be circumvented.

Even with such a model, however, it is important to think carefully about the utility of results obtained via gauge/gravity duals. Although the model may move closer to having QCD-like properties, it is still not QCD, and whatever quantities one calculates are again most useful if they do not vary much over the class of spacetimes with whatever properties were imposed. For example, any result obtained for an arbitrary hot plasma lacking conformal symmetry that is **not** QCD is only useful for understanding QCD in as far as the result is not sensitive to which non-conformal plasma is considered. Put another way, "useful" results for non-conformal hot plasmas only need to be universal across the subset of gravity duals that break conformal symmetry. This idea is discussed at length in [18].

Thus one hopes to capture the properties of a whole class of gauge theories, ideally including QCD, by constructing a simple model with one or two desired properties. Two natural questions then arise. First, are any pathologies introduced into the gauge theory behavior by taking a gravity dual that is not known to solve any equations of motion? Even if one fully trusts the existence of the gauge/gravity correspondence, it only promises consistent and physical dual behavior for backgrounds that are genuinely consistent solutions to a theory of quantum gravity. It is possible that backgrounds that exist in the "gravity swampland", without any extension to a consistent theory of gravity, would predict unphysical behavior. And second, how robust are such models in calculating physical quantities of interest?

To address these issues, in this chapter we construct gravity solutions of varying temperature closely analogous to the solutions of [17], with the same dimensionful parameter in the four-dimensional part of the metric, but which are known to solve the equations of motion for a single scalar field with a potential coupled to gravity [19, 20]; similar scalar/gravity models not designed to directly make contact with [17] include [19, 22, 23]. These solutions are necessarily more complicated than those of [17]. Moreover, these solutions come in a family parameterized not just by the temperature, but by an additional dimensionless quantity, here called α. We then study two properties of our metrics: a bulk property, the speed of sound, which we compare to the speed of sound calculated directly from the model [17], and the jet-quenching parameter $\hat{q}$, which we compare to the results of [18]. Gratifyingly, we find broad agreement, suggesting that the use of the simpler toy model not known to satisfy equations of motion is not problematic in this case.

Moreover, we are able to normalize the temperature scale such that the speed of sound for our family of solutions has the same dependence on temperature regardless of the additional dimensionless parameter α. However, we find that in this physical scale, the form of the jet-quenching parameter varies with temperature differently depending on the value of α. This suggests that our geometries may be quite robust in predicting a speed of sound; but on the other hand may not be as robust for calculating the jet-quenching parameter.

The solutions we construct, although more complicated than those of [17], share the same warp factor for the four-dimensional part of the metric. It is not obvious in general that a whole class of solutions with different temperatures should exist with such a common warp factor. Indeed, we find that the solutions we obtained for varying temperatures have slightly different values of the scalar potential. If the potential varied wildly between solutions, there would be no sense in which we could think of them as states of different temperature in the same theory. We show, however, that for the region of physical interest, the change in the potential is small compared to the potential itself, and thus the associated errors are small. This places a limit on the validity of our approach, where the variation of the potential becomes significant.

Finally, in the model of [17], it was assumed that the one scalar field present was the dilaton, which affects the string metric perceived by the worldsheet in calculations of quantities such as the jet-quenching parameter $\hat{q}$. **A priori**, the single-scalar solutions we construct are agnostic as to whether the scalar field is the dilaton or not. We compare the calculation of $\hat{q}$ between the two cases and find dramatically different behavior with temperature, in one case rising and in the other falling. We suggest that the evolution of the jet quenching parameter with temperature may provide a way of distinguishing whether the spacetime dual to QCD possesses a running dilaton, and hence potentially a strongly-coupled region somewhere in its extent.

We construct our family of solutions in section 2.2. After reviewing the conformal symmetry-breaking model of [17] in section 2.2.1, we detail our solutions in section 2.2.2, and discuss the variation of the scalar potential in section 2.2.3. In section 2.3, we calculate the speed of sound both for the model of [17] and for our solutions, and show how with an appropriate choice of temperature scale, all models have the same functional form for the sound speed. In section 2.4 we calculate the jet-quenching parameter $\hat{q}$ for our models and compare to the result of [18], using both the temperature scale of [18] and the units where the speed of sound is universal. We also compare the behavior of $\hat{q}$ when the scalar field is treated as the dilaton to when it is not. We discuss our results and conclude in section 2.5.

2.2 Probing the Plasma: Models

In an effort to measure how useful a result computed in the gauge/gravity correspondence is to RHIC physics, the authors of [18] offer a pragmatic routine. First, choose a simple metric that preserves all the desired spacetime symmetries and reduces to AdS_5 in the UV, but breaks conformal invariance. Effectively, this allows one to "turn on" a feature of QCD not typically present in pure AdS/CFT. Next, one uses this metric as input to computation in the gauge/gravity correspondence. By studying how the results depend on the conformal symmetry breaking parameter, one hopes to measure the "robustness" of some result to the shift from model to QCD.

In this section, we review the model of Kajantie, Tahkokallio and Yee (KTY) [17] employed by Liu, Rajagopal and Shi [18] to undertake this program, and then construct a class of backgrounds sharing the same conformal-symmetry breaking parameter that explicitly satisfy the equations of motion for one scalar coupled to gravity.

2.2.1 KTY model

Let us review the model of [17]. We use conventions where the action of the gravity/scalar system reads

$$\mathcal{S} = \frac{1}{16\pi G_5}\int d^5x\sqrt{-g}\left(R - \frac{1}{2}(\partial_\mu\Phi)^2 - V(\Phi)\right) . \tag{2.1}$$

In these conventions, the KTY model takes the form

$$ds^2 = \frac{R^2}{z^2}e^{2f(z)}\left[-h(z)dt^2 + d\vec{x}^2 + \frac{dz^2}{h(z)}\right] , \tag{2.2}$$

with

$$2f(z) = -cz^2 , \qquad h(z) = 1 - \frac{z^4}{z_0^4} , \tag{2.3}$$

where the associated temperature is $T = 1/\pi z_0$. The model also contains a running scalar field Φ,

$$\Phi = \sqrt{\frac{3}{2}}\phi z^2 , \tag{2.4}$$

which was interpreted in [17] as the 5D dilaton; we will remain neutral on whether we treat this field as the dilaton or not until section 2.4.[1] If it is the dilaton, the string metric still has the form (2.2) but with

$$2f_{str}(z) = -cz^2 + \frac{4}{3}\Phi_5 = -cz^2 + \sqrt{\frac{2}{3}}\Phi\,. \tag{2.5}$$

The metric and scalar do not solve the equations of motion of the action (2.1), but it was supposed that some additional, otherwise-ignorable matter could be added to generate a true solution.

There are three constant parameters associated to the solution: c, a parameter of nonconformality appearing in the warp factor; ϕ, the overall normalization of the running scalar; and z_0, which controls the temperature. Only two are independent, however: we note that we can change coordinates:

$$t \to \lambda t\,, \qquad \vec{x} \to \lambda \vec{x}\,, \qquad z \to \lambda z\,, \tag{2.6}$$

which is the isometry of pure AdS space (recovered in the limit $c = \phi \to 0, z_0 \to \infty$) associated to scale transformations. The KTY metric is then unchanged if we also scale

$$z_0 \to \lambda z_0\,, \qquad c \to \lambda^{-2} c\,, \qquad \phi \to \lambda^{-2}\phi\,, \tag{2.7}$$

corresponding to the freedom to rescale all mass parameters simultaneously. The two invariant dimensionless combinations can be taken to be,

$$c z_0^2 \propto \frac{c}{T^2}\,, \qquad \alpha \equiv \frac{c}{\phi}\,. \tag{2.8}$$

In addition to the ratio of the temperature to the conformal symmetry-breaking parameter c, we also have the parameter α, encoding the ratio of conformal breaking in the metric to the breaking in the scalar Φ. Thus in addition to the temperature, there is a one-parameter family of conformal-symmetry-breaking geometries. The field theory interpretation of α is in general opaque.

KTY fix α by appealing to the behavior in the meson spectrum of a different metric intended to correspond to the low-energy effective theory on the other side of the confinement phase transition

[1] The canonical normalization for the 5D dilaton, used in [17], is $\Phi_5 \equiv \sqrt{3/8}\Phi$.

[17]:

$$\alpha_{KTY} = \frac{20}{49} \,. \tag{2.9}$$

We shall consider this value, but we will generally leave α arbitrary, and examine the resulting physics for several different choices in the vicinity of (2.9). By considering this parameter, we will be able to quantify how much physical quantities vary as we go from one metric to another at fixed temperature, and hence get an idea of the robustness of our family of solutions.

2.2.2 Model solving equations of motion

We consider a metric ansatz with the general form,

$$ds^2 = e^{2A(r)} \left(-h(r)\, dt^2 + d\vec{x}^2\right) + \frac{e^{2B(r)}}{h(r)} dz^2 \,, \tag{2.10}$$

where r is a suitable radial variable, along with a varying scalar $\Phi(r)$. In papers by Gubser et al., [19, 20] the equations of motion for this system following from the action (2.1) were worked out and found to be,

$$\begin{aligned} A'' - A'B' + \frac{1}{6} &= 0\,, & (2.11)\\ h'' + (4A' - B')h' &= 0\,, & (2.12)\\ 2e^{2B}V + 6A'h' + h(24A'^2 - 1) &= 0\,, & (2.13) \end{aligned}$$

in a gauge where the scalar field itself is used as the radial coordinate, $r = \Phi$; we have neglected to write the scalar equation of motion which is not algebraically independent.

In an attempt to generate a family of solutions to these equations with the same type of conformal symmetry breaking parameter as (2.2), we assume a warp factor for the four-dimensional directions of the same form as (2.3), which using (2.4) and the definition $\alpha \equiv c/\phi$ becomes

$$A(\Phi) = \frac{1}{2} \log\left(\sqrt{\frac{3}{2}} c \frac{R^2}{\alpha}\right) - \frac{1}{2} \log \Phi - \frac{\alpha}{\sqrt{6}} \Phi \,, \tag{2.14}$$

using Φ itself as the radial coordinate. It is then straightforward [19] to solve (2.11) to find

$$B(\Phi) = \log\left(\frac{R}{2}\right) + \frac{1+2\alpha^2}{2\alpha^2} \log\left(1 + \alpha\sqrt{\frac{2}{3}}\Phi\right) - \log \Phi - \frac{1}{\alpha\sqrt{6}}\Phi \,. \tag{2.15}$$

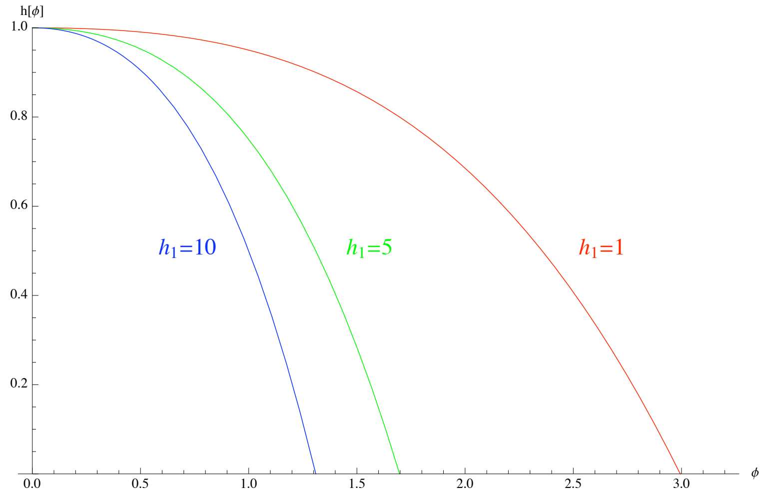

Figure 2.1: Plots of the horizon function $h(\Phi)$ for three different values of the temperature parameter h_1, for $\alpha = 20/49$.

Note that integration constants in both A and B are undetermined by (2.11); we have fixed A to agree with the KTY metric, and B to reduce to AdS space with matching length scale R in the $\Phi \to 0$ limit. Beyond this parameter, this family of metrics depends on the dimensionless ratio α.

We next see from equation (2.12) that the horizon function $h(\Phi)$ consistent with the equations of motion can be obtained by integrating [19]

$$h(\Phi) = h_0 - c^2 R^3 h_1 \int_0^{\Phi} d\Phi' e^{-4A(\Phi')+B(\Phi')}\,, \tag{2.16}$$

with the values of $A(\Phi)$ and $B(\Phi)$ obtained via (2.14) and (2.15). Here we chose the lower bound on the integral for convenience, since any change in it can be subsumed into the constants h_0 and h_1, which are left undetermined by (2.12). We use the freedom in h_0 to impose $h(\Phi = 0) = 1$ to reproduce the AdS limit in the ultraviolet, so $h_0 = 1$. This leaves h_1 as a free parameter in the set of solutions, which we will associate with the temperature.

For a black brane-type geometry we expect h to proceed monotonically from $h = 1$ at the boundary to $h = 0$, which defines the horizon; we are not interested in the space beyond the horizon. To verify that our proposed ansatz leads to actual black brane solutions, we must solve equation (2.16) for $h(\Phi)$. As it turns out, for arbitrary α, the integral in (2.16) is quite complicated, but it can be evaluated for particular choices of α. The result for the KTY value of $\alpha = 20/49$ can be obtained in terms of incomplete gamma functions,

$$
\begin{aligned}
h(\Phi) = 1 \quad - \quad & A h_1 \left[800\,\Gamma\left(\frac{4801}{800}, \frac{801}{800}\right) - 800\,\Gamma\left(\frac{4801}{800}, \frac{267(147 + 20\sqrt{6}\Phi)}{39200}\right) \right. \\
& \left. -801\,\Gamma\left(\frac{4001}{800}, \frac{801}{800}\right) + 801\,\Gamma\left(\frac{4001}{800}, \frac{267(147 + 20\sqrt{6}\Phi)}{39200}\right) \right],
\end{aligned}
\tag{2.17}
$$

where A is the enjoyable constant

$$
A \equiv \frac{163840000000000 \left(\frac{5}{3}\right)^{1/400} 2^{1/160} e^{801/800}}{264116234249604801 \times 89^{1/800}} \approx 0.0017\,. \tag{2.18}
$$

A simpler choice is the nearby $\alpha = 1/2$, for which we find the polynomial result

$$
h(\Phi) = 1 - \frac{h_1}{4320} \left(180\Phi^2 + 60\sqrt{6}\Phi^3 + 45\Phi^4 + 2\sqrt{6}\Phi^5\right)\,. \tag{2.19}
$$

We studied a number of choices of α in the vicinity $0 < \alpha < 1$, where the integrals could be solved; in the remaining sections we will also plot results for $\alpha = 1/5$ and $\alpha = 4/5$.

For the particular value $\alpha = 20/49$ we plot the horizon function for three different values of h_1 in figure 2.1; we see that the function has the correct form, monotonically decreasing to the horizon, and the location of the horizon shrinks as h_1 grows. Similar results hold for other values of α. Given that our solutions do indeed possess a horizon, we can use them to study a non-conformal plasma at finite temperature.

We would like to translate the horizon location Φ_h into a value of the temperature. The temperature T of the geometries is related to the various metric functions by [19]

$$
T = \frac{e^{A(\Phi_h) - B(\Phi_h)} |h'(\Phi_h)|}{4\pi}\,, \tag{2.20}
$$

where the derivative acting on h is with respect to the horizon value Φ_h; note this is not the same as taking a derivative with respect to Φ and then setting $\Phi = \Phi_h$, since in general $h(\Phi)$ is also a function of the parameter Φ_h.

In figure 2.2 we show the relationship between the location of the horizon and the temperature for our solutions, and for the KTY model, for $\alpha = 20/49$; very similar results hold for other α in the range $1/5 < \alpha < 1$. To evaluate this for the model of [18] is a simple exercise in differentiation. For

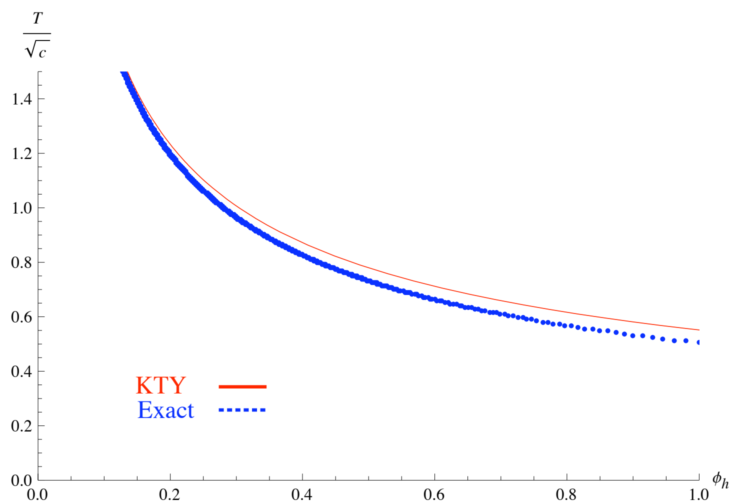

Figure 2.2: Temperature dependence on the horizon location. Deviations increase as $T/\sqrt{c}$ decreases.

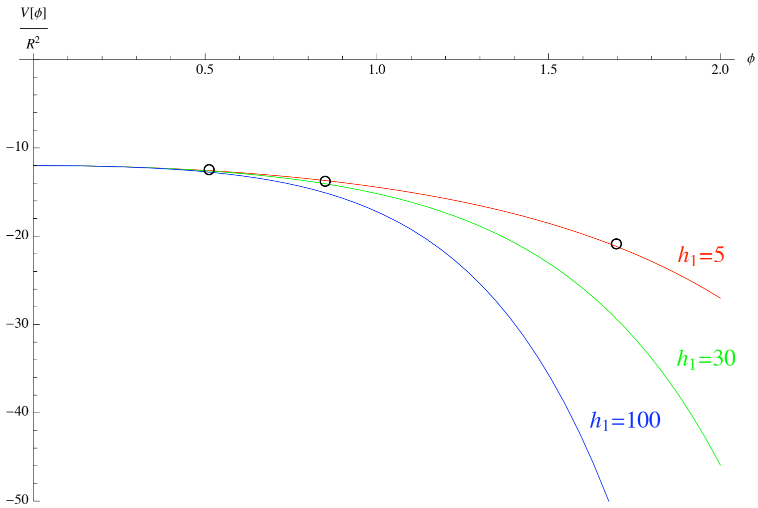

Figure 2.3: A plot of $V(\Phi)/R^2$ for three values of the temperature, and the corresponding horizons indicated as circles. The potential changes substantially, but most of the change is behind the horizon.

the more complicated solution we study here, it requires a numerical routine, where the algorithm obtains the location of the horizon for many values of h_1, finds the corresponding temperature using (2.20), and compares. The two agree in the large-T (small-c) region and deviate only slightly over the range of $1/2 < T/\sqrt{c} < 1$. This range was argued to be of greatest physical interest in [18], through comparison of the thermodynamics of the KTY model to lattice data. This small deviation is perhaps a first suggestion that switching to explicit solutions of the equations of motion does not create a substantial change. For smaller temperatures they diverge more substantially, for reasons we now describe.

2.2.3 Variation of the scalar potential

So far we have discussed equations (2.11) and (2.12), used to determine $B(\Phi)$ and $h(\Phi)$ given $A(\Phi)$. However, we have not considered equation (2.13), which fixes $V(\Phi)$ in terms of the other functions. As was noted in [19], in general this leads to a problem for solving the equations the way we have: there is no guarantee that any given set of functions A, B, and h varying with temperature will lead to the same scalar potential $V(\Phi)$. If the potential changes, then the solutions cannot be thought of as belonging to the same gauge theory dual; instead, as one varies the temperature, one is also changing parameters of the Lagrangian, and producing a vacuum of a different temperature in a **different** theory.

The solutions to the equations of motion we find, assuming the KTY ansatz for $A(\Phi)$ and using (2.13), indeed do not lead to the same potential for different temperatures. While it is possible that there exists *some* arrangement of matter fields for which the potential remains fixed, it is in principle difficult to find. We could also consider a more complicated ansatz, where we do not assume a simple form for $A(\Phi)$, but in addition to the issue of complexity, this defeats the purpose of comparing to the KTY model.[2]

Here we take a practical approach, and see how much it matters. Examining how much the potential is varying with the temperature (that is, the location of the horizon), we find the following. As T changes, $V(0) = -12R^2$ remains fixed, while the largest variation occurs at larger Φ. However, points at sufficiently large Φ are always behind the horizon at Φ_h, and hence the region of largest variation does not contribute to the physics. As the temperature increases, the region where $V(\Phi)$ is varying substantially retreats towards $\Phi = 0$, but at the same time Φ_h retreats in front of it, tending to keep the region of strong variation harmlessly behind the horizon.

We can quantify the change in $V(\Phi)$ at some point Φ as we vary the solutions over the widest physically relevant range: from $T = 0$ to the temperature where that point disappears behind the horizon. We find that the variation in V at a given value of the scalar increases monotonically with Φ; thus for the solution at a given temperature, the point that varies the most over all temperatures to which it contributes is always the point with the largest value of Φ, namely Φ_h itself. We can thus parameterize the variation of V for a solution at a particular temperature T, by how much the potential at the horizon point $V(\Phi_h)$ varies between that solution and the zero-temperature solution.

[2] Solutions to the gravity/scalar system with fixed scalar potential have been studied recently in [22, 23]. These solutions indeed have different warp factors for different values of the temperature.

We have performed this analysis, and for $\alpha = 20/49$ for example we find the values

$$\left.\frac{\Delta V(\Phi_h)}{V(\Phi_h)}\right|_{T/\sqrt{c}=1} = 0.005\,, \qquad \left.\frac{\Delta V(\Phi_h)}{V(\Phi_h)}\right|_{T/\sqrt{c}=1/2} = 0.04\,, \tag{2.21}$$

over the range in $T/\sqrt{c}$ argued in [18] to be most physically relevant. Thus although the solutions to the equations of motion we find are not solutions for precisely the same potential, they are sufficiently similar to lead to only a small error of a couple percent over the region we are interested in. This error, moreover, is over the entire possible range of temperatures; for a practical calculation comparing two solutions with similar temperatures the error will be smaller.

In general we find that smaller values of $T/\sqrt{c}$ have worse behavior; thus the larger the conformal symmetry-breaking, the more the effect matters. Similar results hold for other values of α, and as α increases, the "safe" region moves further in towards smaller values of $T/\sqrt{c}$ (and vice versa). In the sections that follow, we arbitrarily choose a largest error in $\Delta V/V$ that we will tolerate of five percent, and truncate the results for various values of α each at this cut-off. The remaining points should be robust to the variation of the potential to within a few percent.

This is a trade-off for attempting to find exact solutions that, while more complicated than the KTY model, are still relatively simple; in principle there should exist solutions with precisely the same value of $V(\Phi)$ for all temperatures, but these are in general hard to obtain, and additionally, most of these solutions will bear no particular resemblance to the KTY metric for any value of c.

It is also possible to vary our one other parameter, α, as we vary $T/\sqrt{c}$, to try and mitigate the variation of the potential; that is, we can try to find the path through the two-dimensional parameter space of $T/\sqrt{c}$ and α that minimizes the variation of $V(\Phi)$. It is possible to decrease the variation of the potential by several orders of magnitude by making a compensating change in α, though one cannot cancel it precisely. We will not attempt to systematically perform this compensation, since the error from simply changing $T/\sqrt{c}$ is already small for the region we are most interested in.

2.3 The speed of sound

Having our solutions in hand, we would like to compare their predictions to those of the KTY model, to try and see whether the use of metrics not solving known equations of motion still leads to reasonable and robust results. We will compare two quantities: first, a “bulk” quantity not involving the string worldsheet, the speed of sound. In the next section, we shall consider a worldsheet-related number, the jet-quenching parameter.

In a non-conformal plasma, one expects richer thermodynamic behavior than in the conformal case. For example, conformal invariance fixes the speed of sound, defined in terms of the pressure P and energy density ϵ as

$$c_s^2 \equiv \frac{\partial P}{\partial \epsilon}\,, \tag{2.22}$$

at $c_s^2 = 1/3$. This condition comes from the tracelessness of the energy-momentum tensor, as mandated by invariance under dilations. In a non-conformal plasma, on the other hand, c_s^2 can vary.

A convenient formula for the speed of sound is

$$c_s^2 = \frac{d \log T}{d \log s} = \frac{d \log T}{d\Phi_h}\left(\frac{d \log s}{d\Phi_h}\right)^{-1}\,, \tag{2.23}$$

valid in the limit of zero net baryon density, a reasonable approximation in the heavy-ion fireball. Besides the temperature it requires knowledge of the entropy density s, which for our systems is simply proportional to the horizon area of the black brane, taking the form

$$s = \frac{e^{3A(\Phi_h)}}{4\pi G_5}\,, \tag{2.24}$$

and since both T and s vary with Φ_h, it is easiest for us to compute (2.23) in terms of the variation of each quantity with Φ_h, as indicated.

For the KTY model, the speed of sound is straightforward to evaluate:

$$c_s^2 = \frac{1}{3(1 + \frac{c}{\pi^2 T^2})}\,. \tag{2.25}$$

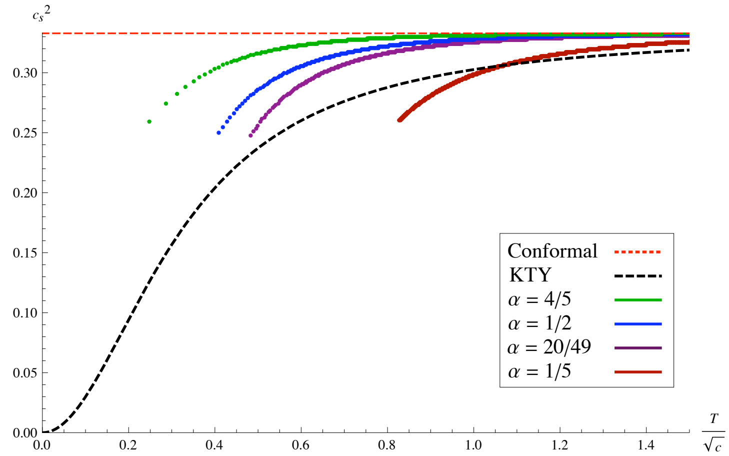

Figure 2.4: Behavior of the squared speed of sound with respect to the dimensionless quantity $T/\sqrt{c}$ plotted for several values of the parameter α. Also shown is the conformal value ($c_s^2 = 1/3$), and the result given by the KTY model.

Note that this formula is independent of α, which for the KTY model entered only into the scalar field and not into the metric (which controls s and T). The result is plotted in figure 2.4.[3] This expression clearly has the right limit of $c_s^2 \to 1/3$ as we restore conformal symmetry $c \to 0$, and it monotonically decreases as the temperature gets small to approach zero in the limit of zero T. This decrease below the conformal value is reasonable on physical grounds.[4]

For the family of solutions obtained in this chapter, calculating the speed of sound in general requires a numerical routine. The algorithm is simply to scan over many values of the horizon location Φ_h by varying h_1, and calculating the resulting values of the temperature and entropy. We then compare neighboring values of Φ_h to calculate the speed of sound. Note that because this calculation involves comparing two solutions with distinct temperature, it is particularly sensitive to the variation of the potential between those solutions; we should not expect this to be a reliable calculation in the limit that the potential variation becomes substantial.

Crucially, the results of this calculation vary depending on the value of α chosen. In figure

[3] A very similar functional form for the sound speed was found in [24], based on the model in [25] which resembles [17] without a running scalar.

[4] For example, in the simpler case of the perfect fluid $P = w\epsilon$, we have $c_s^2 = w$ and the interpolation between $c_s^2 = 1/3$ and $c_s^2 = 0$ is just the progression from ultrarelativistic to non-relativistic species. This plasma would have no quasiparticle description, but the behavior of the speed of sound is analogous.

2.4 we plot the results for a few representative values of this parameter, along with the single result (2.25) for the KTY model. For our results, as each model approaches smaller values of $T/\sqrt{c}$ the error due to the variation of the potential becomes larger. We have therefore imposed a somewhat arbitrary cutoff, including only results with $\Delta V/V < 0.05$. Following the results beyond this cutoff eventually results in pathological behavior, in particular the speed of sound squared going below zero at nonzero temperature.

For all values of α, the speed of sound asymptotes to the conformal value at large temperature and decreases at smaller temperature, analogous to the KTY model. The curvatures of our solutions are slightly different from KTY, being initially flatter and then dropping more abruptly as the temperature is lowered. Smaller values of α give a lower speed of sound at fixed temperature, while larger values give a greater speed. Unfortunately, the variation of the potential and the associated curve truncation do not allow us to determine the small $T/\sqrt{c}$ behavior of the speed of sound. As discussed in [26], lattice simulations for hot QCD matter predict a "strong" drop in the speed of sound near the critical temperature ($T_c \sim 170$ MeV), followed by a rise below it. Obviously, such behavior is not present in the KTY model, which monotonically approaches $c_s^2 = 0$ as $T/\sqrt{c} \to 0$. This is because we work exclusively with the "deconfined phase" geometry, which corresponds to $T > T_c$. For an attempt to realize this behavior in a gravity dual, see [19, 46].

We have plotted our results in terms of $T/\sqrt{c}$ in order to make comparisons with [18]; they naturally used c as a reference parameter since only it appears in the metric, which controls the quantities of interest. For full solutions to the equations of motion, however, the parameter ϕ feeds back into the metric as well via the parameter α. It is not obvious that $T/\sqrt{c}$, as opposed to $T/\sqrt{\phi}$ or any combination of the two massive parameters, is the most useful scale to employ. In other words, our additional dimensionless parameter makes it unclear which units are the natural ones to use.

We can use our results for the speed of sound to try and resolve this issue physically. The speed of sound is a calculable quantity with physical consequences. We may choose, if we can, to set our scale for each model precisely so that in these units, the same temperature always gives

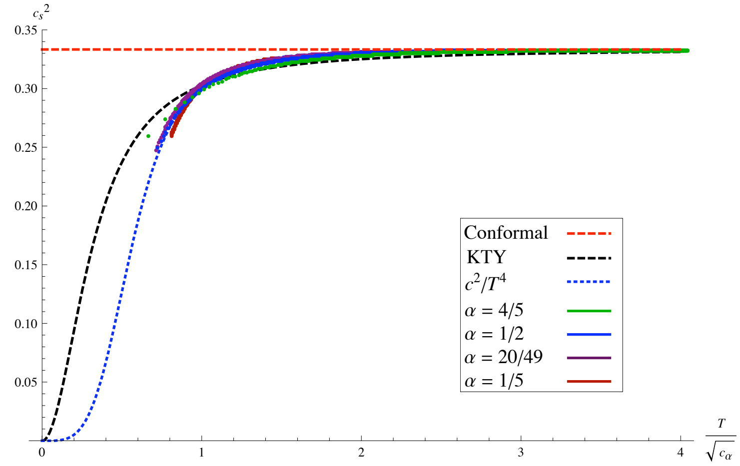

Figure 2.5: Speed of sound curves measured in rescaled units $T/\sqrt{c_\alpha}$. In these units, our model makes one prediction for the dependence of the speed of sound on the ratio of temperature to a dimensionful combination of the parameters ϕ and c. We also compare to the KTY result and an analogous function depending on T^4.

the same value of the speed of sound. That is, we can seek to measure T relative to whatever combination of c and ϕ we need to make the speed of sound curve look identical for all values of α.

We find that plotting the speed of sound as a function of $T/\sqrt{c_\alpha}$, where c_α is an α-dependent rescaling of c given by $(c_{4/5}, c_{1/2}, c_{20/49}, c_{1/5}) = (0.14c, 0.32c, 0.46c, 1.05c)$ with similar scalings for other values of α, creates a convergence between the various curves of our model, all agreeing substantially with each other over their region of validity. This suggests that the appropriate units to measure our results with respect to are $T/\sqrt{c_\alpha}$, which we will do. Since this rescaling depends on α, we can think of c_α as a combination of the massive parameters c and ϕ. In figure 2.5, we plot our rescaled sound speeds, along with the KTY result (2.25) and also the function

$$c_s^2 \approx \frac{1}{3(1+\frac{c_\alpha^2}{\pi^2 T^4})}\,, \tag{2.26}$$

which is a better fit to our unified result for the speed of sound.

We can compare our result to the calculation of the speed of sound in other models, such as that for the $\mathcal{N} = 2^*$ theory in [27]. In terms of conformal symmetry breaking parameters m_f and

m_b, they found to leading order in each m_f/T and m_b/T,

$$c_s = \frac{1}{\sqrt{3}}\left(1 - \frac{[\Gamma(3/4)]^2}{3\pi^4}\left(\frac{m_f}{T}\right)^2 - \frac{1}{18\pi^4}\left(\frac{m_b}{T}\right)^4 + \dots\right) , \tag{2.27}$$

which broadly matches KTY and our results in the leading behavior: all decrease from the conformal value as the temperature goes down. For generic values of m_f and m_b (including the $\mathcal{N} = 2$ limit $m_f = m_b$), the $(m_b/T)^4$ term will be subleading, and in this case the $\mathcal{N} = 2^*$ speed of sound matches the KTY model to order $1/T^2$ (including the sign) as long as we identify the symmetry-breaking parameters $c = 2[\Gamma(3/4)]^2 m_f^2/3\pi^2$. In the limit $m_f \ll m_b$, however (including $m_f = 0$), the $\mathcal{N} = 2^*$ models predict the first subleading term to be proportional to $-1/T^4$, which is a better match to our models and the form (2.26). It is possible that the best fit to our models contains both terms at leading order, as in (2.27).[5]

We have seen that as long as we use the right units, our determination of the speed of sound is quite robust, and broadly similar to the KTY result though not of precisely the same form. As a consequence, we can use the physical quantity of the speed of sound to circumvent our ignorance about the physical meanings of c and ϕ and use the running of the speed of sound itself as our effective scale. Let us now examine a worldsheet-dependent quantity, the jet-quenching parameter $\hat{q}$.

2.4 Jet-quenching parameter

The authors of [18] calculate a number of observables associated to the propagation of quarks in the plasma defined by the KTY model, which on the gravity side are associated to worldsheet calculations. Here we subject our class of models to the calculation of one of these, the jet-quenching parameter $\hat{q}$.

[5] Other theories that approach $c_s^2 = 1/3$ from below in the high-T limit include the model of [24, 25] which is closely related to KTY, the finite-temperature Klebanov-Strassler cascade [28, 29], the Gubser-Nellore model [19], and the Gürsoy-Kiritsis-Mazzanti-Nitti solutions [22, 23]. Models with constant $c_s^2 < 1/3$ also exist, including the Sakai-Sugimoto model [30], the Chamblin-Reall models [19] and the model of Springer [31, 32].

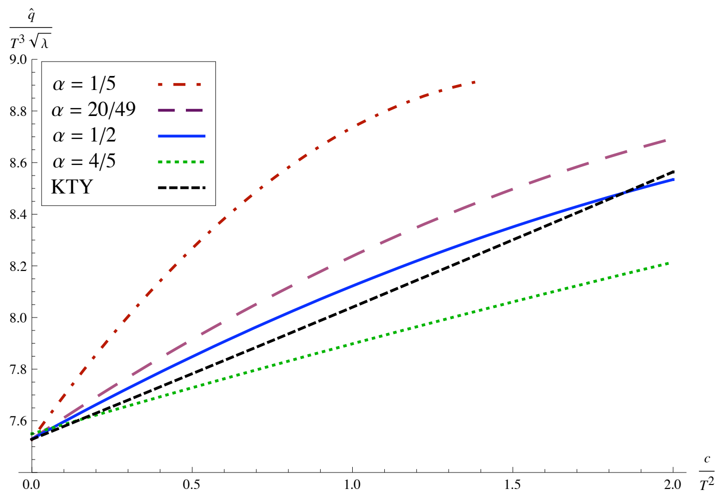

Figure 2.6: Jet-quenching parameter plotted against c/T^2 for several values of α, and in the KTY model. The definition of the quantity λ follows [18].

The parameter is computed via the integral[6]

$$\hat{q} = \frac{1}{\pi\alpha'}\left(\int_0^{\Phi_h} \frac{d\Phi}{\sqrt{\bar{h}(\Phi)[1-\bar{h}(\Phi)]\exp[6\bar{A}(\Phi)-2\bar{B}(\Phi)]}}\right)^{-1} \tag{2.28}$$

where α' is the string tension, and the bars above the metric functions are reminders that they must be transformed into string frame. We can calculate this quantity for our model as well. Note that to do this, we must make a choice as to whether Φ corresponds to the dilaton or not, since (2.28) is sensitive to the string metric. Seeking to have things all ways, we will try both choices and compare.

First we calculate $\hat{q}$ for various values of α assuming the scalar is the dilaton, and plot it with respect to $T/\sqrt{c}$ in figure 2.6, along with the value obtained by [18]. Following [18], we show $\hat{q}$ relative to $T^3\sqrt{\lambda}$, taking into account that many energy loss models used to describe jet quenching at RHIC take $\hat{q}$ to scale like T^3 [38]. We notice a few things: first of all, the high-temperature (conformal) limit is robust, with the KTY model and our solutions for various α all approaching the same value at $\hat{q}/(T^3\sqrt{\lambda}) \approx 7.5$. However, the functional forms of the various values of α diverge substantially as conformal symmetry breaking is introduced, with small α possessing the greatest

[6] The definition used by [18, 35, 36], as proposed by [33, 34], has been called into question by [37]; since our primary motivation is to compare to the [18] computation we will use their definition.

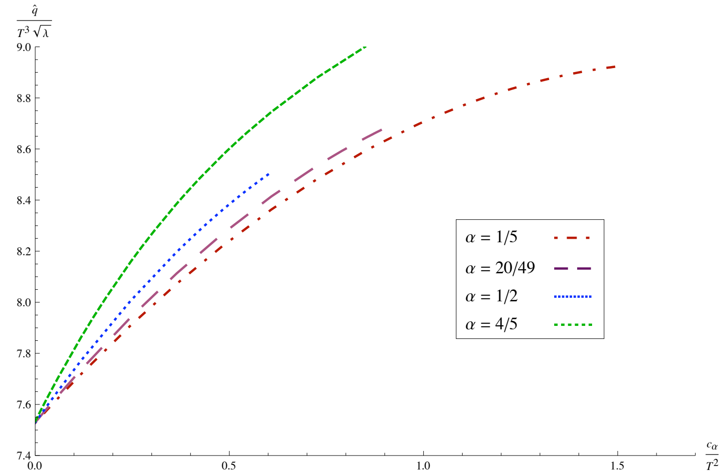

Figure 2.7: Jet-quenching parameter in scaled coordinates. The universality observed in the speed of sound calculation is no longer present; our model does not seem to uniquely determine the temperature dependence of $\hat{q}$.

slope.

We established in the previous subsection, however, that a more physical scale is to measure quantities relative to $T/\sqrt{c_\alpha}$, since in this scale, every value of α has the same speed of sound. Thus if the jet-quenching parameter varies when measured relative to $T/\sqrt{c_\alpha}$, this represents a physical difference between models and not just an unknown and arbitrary rescaling of the reference scale.

In figure 2.7 we plot the same results relative to the physical scale. Interestingly, we still find distinct curves for $\hat{q}$ at different values of α. Thus the variation of α represents a true physical deformation, allowing us to vary the functional form of the jet quenching while keeping the "bulk" property of the speed of sound fixed. Notably, the relative positions of the different values of α have flipped, with large α now having greater slope.

We can compare this result to the case where the scalar Φ is not treated as the dilaton, so the string metric warp factors are identical to the Einstein cases (2.14), (2.15); the results are plotted in figures 2.8, 2.9. We note that the functional form of $\hat{q}$ changes substantially between the two cases. For a running dilaton, regardless of α the ratio $\hat{q}/(T^3\sqrt{\lambda})$ increased as the temperature dropped; for the absence of a running dilaton we find the opposite, with the ratio generally falling, more

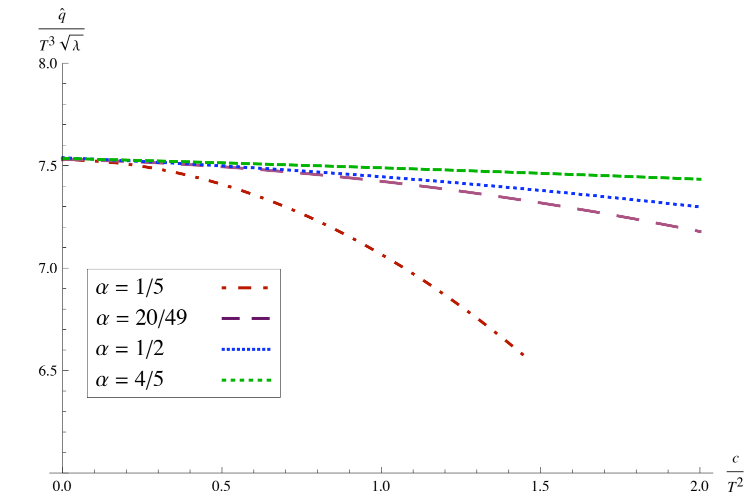

Figure 2.8: Jet-quenching parameter when Φ is not the dilaton, in unscaled coordinates.

pronouncedly in the scaled (physical) coordinates. Again the switch to scaled coordinates $T/\sqrt{c_\alpha}$ also exchanges the ordering of the models. We discuss these results in the final section.

2.5 Discussion

We set out to try and understand whether the use of simple model geometries not known to solve any equation of motion but possessing a key desired characteristic was reasonable and robust. At this point we can attempt to address these questions.

There is no indication whatsoever that the use of the KTY model leads to unphysical results, or indeed results particularly at odds with the class of solutions to the scalar/gravity system we construct. For both the speed of sound and the jet-quenching parameter, the KTY model makes predictions solidly in the middle of the range of results of our solutions, and with similar functional forms. So this is reassuring: if there is a hidden difficulty with such a simple model, we have not found it.

Moreover, we have found that the functional form of the speed of sound is universal across our models, regardless of our tunable parameter α, as long as we measure it in the right units; it also agrees with the leading-order behavior of a class of $\mathcal{N} = 2^*$ models [27]. Thus the predictions

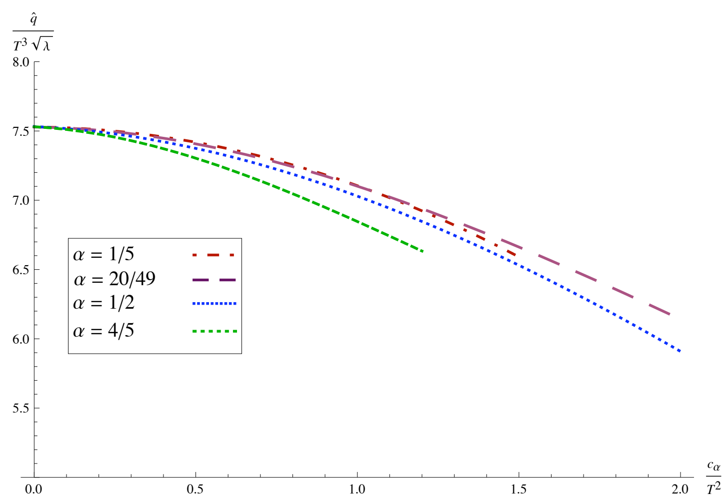

Figure 2.9: Jet-quenching parameter when Φ is not the dilaton, in scaled coordinates.

of the sound speed are independent of whichever representative of our solutions one chooses to use, and hence can be said to be significantly robust. This does not imply that they are universal across all non-conformal plasmas, but are part of a broader class including the KTY model and others that approaches the conformal value from below as the temperature gets large.

For examining the results for the jet-quenching parameter $\hat{q}$, it is useful for us to distinguish two different notions of "robustness". As a first point of comparison, we can look at the $\hat{q}$ results in the context of the results of Liu, Rajagopal and Yee [18]. In this work, a dominant thrust was to identify whether or not a given result was "robust" to the introduction of non-conformality. The idea is that a "robust" quantity would change its value little as the conformal symmetry breaking parameter relative to the temperature was varied across some physically interesting range. Although the variation of the potential does not allow us to scan an arbitrary range of, say, c/T^2, we can nevertheless make an comparison of most of our models over the range considered in [18].

For the α values 20/49, 1/2 and 4/5, we can follow $\hat{q}$ all the way from $c/T^2 = 0$ to 4. Over this range, one finds that the value of $\hat{q}/T^3\sqrt{\lambda}$ changes by about 15% for all α values. By comparison, over the same range the KTY result was found in [18] to increase by about 28%. From figure 2.6 it is easy to see that the largest variation is expected from $\alpha = 1/5$. Unfortunately the variation of the potential limits us in this case to the range $0 \leq c/T^2 \leq 1.4$, across which $\hat{q}$ changes by 18%. When the scalar field is *not* the dilaton, figure 2.8, the jet quenching parameter will again change most when $\alpha = 1/5$ — here 13 % for $0 \leq c/T^2 \leq 1.4$. When $\alpha = 4/5, 1/2$ or $20/49$, we can explore the range $0 \leq c/T^2 \leq 4$, for which we find a 5%, 10%, and 10% change respectively. Accordingly, over these ranges in c/T^2, the value of $\hat{q}$ for a given α is relatively robust to the introduction of the conformal symmetry breaking parameter c following the definition of [18].

There is another important way in which our results may be judged for "robustness". It is evident that none of the geometries we have studied is QCD itself, so their predictions are valuable exactly as far as they are not particularly dependent on the details of the model picked, as we have discussed. The ideal would be to pick a simple model with a few constraints — no conformal symmetry, the right kind of matter, and so on — and hope that the physical results (for at least some quantities) would then be independent of details of which model we have picked — in our case, of which value of the dimensionless parameter α was used. We found that the choice of α could be used to fix a unit system natural for the bulk property of the speed of sound, so we can normalize the variation of the sound curve across all models. Even with this normalization, however, the jet-quenching parameter had substantial variation even over the narrow window of α-values we were able to explore.

Thus, on the one hand we find that the speed of sound is quite resilient. All of our models lead to the same functional form for the sound speed over their regions of validity, which can be made to coincide in the proper set of units; they closely resemble the model of KTY [17] as well.

On the other hand, although our calculation of the jet-quenching parameter seems quite physical, it is less robust in this second sense, at least away from the conformal limit, as its functional form varies significantly with α. Without knowing the true field-theory dual, it is impossible to know what α corresponds to, and hence which value should be picked, and therefore which curve to use. Moreover, we could have chosen a more complicated starting point for our ansatz with more dialable parameters, and there is no reason to think the variation of $\hat{q}$ would not also persist over such a multi-dimensional parameter space.

Thus if we want to extract universal properties of something like the jet-quenching parameter, we either have to provide new input constraints into our models, or look for a property insensitive to fine details, caring only about a gross behavior of the quantity. One example of the latter might be the substantial difference in the behavior of $\hat{q}$ between when Φ was treated as the dilaton and not. Although the details of the curves vary, one could try to extract an overall lesson that a running dilaton leads to a growth of $\hat{q}/T^3\sqrt{\lambda}$ as the temperature diminishes, while a constant dilaton leads to the opposite. Currently, many energy loss models used to describe jet quenching at RHIC take $\hat{q}$ to scale like T^3 [38], giving no preference for the fate of our scalar field. Determining higher order temperature dependence would constitute another input into future models of the plasma, and place constraints on the available freedoms.

In conclusion, we have found no reason to avoid simple models of the QCD plasma, but we have reinforced that the robustness of their predictions must be handled with care. Some quantities such as the sound speed may be quite robust, while others such as the jet-quenching parameter may be somewhat robust over the variation of a single parameter but less so once additional dialable parameters are introduced to the family of models. Even so, they may contain useful information such as the relationship between the dilaton and the global behavior of the function $\hat{q}(T)$. Further study of these questions in the future is surely warranted.

Chapter 3

A holographic critical point

3.1 Overview

At zero chemical potential μ for baryon number, quantum chromodynamics (QCD) appears to have a smooth but rapid crossover at a temperature T_c whose value is within about 10% of 175 MeV. It is believed that this crossover sharpens into a line of first order phase transitions at finite μ. The position of the critical point that terminates this line is of considerable experimental interest, but it is hard to determine theoretically due to being in a region of strong coupling, and also because lattice techniques are not well adapted to finite real μ. A theory review can be found in [39]. Recent lattice results can be found in for example [40, 41, 42]. The aims of the recently initiated beam-energy scan at RHIC are laid out in [89] and the fixed-target CBM project at FAIR is discussed in [44].

It was shown in [45, 46] that simple gravitational theories in five dimensions are capable of producing black holes which approximately reproduce the equation of state of QCD, including the crossover, at vanishing chemical potential; see also [22, 23, 47, 48, 49] and the review [50]. The gravitational theories include just two fields: the spacetime metric, and a real scalar field whose profile breaks conformal invariance and can be understood roughly as the running coupling of QCD. A natural generalization of such models is to include a chemical potential for baryon number as well. Adding a single additional field, a $U(1)$ gauge field dual to the baryon number current, one may generate a chemical potential by turning on an appropriate electric field in the black hole geometry.

In this chapter, we study the coupled metric-scalar-gauge field system and numerically obtain solutions for charged black holes filling out the T-μ phase diagram of the field theory dual. The minimal Lagrangian for these theories contains some freedom, encoded in the choice of scalar potential and gauge kinetic function. We elect to fix both these functions by matching to lattice results for QCD at zero chemical potential. The scalar potential is fixed by demanding a QCD-like equation of state that captures the chiral symmetry breaking crossover, as in [45, 46]. We show how the gauge kinetic function can be determined by similarly matching quark susceptibilities, in principle removing all freedom from the construction.

We then investigate how black holes behave at finite chemical potential. We find that just as is expected for QCD, at finite μ the crossover turns into a line of true first-order phase transitions ending in a critical point. We locate the first-order line by looking for characteristic thermodynamically unstable solutions, and identify the critical point as the end of this line; the location of the critical point is at physically reasonable values of T and μ.

We then turn to a study of the critical exponents of this point. We find a set of exponents that are nontrivially self-consistent due to satisfying two scaling relations. Thus our black holes built from just three fields reproduce a realistic phase diagram near the critical endpoint for a QCD-like theory. In QCD, the critical point is expected to lie in the same universality class as the 3D Ising model and the fluid liquid/gas transition. The critical exponents we obtain are consistent with mean-field scaling. This is reasonable since our black hole constructions are classical, corresponding to an implicit large N limit on the field theory side that suppresses quantum corrections. Further realism lies, presumably, in the inclusion of $1/N$ corrections.

The organization of the rest of this chapter is as follows. In section 3.2 we describe our gravity theory and summarize our results for the location of the critical point in the T-μ plane and the values of its critical exponents. In section 3.3 we provide a self-contained summary of the aspects of thermodynamics which we will require in the rest of the chapter, as well as brief remarks on the phase structure of QCD. Experts will have no reason to read this section, which contains no new results. In section 3.4 we analyze the equations of motion following from our gravity theory, explain how to extract thermodynamic quantities from the black hole solutions, and summarize our numerical strategy. In section 3.5 we will explain how the gauge kinetic function can be chosen to match lattice data for the baryon susceptibility at $\mu = 0$. In section 3.6 we describe locating the critical point on the phase diagram, and in section 3.7 we analyze its properties, calculating the critical exponents and finding them consistent with mean-field scaling. In section 3.8 we compare our result for the location of the critical point to others in the literature, and conclude with some discussion.

3.2 Gravity Theory and Summary of Results

Our model falls in a class of five-dimensional gravitational theories including a real scalar ϕ and an abelian gauge field A_μ along with the spacetime metric, defined by the Lagrangian

$$\mathcal{L} = \frac{1}{2\kappa^2}\left[R - \frac{f(\phi)}{4}F_{\mu\nu}^2 - \frac{1}{2}(\partial\phi)^2 - V(\phi)\right], \tag{3.1}$$

where we use mostly plus conventions. With energy dimensions assigned so that $[\kappa] = -3/2$, $[g_{\mu\nu}] = [A_\mu] = [\phi] = 0$, one finds that 3.1 is almost[1] the most general action using this field content one can have with at most two derivatives. Arbitrary functions of ϕ multiplying the Einstein-Hilbert and scalar kinetic terms can be removed by conformal transformations of the metric and reparametrizations of ϕ, respectively.

The black hole geometries consist of metrics taking the form

$$ds^2 = e^{2A(r)}\left[-h(r)dt^2 + d\vec{x}^2\right] + \frac{e^{2B(r)}}{h(r)}dr^2, \tag{3.2}$$

along with an ansatz for the scalar field and electrostatic potential depending only on the radial coordinate r:

$$\phi = \phi(r), \qquad A_\mu dx^\mu = \Phi(r)dt. \tag{3.3}$$

The coordinates $(t, \vec{x})$ cover Minkowski space, $\mathbf{R}^{3,1}$, while the radial coordinate r represents the holographic direction.

[1] The exception is that one could add a Chern-Simons term $A \wedge F \wedge F$, but this term has no effect on the classical equations of motion, which are what we will study; in addition it vanishes for the solutions we are going to consider, because they have only electric charge, not magnetic. Thus we neglect it.

As explained in [45] in the case of vanishing gauge field, a choice of the scalar potential $V(\phi)$ can be translated into a dependence of the entropy on temperature T. ([45] chooses to work equivalently with the speed of sound $c_s^2 = d\log T/d\log s$.) In fact, if a desired dependence $s(T)$ is specified, then—within certain limits—one can find the $V(\phi)$ that leads to it. A reasonable fit, not too far from T_c, to lattice results for $s(T)$, is achieved with the simple choice[2] [46]

$$V(\phi) = \frac{-12\cosh\gamma\phi + b\phi^2}{L^2} \qquad \text{with } \gamma = 0.606 \text{ and } b = 2.057\,, \tag{3.4}$$

and L a constant related to the number of degrees of freedom.

The black holes describing matter at finite chemical potential include a nonzero gauge field as well. This introduces the problem of specifying the gauge kinetic function $f(\phi)$. We can always use the freedom to rescale A_μ to set $f(0) = 1$. The matching of the speed of sound described in the last paragraph is completely insensitive to the choice of $f(\phi)$. However, $f(\phi)$ can be fixed if one knows the baryon number susceptibility at $\mu = 0$. This susceptibility is in fact fairly well known from the lattice [40]. In this chapter, we will not be systematic in finding $V(\phi)$ and $f(\phi)$ through a fit. Instead, we will focus on the above choice of $V(\phi)$ and a similarly simple form for $f(\phi)$, namely

$$f(\phi) = \frac{\operatorname{sech}\left[\frac{6}{5}(\phi-2)\right]}{\operatorname{sech}\frac{12}{5}}\,, \tag{3.5}$$

which as we will discuss in section 3.5 leads to susceptibilities in good agreement with lattice results.

It is probably impossible to find a string theory construction that leads precisely to the potential 3.4 and gauge kinetic function 3.5. Thus we cannot claim that the theory 3.1 is dual to a specific known field theory. However, string theory constructions do typically lead to potentials which include sums of exponentials of canonically normalized scalars. Thus these functions are at least in the ballpark of expressions that can be derived from string theory, and it is reasonable to place the dual to our model in the broad class of strongly coupled, large-N gauge theories.

Having fit $V(\phi)$ and $f(\phi)$ to lattice quantities at $\mu = 0$, we are able to use black hole constructions to extrapolate outward into the T-μ plane, where we indeed find a critical endpoint.

[2] The constant γ in 3.4 is unrelated to the critical exponent which will appear later in the chapter.

Through methods explained in sections 3.5 and 3.6, we estimate the location of this critical point to be

$$T_c = 143 \text{ MeV} \qquad \mu_c = 783 \text{ MeV} . \tag{3.6}$$

We will compare this result to other estimates in the literature in the conclusions.

Because we have not made a systematic study of the forms of $V(\phi)$ and $f(\phi)$ that approximately match lattice data at $\mu = 0$, we are not in a position to provide theoretical error bars for the result 3.6. It is best to view this result as a proof of principle that you can get a critical endpoint in the T-μ plane using AdS/CFT methods, and that the values 3.6 are within the theoretical error bars. It is also noteworthy that we ignore fluctuations in our analysis: the black holes we construct are fixed, classical geometries. This means that we are not capturing all the physics that is expected to go into the critical endpoint.

Analyzing the thermodynamics near the critical point and performing linear regression fits to the data, we obtain results for four critical exponents,

$$\alpha = 0 , \qquad \beta \approx 0.482 , \qquad \gamma \approx 0.942 , \qquad \delta \approx 3.035 . \tag{3.7}$$

These results are, as we shall discuss, non-trivially consistent with scaling relations, and consistent also with the mean field exponents $\alpha = 0$, $\beta = 1/2$, $\gamma = 1$, $\delta = 3$.

3.3 Thermodynamics with a finite chemical potential

Before discussing the solution of the equations of motion in the gravity system 3.1 and the exploration of the phase diagram, in this section we review a few essential aspects of thermodynamics and critical phenomena.

3.3.1 Thermodynamics of a fluid

A fluid is characterized by the extensive quantities entropy S, volume V and particle number (or net charge) N, and their conjugate intensive variables temperature T, pressure p and chemical potential μ. The internal energy $U = U(S, V, N)$ depends on the extensive variables, which can be thought of as characterizing the system itself, with small changes described by the first law,

$$dU = TdS - pdV + \mu dN \,. \tag{3.8}$$

The intensive variables, sometimes called "fields," can be thought of as properties imposed on the system by contact with a reservoir.

For systems like the quark-gluon plasma, we are not interested in a fixed volume, but instead in volume densities for the extensive quantities. Define the energy density ϵ, entropy density s and number density ρ,

$$\epsilon \equiv U/V \,, \qquad s \equiv S/V \,, \qquad \rho \equiv N/V \,. \tag{3.9}$$

Then, using the thermodynamic relation,

$$U = TS - pV + \mu N \,, \tag{3.10}$$

one can show that the first law of thermodynamics 3.8 rewritten in terms of densities becomes

$$d\epsilon = Tds + \mu d\rho \,, \tag{3.11}$$

naturally reducing the system to a two-variable problem. It is useful to define the corresponding free energy density $f(T, \mu)$ depending on the field variables T and μ using the usual Legendre transformation,[3]

$$f(T, \mu) \equiv \epsilon - sT - \mu\rho \,, \tag{3.12}$$

which obeys

$$df = -sdT - \rho d\mu \,. \tag{3.13}$$

Furthermore, it is easy to see the thermodynamic relation 3.10 implies that the pressure reappears in the analysis as just minus the free energy,

$$p = -f \,. \tag{3.14}$$

[3] The free energy density should not be confused with the function $f(\phi)$ in the gravity Lagrangian.

The phase diagram is the plot of "field" variables T and μ. At each point on the phase diagram, a physical phase corresponds to values of the extensive variables (or densities of extensive variables in our case, s and ρ) which extremize the free energy. In general, it is possible for more than one extremum to exist at a given point on the diagram, corresponding to the existence of multiple phases. The preferred phase is the one minimizing the free energy f; this is the condition of global stability and ultimately stems from the second law of thermodynamics.

In addition to global stability, one must consider local stability, which is characterized by stability under small fluctuations. This is equivalent to the statement of positive-definiteness of the matrix of susceptibilities:

$$\mathcal{S} \equiv \begin{pmatrix} -\frac{\partial^2 f}{\partial T^2} & -\frac{\partial^2 f}{\partial \mu \partial T} \\ -\frac{\partial^2 f}{\partial T \partial \mu} & -\frac{\partial^2 f}{\partial \mu^2} \end{pmatrix} = \begin{pmatrix} \frac{\partial s}{\partial T} & \frac{\partial s}{\partial \mu} \\ \frac{\partial \rho}{\partial T} & \frac{\partial \rho}{\partial \mu} \end{pmatrix}, \tag{3.15}$$

where all derivatives of T or μ are taken with the other fixed. We note that the upper-left diagonal element is related to the specific heat at constant chemical potential C_μ:

$$C_\mu \equiv T \left(\frac{\partial s}{\partial T} \right)_\mu = -T \left(\frac{\partial^2 f}{\partial T^2} \right)_\mu, \tag{3.16}$$

while the lower-right diagonal quantity is related to the isothermal compressibility,

$$\kappa_T \equiv \frac{1}{\rho^2} \left(\frac{\partial \rho}{\partial \mu} \right)_T. \tag{3.17}$$

In QCD, one usually considers in place of κ_T the quark susceptibility,

$$\chi_2 \equiv \left(\frac{\partial \rho}{\partial \mu} \right)_T = -\left(\frac{\partial^2 f}{\partial \mu^2} \right)_T = \rho^2 \kappa_T \,. \tag{3.18}$$

The statement that the matrix of susceptibilities is positive definite is equivalent to requiring

$$C_\rho > 0\,, \qquad \chi_2 > 0\,, \tag{3.19}$$

where C_ρ is the specific heat at constant volume,

$$C_\rho \equiv T \left(\frac{\partial s}{\partial T} \right)_\rho = -T \left[\frac{\partial^2 f}{\partial T^2} - \frac{\left(\partial^2 f / \partial T \partial \mu\right)^2}{\left(\partial^2 f / \partial \mu^2\right)} \right]. \tag{3.20}$$

In the last expression all T and μ derivatives are taken with the other fixed. Note that the Jacobian of the susceptibility matrix is simply

$$\det \mathcal{S} = \frac{1}{T}\chi_2 C_\rho \,. \tag{3.21}$$

Generally speaking, local stability (i.e. positive definite $\mathcal{S}$) is a requirement in order for a configuration to be considered a well-defined phase of the system.

When two phases have equal free energies at a given (T, μ), a first-order phase transition occurs at that point; typically the locus of first-order transitions has codimension one and so describes a line. On one side of the line one phase is favored, while on the other the other is favored; at the first-order line, a discontinuity exists in the densities, Δs and $\Delta\rho$, as the system jumps from one phase to another. The discontinuity in the entropy gives rise to the latent heat $L = T\Delta S$.

A first-order line may terminate on a second-order point, also called a critical point. Here the two distinct phases merge into one; consequently the discontinuities in the densities approach zero as one moves along the first-order line to the critical point. However, although these first derivatives of the free energy become well-behaved, the second derivatives, that is the susceptibilities, may diverge at the critical point. The nature of these divergences characterize some of the critical exponents associated to the critical point, as we will describe momentarily. Critical points in different systems with different variables may share the same critical exponents, a phenomenon called "universality;" the systems are said to lie in the same universality class. Beyond the critical endpoint on the phase diagram there is no discontinuous behavior, but the densities may change rapidly along the extension of what would have been the first-order line. This behavior is called a crossover.

3.3.2 Phase diagram for QCD

A great deal of work has gone into predicting the phase structure of QCD, and it is believed to be quite rich; for reviews, see [86, 87, 88]. At small values of the baryon chemical potential, the QCD phase diagram is dominated by the chiral symmetry breaking transition, and this will be our focus.

When all quarks are assumed to be massless, chiral symmetry is an exact symmetry of the QCD Lagrangian, and the broken symmetry phase at low T and μ and the restored symmetry phase at high T and/or μ are distinct and must be separated by a line of true phase transitions. Near the μ-axis, the transition is expected to be first-order. Near the T-axis, the order of the transition depends on the number of massless quarks. For two massless quarks, the transition on the T-axis is second order and in the universality class of the $O(4)$ model; this transition is expected to be the end of a line of second-order transitions extending into the T-μ plane and meeting the first-order line rising from the μ-axis at a tricritical point. For three massless quarks, on the other hand, the transition on the T-axis is expected to be first-order.

In the real world, quarks are massive and chiral symmetry is not an exact symmetry of QCD. On the T-axis, the transition is known from lattice studies not to be a sharp transition but instead a crossover. It is widely expected that at sufficiently large chemical potential μ the first-order line returns; it then terminates at a critical endpoint at some (T_c, μ_c). This is displayed in figure 3.1.

The critical endpoint is an object of substantial interest and speculation. It is difficult to explore it theoretically, as the theory is strongly coupled and lattice calculations are difficult at finite μ. A number of models have been constructed to analyze its properties. It is expected to lie in the universality class of the 3D Ising model, like the standard liquid/gas transition of fluids. It is anticipated that depending on its location on the phase diagram, future heavy ion experiments such as those at RHIC, LHC or FAIR may produce a quark-gluon plasma lying close to the critical point at freeze-out, which could lead to information about its properties (see for example [89, 44, 54].)

Other phases of QCD are anticipated to exist, in particular regions at large μ characterized by color superconductivity. We will have little to say about these phases in this chapter other than a brief speculation in section 3.6.2.

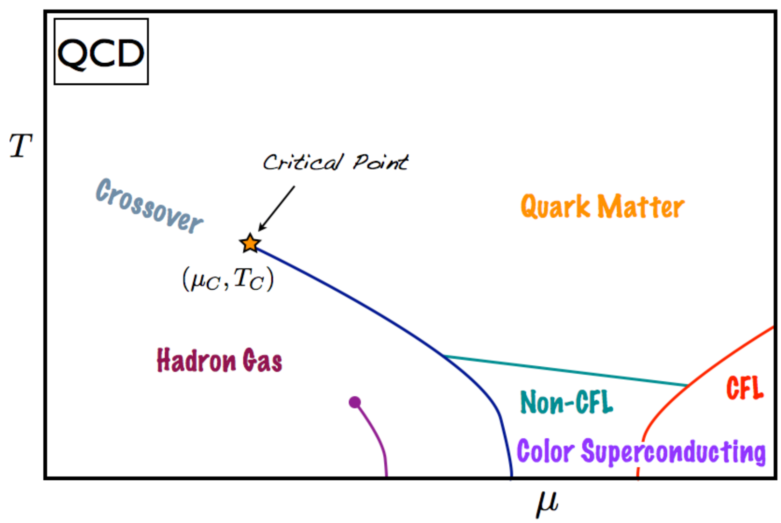

Figure 3.1: The expected phase diagram of QCD. The line ending in a star is the first-order chiral transition and its critical endpoint, which we focus on. Below is the nuclear matter transition. At lower right are color superconducting phases, color-flavor locked and otherwise.

3.3.3 Critical behavior

Near the critical point various first and second derivatives of the free energy go to zero or diverge as power laws, and it is the "critical exponents" associated with these power laws that are universal — meaning they may take the same values from one physical system to another, even among systems with quite different microscopic properties. Describing them is at the heart of the study of critical phenomena.

We will calculate four standard thermodynamic critical exponents α, β, γ and δ.[4] In calculating the exponents, it is vital to specify whether one is approaching the critical point along the axis defined by the first order line, or by another direction. The exponent α is defined by the power law behavior of the specific heat at constant ρ as the critical point is approached along the axis defined by the first order line:

$$C_\rho \sim |T - T_c|^{-\alpha}\,, \qquad \text{along first order axis}\,. \tag{3.22}$$

The exponent β comes from the discontinuity of ρ across the first-order line. $\Delta\rho$ is finite at a generic point on the first-order line, and goes to zero as one approaches the critical point along the line:

$$\Delta\rho \sim (T_c - T)^{\beta}\,, \qquad \text{along first order line}\,. \tag{3.23}$$

The exponent γ is analogous to α, but instead of C_ρ, it is χ_2 that is tracked along the first-order axis:

$$\chi_2 \sim |T - T_c|^{-\gamma}\,, \qquad \text{along first order axis}\,. \tag{3.24}$$

Finally, δ is defined at the critical isotherm $T = T_c$ by the relation between $\rho - \rho_c$ and $\mu - \mu_c$:

$$\rho - \rho_c \sim |\mu - \mu_c|^{1/\delta}\,, \qquad \text{for } T = T_c\,. \tag{3.25}$$

The same power law will manifest for any approach **not** parallel to the first-order line. The paths through the phase diagram associated to the four exponents are summarized in figure 3.2.

[4] Two other commonly-used critical exponents, ν and η, require knowledge of the spatial distribution of correlation functions and will not be calculated here.

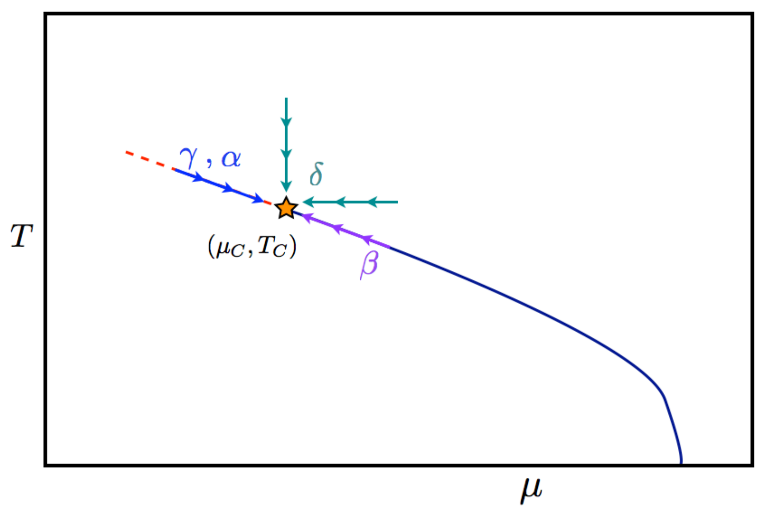

Figure 3.2: A cartoon of the first-order line terminating at the critical point (star) with the directions of approach of the various critical exponents indicated.

The four thermodynamic exponents are not all independent; in general they obey so-called scaling relations, which follow from the scaling behavior of the free energy at the critical point, determining two exponents in terms of the other two. One has

$$\begin{aligned} \alpha + 2\beta + \gamma &= 2, \\ \alpha + \beta(1+\delta) &= 2\,. \end{aligned} \tag{3.26}$$

Different critical exponents are characteristic of distinct universality classes. Calculations in Landau-Ginzburg, or mean-field, theory capture the tree-level values of the critical exponents; in general this neglects quantum corrections, which can be captured by the more sophisticated techniques of the renormalization group. The critical point of QCD is expected to lie in the universality class of the 3D Ising model, as does the standard liquid/gas transition. The results from mean field (van der Waals) theory, the full quantum 3D Ising model, and experiments in non-QCD fluids are summarized in the table [55]:

	Mean field	3D Ising	Experiment
α	0	0.110(5)	0.110 - 0.116
β	1/2	0.325 $\pm$ 0.0015	0.316 - 0.327
γ	1	1.2405 $\pm$ 0.0015	1.23 - 1.25
δ	3	4.82(4)	4.6 - 4.9

These are the results we will compare our holographic system to.

3.4 Black hole solutions

We now turn to an analysis of the equations of motion for the gravity system. From the action 3.1 one can derive four second order equations of motion and a zero-energy constraint. The second order equations (simplified slightly using the zero-energy constraint) are

$$A'' - A'B' + \frac{1}{6}\phi'^2 \quad = 0 \tag{3.27}$$

$$h'' + (4A' - B')h' - e^{-2A} f(\phi)\Phi'^2 \quad = 0 \tag{3.28}$$

$$\Phi'' + (2A' - B')\Phi' + \frac{d \log f}{d\phi}\phi'\Phi' \quad = 0 \tag{3.29}$$

$$\phi'' + \left(4A' - B' + \frac{h'}{h}\right)\phi' - \frac{e^{2B}}{h}\frac{\partial V_{\text{eff}}}{\partial \phi} \quad = 0\,, \tag{3.30}$$

where

$$V_{\text{eff}}(\phi, r) \equiv V(\phi) - \frac{1}{2}e^{-2A-2B} f(\phi)\Phi'^2\,. \tag{3.31}$$

The zero-energy constraint is

$$h(24A'^2 - \phi'^2) + 6A'h' + 2e^{2B}V(\phi) + e^{-2A} f(\phi)\Phi'^2 = 0\,. \tag{3.32}$$

The equation of motion for Φ can be integrated once to show the conservation of the Gauss charge Q_G for the $U(1)$ gauge field:

$$\frac{dQ_G}{dr} = 0 \qquad \text{where} \qquad Q_G = f(\phi)e^{2A-B}\Phi'\,. \tag{3.33}$$

One other conserved quantity can be guessed from scaling symmetries, as in [45]:

$$\frac{dQ_N}{dr} = 0 \qquad \text{where} \qquad Q_N = e^{2A-B}[e^{2A}h' - f(\phi)\Phi\Phi']\,. \tag{3.34}$$

3.4.1 Near-horizon asymptotics

Let's assume that h has a simple zero at r_H and that it has no additional zeroes between r_H and the boundary. Then r_H is the location of a regular black hole horizon. A series solution to the equations 3.27 and 3.32 can be developed simply by expanding

$$X(r) = X_0 + X_1(r - r_H) + X_2(r - r_H)^2 + \dots\,, \tag{3.35}$$

where X is any of A, B, h, Φ, and ϕ. $B(r)$ may be fixed to be anything by a choice of the coordinate r, so all the B_n are arbitrary. All but finitely many of the other coefficients, however, are determined in terms of the first few. To be more precise: $h_0 = 0$ by assumption; $A_0 = 0$ can be arranged by rescaling t and $\vec{x}$ by a common factor; $h_1 = 1/L$ can be arranged by rescaling only t; $\Phi_0 = 0$ is a choice one must make in order for Φdt to be well-defined at the horizon; and all other coefficients are determined once one chooses ϕ_0 and Φ_1. In other words, the solutions to 3.27 and 3.32 may be parametrized by (ϕ_0, Φ_1). It helps our intuition to recall that ϕ_0 is the value of the scalar field at the horizon, while Φ_1 is essentially the electric field in the radial direction, also evaluated at the horizon. Given the assumptions just stated, it is easy to show that

$$\begin{aligned} Q_G &= e^{-B_0} f(\phi_0) \Phi_1 && (3.36) \\ Q_N &= \frac{1}{L} e^{-B_0} \,. && (3.37) \end{aligned}$$

It does not seem to be practical to find solutions of the equations of motion through high-order series expansions, because the expressions for high-order coefficients quickly become quite complicated. In practice we stopped at fourth order. The resulting expansions are suitable for providing initial values for numerical integration of the differential equations 3.27 at a radius slightly outside the horizon.

3.4.2 Far region asymptotics

To discuss asymptotic behavior far from the horizon it helps to pick a gauge, so we fix $B = 0$. We can write the potential $V(\phi)$ as

$$V(\phi) = -\frac{12}{L^2} + \frac{1}{2} m_\phi^2 \phi^2 + \mathcal{O}(\phi^3) \,, \tag{3.38}$$

demonstrating L is the radius of curvature of the asymptotic AdS_5 geometry, and we can define Δ_ϕ, the ultraviolet dimension of the operator dual to ϕ, according to

$$m_\phi^2 L^2 \equiv \Delta_\phi (\Delta_\phi - 4) \,. \tag{3.39}$$

Following [46], we have assumed that this operator is essentially $\operatorname{tr} F^2$ and that the ultraviolet limit is to be matched to QCD at a scale significantly above T_c but not parametrically large. Thus Δ_ϕ should be only slightly less than 4, and in our potential $\Delta_\phi \approx 3.93$.

One can then straightforwardly show that

$$\begin{aligned}
A(r) &= \alpha(r) + A_{2\nu}^{\rm far} e^{-2\nu\alpha(r)} + \ldots \\
h(r) &= h_0^{\rm far} + h_4^{\rm far} e^{-4\alpha(r)} + h_{4+2\nu}^{\rm far} e^{-(4+2\nu)\alpha(r)} + \ldots \\
\Phi(r) &= \Phi_0^{\rm far} + \Phi_2^{\rm far} e^{-2\alpha(r)} + \Phi_{2+\nu}^{\rm far} e^{-(2+\nu)\alpha(r)} + \ldots \\
\phi(r) &= \phi_A e^{-\nu\alpha(r)}(1 + a_\nu e^{-\nu\alpha(r)} + a_{2\nu} e^{-2\nu\alpha(r)} + \ldots) \\
&\quad + \phi_B e^{-\Delta_\phi \alpha(r)} + \ldots
\end{aligned} \tag{3.40}$$

where

$$\alpha(r) \equiv A_{-1}^{\rm far} \frac{r}{L} + A_0^{\rm far} \tag{3.41}$$

and

$$\nu \equiv 4 - \Delta_\phi \,. \tag{3.42}$$

The zero-energy constraint 3.32 implies

$$A_{-1}^{\rm far} = \frac{1}{\sqrt{h_0^{\rm far}}} \,. \tag{3.43}$$

Given 3.40, it is straightforward to show that the conserved charges in terms of the far-region quantities evaluate to

$$\begin{aligned}
Q_G &= -\frac{2}{L} A_{-1}^{\rm far} \Phi_2^{\rm far} \\
Q_N &= \frac{2}{L} A_{-1}^{\rm far} (-2h_4^{\rm far} + \Phi_0^{\rm far} \Phi_2^{\rm far}) \,.
\end{aligned} \tag{3.44}$$

Thus $A_{-1}^{\rm far}$, $h_4^{\rm far}$, and $\Phi_2^{\rm far}$ can be determined in terms of $h_0^{\rm far}$ and $\Phi_0^{\rm far}$ once Q_G and Q_N are known. It is notable that in the absence of a scalar (or if for some reason $\phi \to 0$ at the boundary faster than $e^{-2\alpha(r)}$) then the next correction to $h(r)$ after $h_4^{\rm far} e^{-4\alpha(r)}$ is $h_6^{\rm far} e^{-6\alpha(r)}$, and the equation of motion for h can be used to show that

$$h_6^{\rm far} = \frac{1}{3} (\Phi_2^{\rm far})^2 \,. \tag{3.45}$$

However, for the solutions we will study numerically, the scalar doesn't vanish fast enough for the $h_6^{\rm far} e^{-6\alpha(r)}$ term to be interesting.

Evidently, the expansions 3.40 are qualitatively more intricate than the Taylor expansions 3.35 around the horizon because the powers of $e^{-\alpha(r)}$ are not (for practical purposes) commensurate, owing to $\nu \approx 0.07$ not being the ratio of small integers. The fact that $\nu \ll 1$ also leads to some difficulties in finding robust numerical solutions to the equations of motion. We will discuss these issues at greater length in subsection 3.4.4.

The expansion of $\phi(r)$ in 3.40 is split into the part dual to a deformation (proportional to ϕ_A) and the part dual to an expectation value (proportional to ϕ_B). Each solution carries a series of corrections, which we have shown only for the solution proportional to ϕ_A. The correction term $a_\nu e^{-\nu\alpha(r)}$ is present only when $V'''(0) \neq 0$, so for even potentials like 3.4 the leading correction is $a_{2\nu} e^{-2\nu\alpha(r)}$. For small enough ν, this correction, and even higher corrections proportional to ϕ_A, dominate over the $\phi_B e^{-\Delta_\phi \alpha(r)}$ term. Thus the terms not shown explicitly in the expansion for $\phi(r)$ are subleading either to $\phi_A e^{-\nu\alpha(r)}$ or to $\phi_B e^{-\Delta_\phi \alpha(r)}$—or to both. In all the other expansions in 3.40, the omitted terms are all subleading to the terms shown explicitly.

3.4.3 Thermodynamic quantities

The solutions we are interested in have $\phi_A \neq 0$, because they are to be understood as renormalization group flows triggered by deformation of a very slightly relevant operator. This is not exactly how QCD works, but it is sufficiently close to be an interesting approximation. In order to compare solutions meaningfully, one should ideally arrange for ϕ_A always to be the same. This can be accomplished through a coordinate transformation, provided $\phi(r)$ always has the same sign at the boundary.[5] More specifically: suppose we obtain a solution numerically which has some positive value of ϕ_A. Then we wish to perform a coordinate transformation on this solution to bring it into the form

$$d\tilde{s}^2 = e^{2\tilde{A}(\tilde{r})}(-\tilde{h}(\tilde{r})d\tilde{t}^2 + d\tilde{\vec{x}}^2) + \frac{d\tilde{r}^2}{\tilde{h}(\tilde{r})} \tag{3.46}$$

$$\tilde{A}_\mu d\tilde{x}^\mu = \tilde{\Phi}(\tilde{r})d\tilde{t} \qquad \tilde{\phi} = \tilde{\phi}(\tilde{r}) \tag{3.47}$$

[5] If $\phi(r)$ becomes negative at the boundary, the following expressions for far-zone coefficients and thermodynamic quantities can still be used if $|\phi_A|$ is substituted for ϕ_A.

where

$$\begin{aligned}
\tilde{A}(\tilde{r}) &= \frac{\tilde{r}}{L} + \mathcal{O}(e^{-2\nu\tilde{r}/L}) \\
\tilde{h}(\tilde{r}) &= 1 + \tilde{h}_4^{\mathrm{far}} e^{-4\tilde{r}/L} + \mathcal{O}(e^{-(4+2\nu)\tilde{r}/L}) \\
\tilde{\Phi}(\tilde{r}) &= \tilde{\Phi}_0^{\mathrm{far}} + \tilde{\Phi}_2^{\mathrm{far}} e^{-2\tilde{r}/L} + \mathcal{O}(e^{-(2+\nu)\tilde{r}/L}) \\
\tilde{\phi}(\tilde{r}) &= e^{-\nu\tilde{r}/L} + \mathcal{O}(e^{-2\nu\tilde{r}/L})
\end{aligned} \tag{3.48}$$

Setting $ds^2 = d\tilde{s}^2$, $A_\mu dx^\mu = \tilde{A}_\mu d\tilde{x}^\mu$, and $\phi(r) = \tilde{\phi}(\tilde{r})$, one finds immediately that

$$\begin{aligned}
\tilde{t} &= \phi_A^{1/\nu} \sqrt{h_0^{\mathrm{far}}}\, t \\
\tilde{\vec{x}} &= \phi_A^{1/\nu} \vec{x} \\
\frac{\tilde{r}}{L} &= \alpha(r) - \log(\phi_A^{1/\nu}) = A_{-1}^{\mathrm{far}} \frac{r}{L} + A_0^{\mathrm{far}} - \log(\phi_A^{1/\nu})
\end{aligned} \tag{3.49}$$

and

$$\begin{aligned}
\tilde{A}(\tilde{r}) &= A(r) - \log(\phi_A^{1/\nu}) \\
\tilde{h}(\tilde{r}) &= \frac{1}{h_0^{\mathrm{far}}}\, h(r) \\
\tilde{\Phi}(\tilde{r}) &= \frac{1}{\phi_A^{1/\nu}\sqrt{h_0^{\mathrm{far}}}}\, \Phi(r)\,,
\end{aligned} \tag{3.50}$$

which implies

$$\begin{aligned}
\tilde{\Phi}_0^{\mathrm{far}} &= \frac{\Phi_0^{\mathrm{far}}}{\phi_A^{1/\nu}\sqrt{h_0^{\mathrm{far}}}} \\
\tilde{\Phi}_2^{\mathrm{far}} &= \frac{\Phi_2^{\mathrm{far}}}{\phi_A^{3/\nu}\sqrt{h_0^{\mathrm{far}}}} \\
\tilde{h}_4^{\mathrm{far}} &= \frac{h_4^{\mathrm{far}}}{\phi_A^{4/\nu} h_0^{\mathrm{far}}}\,.
\end{aligned} \tag{3.51}$$

Intensive thermodynamic quantities can now be readily extracted using these relations along with standard expressions in the $(\tilde{t}, \tilde{\vec{x}}, \tilde{r})$ coordinate system and the assumptions stated following 3.35:

$$\begin{aligned}
T &= \frac{e^{\tilde{A}(\tilde{r}_H)}}{4\pi} \left(\frac{d\tilde{h}}{d\tilde{r}}\right)_{\tilde{r}=\tilde{r}_H} = \frac{1}{4\pi} \frac{1}{L\phi_A^{1/\nu}\sqrt{h_0^{\mathrm{far}}}} \\
\mu &= \frac{\tilde{\Phi}_0^{\mathrm{far}}}{L} = \frac{\Phi_0^{\mathrm{far}}}{L\phi_A^{1/\nu}\sqrt{h_0^{\mathrm{far}}}}\,.
\end{aligned} \tag{3.52}$$

Densities of extensive thermodynamic quantities can likewise be computed:

$$\begin{aligned} s &= \tfrac{2\pi}{\kappa^2} e^{3\tilde{A}(\tilde{r}_H)} = \tfrac{2\pi}{\kappa^2} \tfrac{1}{\phi_A^{3/\nu}} \\ \rho &= -\tfrac{\tilde{\Phi}_2^{\rm far}}{\kappa^2} = -\tfrac{\Phi_2^{\rm far}}{\kappa^2 \phi_A^{3/\nu} \sqrt{h_0^{\rm far}}} \,. \end{aligned} \tag{3.53}$$

Thus knowledge of the four asymptotic scaling parameters ϕ_A, $h_0^{\rm far}$, $\Phi_0^{\rm far}$ and $\Phi_2^{\rm far}$ determines the standard thermodynamic variables T, μ, s and ρ. Subleading parameters in the field expansions will depend on these in general. For example, using the constancy of the Noether charge 3.34 and its asymptotic expressions 3.36 and 3.44, for $h_4^{\rm far}$ one can show

$$\frac{h_4^{\rm far}}{\phi_A^{4/\nu} h_0^{\rm far}} = \tilde{h}_4^{\rm far} = -\frac{\kappa^2 L}{2}(sT + \mu\rho) = -\frac{\kappa^2 L}{2}(\epsilon + p)\,, \tag{3.54}$$

where in the last step we used the thermodynamic relation (3.10) to express the result in terms of the sum of the pressure and energy density. Note that this is the only combination of ϵ and p we have access to from these calculations. The pressure by itself is equivalent to the free energy density (3.14), which to calculate we would need to evaluate the full renormalized action including counterterms to cancel divergences. It is possible to get the results we're interested in — in particular the position of the critical point and the values of its critical exponents — with just T, μ, s, and ρ.

We can also use the Gauss charge to relate a certain combination of the near-horizon parameters (ϕ_0, Φ_1) to the asymptotic parameters, and thus the thermodynamics. One finds that the Gauss charge is proportional to the inverse of the entropy per baryon:

$$Q_G = f(\phi_0)\Phi_1 = \frac{4\pi}{L}\frac{\rho}{s}\,. \tag{3.55}$$

This is the only analytic relation between the initial conditions at the horizon and the thermodynamic parameters.

3.4.4 Numerical strategy

It is straightforward in principle to obtain a numerical black hole solution by integrating the second-order equations of motion 3.27 starting at some point slightly outside the horizon with the functions and their derivatives initialized from the horizon series expansions described in section 3.4.1, with initial conditions (ϕ_0, Φ_1). Then a fit can be performed of the numerically known functions $A(r)$, $h(r)$, $\Phi(r)$, and $\phi(r)$ to the asymptotic forms 3.40 to extract the quantities $h_0^{\rm far}$, $\Phi_0^{\rm far}$, $\Phi_2^{\rm far}$, and ϕ_A in terms of which T, μ, s, and ρ can be determined. Thus for each input value of (ϕ_0, Φ_1), we obtain a black hole characterized by thermodynamic quantities (T, μ, s, ρ). Certain values of (ϕ_0, Φ_1) may lead to a solution that does not converge to an asymptotically-AdS_5 solution. Typically, these spacetimes are singular. They are not of the class we are interested in, so they are discarded.

Numerical integrations can be made vastly more efficient by noting that $h(r)$ and $\Phi(r)$ converge much faster to their asymptotic values than $\phi(r)$ and $A'(r)$. A good strategy, then, is to figure out the value $r = r_*$ beyond which the non-constant corrections to $h(r)$ and $\Phi(r)$ have no more influence on the equations of motion for A and ϕ than round-off errors do; then join a solution of the full equations of motion from a point just outside the horizon to $r = r_*$ to a solution to simplified equations of motion, obtained by replacing h by $h_0^{\rm far}$ and Φ by $\Phi_0^{\rm far}$, from $r = r_*$ to a value of r large enough to reliably compute ϕ_A. As discussed following 3.44, $\Phi_2^{\rm far}$ can be determined once $h_0^{\rm far}$ and $\Phi_0^{\rm far}$ are known. Thus in order to extract T, μ, s, and ρ using 3.52-3.53, the only quantities one needs from numerics are $h_0^{\rm far}$, $\Phi_0^{\rm far}$, and ϕ_A. We implemented the strategy described here in Mathematica, where the basic ODE's 3.27 are solved using `NDSolve`.

3.5 Quark susceptibility at zero chemical potential

Because lattice calculations at finite chemical potential are problematic, it has been difficult to make precise predictions for the behavior of QCD off the T-axis. However, at $\mu = 0$, lattice studies have been carried out extensively. The potential $V(\phi)$ from [45, 46] was engineered to reproduce the equation of state $s(T)$ known from lattice simulations.

We would like to also constrain the gauge kinetic function $f(\phi)$ using known lattice results at $\mu = 0$. The extrapolation to finite μ is then completely determined by known physics at $\mu = 0$, and represents the unique prediction for the phase diagram of the large-N gauge theory defined to emulate the thermodynamics of QCD on the T-axis.

The gravity calculation of $s(T)$ at $\mu = 0$ is completely insensitive to $f(\phi)$, since the gauge field is zero in these solutions. Instead we may examine the quark susceptibility 3.18 at vanishing μ as a function of temperature, as this has also been calculated extensively on the lattice and as we will see, depends on the choice of $f(\phi)$. In section 3.5.1 we find a gravity formula for the quark susceptibility at zero chemical potential, and in section 3.5.2 we use this to justify our choice of $f(\phi)$.

3.5.1 A formula for quark susceptibility

The black holes with $\mu = 0$ have vanishing gauge field A_μ, and $\rho = 0$ as well. To calculate the quark susceptibility 3.18, we make use of the key observation that the gauge field equation of motion is linear and homogeneous in Φ, while Φ appears only quadratically in the remaining equations 3.27. We thus proceed by treating Φ as a linear perturbation, solving the gauge field equation in the fixed background of the $\mu = 0$ black hole, and then determine χ_2 by noting that on the T-axis, its definition 3.18 becomes

$$\chi_2(\mu{=}0) = \lim_{\mu\to 0} \frac{\rho(\mu)}{\mu} \,. \tag{3.56}$$

Moreover, in the linearized approximation, the overall normalization of Φ is arbitrary as far as the equations of motion are concerned and will cancel out of 3.56, so we can set it to $\Phi_1 = 1/L$.

We can in fact obtain a formula for 3.56 that reduces to quantities only involving the metric and scalar, which are unchanged in the linearized approximation and thus can be taken from the solution for the background $\mu = 0$ black hole. Since it is common in the literature to plot χ_2 normalized by T^2, which approaches a constant at large T, we will find a formula for $\hat{\chi}_2 \equiv \chi_2/T^2$. Using equations 3.52-3.53, we have

$$\hat{\chi}_2(\mu{=}0) = \frac{\rho}{\mu T^2} = -\frac{(4\pi)^2 L^3}{\kappa^2} \frac{\Phi_2^{\text{far}} h_0^{\text{far}}}{\Phi_0^{\text{far}}} \,, \tag{3.57}$$

and making use of the expression 3.44 for the Gauss charge Q_G, we may simplify 3.57 to

$$\hat{\chi}_2(\mu{=}0) = \frac{8\pi^2 L^4}{\kappa^2}(h_0^{\rm far})^{3/2}\frac{Q_G}{\Phi_0^{\rm far}}\,. \tag{3.58}$$

Now recall that $\Phi \to 0$ at the horizon $r = r_H$. As a result,

$$\Phi_0^{\rm far} = \int_{r_H}^{\infty} dr\,\Phi' = Q_G \int_{r_H}^{\infty} dr\, e^{-2A} f(\phi)^{-1}\,, \tag{3.59}$$

where in the second step we have employed the definition 3.33 of the Gauss charge. Plugging 3.59 into 3.58 results in

$$\hat{\chi}_2(\mu{=}0) = \frac{8\pi^2 L^4}{\kappa^2}\frac{(h_0^{\rm far})^{3/2}}{\int_{r_H}^{\infty} dr\, e^{-2A} f(\phi)^{-1}}\,. \tag{3.60}$$

Note at this point that all explicit dependence on the gauge field Φ has dropped out. One can illuminate this further by noting that

$$\frac{s}{T^3} = \frac{128\pi^4 L^3}{\kappa^2}\,(h_0^{\rm far})^{3/2}\,, \tag{3.61}$$

so that finally

$$\hat{\chi}_2(\mu{=}0) = \frac{L}{16\pi^2}\,\frac{s}{T^3}\,\frac{1}{\int_{r_H}^{\infty} dr\, e^{-2A} f(\phi)^{-1}}\,. \tag{3.62}$$

This expression may now be evaluated on $\mu = 0$ black holes directly, without having to solve the linearized Φ equation explicitly.

Our final expression 3.62 is suggestive because in lattice simulations, s/T^3 and $\hat{\chi}_2 \equiv \chi_2/T^2$ have qualitatively similar behavior as functions of temperature at $\mu = 0$: both start near zero for low temperatures, then rapidly cross over to a large value in the region of T_c, and asymptote to a finite value at large T. Hence from (3.62) we come to expect the realistic behavior of $\hat{\chi}_2$ will to some extent be inherited from the analogous behavior of s/T^3.

The effects of the integral in the denominator of 3.62 do play an important role, however. This integral introduces a dependence of the quark susceptibility on the function $f(\phi)$, which s/T^3 alone was insensitive to. Thus differences between the functional forms of $\hat{\chi}_2$ and s/T^3 are due entirely to the effects of $f(\phi)$.

3.5.2 Matching to lattice data at zero chemical potential

We now discuss the matching of lattice data to black hole results at $\mu = 0$ and justify our choice 3.5 for $f(\phi)$. Since the precise field theory dual of our model is unknown, we will not try to translate the quantities κ, L into field theory language. Instead, we will make the arbitrary choice $\kappa = L = 1$ and parametrize our ignorance by allowing separate overall constant rescalings between the lattice quantities and the black hole quantities:

$$[s]_{\text{lattice}} = \lambda_s [s]_{\text{BH}}\,, \quad [T]_{\text{lattice}} = \lambda_T [T]_{\text{BH}}\,, \quad [\rho]_{\text{lattice}} = \lambda_\rho [\rho]_{\text{BH}}\,, \quad [\mu]_{\text{lattice}} = \lambda_\mu [\mu]_{\text{BH}}\,. \tag{3.63}$$

As described previously, to compute the entropy density at $\mu = 0$ one doesn't need any information about $f(\phi)$ at all. In figure 3.3A we show how the entropy density compares between lattice and black holes based on the potential 3.4. For lattice data we used the right hand plot in Figure 3 of [40][6] , with points from asqtad $N_\tau = 6$ simulations from $T = 150\,\text{MeV}$ out to $T = 382\,\text{MeV}$, and then points from p4 $N_\tau = 6$ simulations out to $T = 720\,\text{MeV}$. We determined $T_c \approx 191\,\text{MeV}$ as the temperature at which s/T^3 reaches $1/e$ of its largest value as obtained from the highest temperature data point.[7] For black hole data, we constructed black holes starting with our standard choice 3.4 of scalar potential, and for ϕ_0 ranging from 1.5 to 7.5 in 20 steps, uniform on a log scale.

Our conventions are for all lattice quantities to have units which are powers of MeV, while with $\kappa = L = 1$, all black hole quantities are dimensionless. Thus λ_s and λ_T have units which are also powers of MeV. We found a good fit between lattice data and black holes with

$$\lambda_s = (121\ \text{MeV})^3\,, \qquad \lambda_T = 252\ \text{MeV}\,. \tag{3.64}$$

Turning to the quark susceptibility, in figure 3.3B we show how susceptibilities computed starting from the choice 3.5 for $f(\phi)$ compare with lattice data. For lattice data we used the same reference

[6] We chose [40] to have a definite lattice result to compare to, but there is still disagreement in the literature; for another determination of the equation of state, see [42]. We expect small changes to our model could accomodate variations in the lattice results.

[7] $T_c \approx 191\,\text{MeV}$ is somewhat larger than the value $T_c \approx 175\,\text{MeV}$ mentioned in section 3.1; however it is in line with estimates of [56]. Lower values for T_c are favored, for example, in [57, 58, 59]. We do not aim here to probe the apparent discrepancy; instead we are largely opting for the higher values because all the lattice data we use directly is from [40].

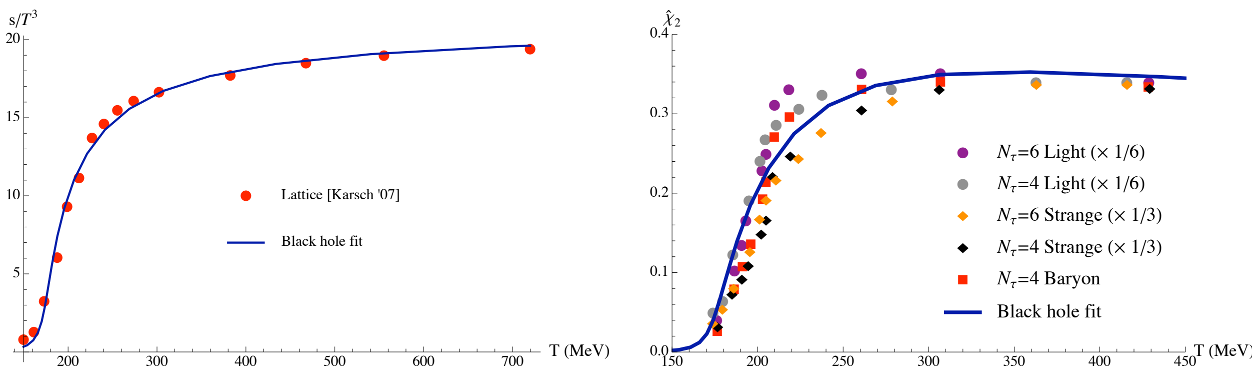

Figure 3.3: The normalized entropy s/T^3 and quark susceptibility $\hat{\chi}_2 \equiv \chi_2/T^2$ at $\mu = 0$, computed on the lattice and fit by black holes in the gravity theory defined by our choices of $V(\phi)$ and $f(\phi)$ (equations 3.4 and 3.5). Lattice data is taken from [40].

as for the entropy [40], with light quark results from the left hand plot in Figure 5, and strange quark and total baryon number results from the two sides of Figure 6; we scaled the light quark and strange quark curves appropriately to asymptote to the same value as that of the baryon number, $\hat{\chi}_2 = 1/3$, at high temperatures. For black hole data we used the same black holes as in the entropy plot, and we employed 3.62 with $L = 1$ (and implicitly also $\kappa = 1$ as before). We used the value of λ_T in 3.64 to rescale the temperature axis, and we adjusted the overall scale of $\hat{\chi}_2$ arbitrarily to optimize the fit to lattice over the range shown in the figure 3.3B. The rescaling of the susceptibility is thus

$$[\chi_2]_{\rm BH} \equiv \left[\frac{\partial\rho}{\partial\mu}\right]_{\rm BH} = \frac{\lambda_\mu}{\lambda_\rho}[\chi_2]_{\rm lattice} \,. \tag{3.65}$$

Thus, knowing $[\chi_2]_{\rm BH}$ and $[\chi_2]_{\rm lattice}$ at the same temperature tells us λ_μ/λ_ρ. In order to find λ_μ and λ_ρ separately, we must recall that the relation for the free energy 3.12 holds equally in lattice units and in the black hole setup. Thus

$$\lambda_T\lambda_s = \lambda_\mu\lambda_\rho = \lambda_\epsilon = \lambda_f \,. \tag{3.66}$$

Putting 3.65 and 3.66 together, we find

$$[\hat{\chi}_2]_{\rm BH} \equiv \left[\frac{1}{T^2}\frac{\partial\rho}{\partial\mu}\right] = \frac{1}{\lambda_T^2}\frac{\lambda_\mu^2}{\lambda_\rho\lambda_\mu}[\hat{\chi}_2]_{\rm lattice} = \frac{\lambda_T\lambda_\mu^2}{\lambda_s}[\hat{\chi}_2]_{\rm lattice} \,, \tag{3.67}$$

which can be recast as

$$\lambda_\mu = \sqrt{\frac{\lambda_s}{\lambda_T}\frac{[\hat{\chi}_2]_{\rm BH}}{[\hat{\chi}_2]_{\rm lattice}}}\,. \tag{3.68}$$

Let us now describe how we arrived at the choice 3.5 for functional form for the gauge kinetic function. The value of $f(\phi)$ near the horizon is particularly important, because the factor e^{-2A} in the integral 3.62 puts significant weight on the near-horizon region. In particular, if $f(\phi)$ is large at the horizon, the integral will be relatively small compared to when $f(\phi)$ is small at the horizon. Since $\hat{\chi}_2$ stays close to its high-temperature value down to a lower temperature than s/T^3 before plunging rapidly to small values, a reasonable conjecture is that as ϕ goes from 0 to positive values, one needs $f(\phi)$ first to increase as a function of ϕ, then to decrease rapidly. The functional form 3.5 was chosen with these desired features in mind, and also with the thought that asymptotically exponential behavior at large ϕ is typical of supergravity theories.

Operationally, the way we determined λ_μ was to use the correct Stefan-Boltzmann value $\hat{\chi}_2 = 1/3$ for baryon number as the value for $[\hat{\chi}_2]_{\rm lattice}$, and to evaluate $[\hat{\chi}_2]_{\rm BH}$ at $T = 460\,\text{MeV}$. This is a reasonable approach because the lattice data converges quickly to the Stefan-Boltzmann value at high temperature. The result is

$$\lambda_\mu = 972 \text{ MeV}\,, \qquad \lambda_\rho = (77 \text{ MeV})^3\,. \tag{3.69}$$

Again it should be emphasized that our choice 3.5 of $f(\phi)$ is to a degree *ad hoc*, and it should be understood as providing a proof of principle that an approximate fit to χ_2 can go with a critical endpoint in the T-μ plane based on AdS/CFT techniques.

3.6 Searching for the critical point

Having settled on a functional form for $V(\phi)$ and $f(\phi)$ by matching to lattice thermodynamics at $\mu = 0$, our Lagrangian is now completely determined. We can next turn to numerically solving for a set of black holes to fill in the phase diagram. An expectation is that the crossover that takes place on the T-axis is sharpened into a first-order line lying out in the T-μ plane, and that this first-order line ends at a critical point somewhere in the vicinity of the crossover. Our first task therefore is to search for this critical point.

3.6.1 Scanning the thermodynamics of black holes

For a first pass at mapping out the thermodynamic behavior of black holes across the T-μ plane, we generated approximately 2500 numeric solutions to the equations 3.27 and 3.32, seeded by initial conditions near the horizon as described in section 3.4.1. Each solution is specified by the value of (ϕ_0, Φ_1) that was used to generate the near-horizon asymptotics. We remind the reader that ϕ_0 is the value of the scalar field at the horizon, which we took always to be positive, and Φ_1 is essentially the electric field at the horizon pointing upward in the fifth dimension. We worked exclusively in the gauge $B = 0$.

To choose a suitable range for ϕ_0, we note first of all that the fits discussed in the previous section involved values of ϕ_0 no larger than 7.5. We went from $\phi_0 = 1$ to $\phi_0 = 15$ in order to obtain the best global picture of the thermodynamics that we could, but any features seen at ϕ_0 significantly larger than 7.5 should be regarded with some degree of skepticism, since in principle one could adjust $V(\phi)$ and/or $f(\phi)$ for $\phi > 7.5$ to make any desired phenomenon occur in that region.[8] It is notable, however, that both $V(\phi)$ and $f(\phi)$ are fairly featureless for $\phi \gtrsim 4$, both being close to a simple exponential function over that domain.

To choose a suitable range for Φ_1, we demonstrate that there is an upper bound on possible Φ_1 values leading to an asymptotically-AdS black hole. To see this, first note that the first equation of 3.27 with $B = 0$ shows that A is concave down as a function of r. But it must be increasing at large r in order for the spacetime to be asymptotically AdS_5. Therefore A must be increasing at the horizon, which is to say $A_1 > 0$. Using the zero-energy constraint 3.32, A_1 can be re-expressed as

$$A_1 = -\frac{L}{6}\left[2V(\phi_0) + f(\phi_0)\Phi_1^2\right] . \tag{3.70}$$

[8] In fact, constraints on $f(\phi)$ come from a narrower range of ϕ, extending only up to $\phi_0 = 5$. Thus, baryon-specific physics is most reliably studied in our model at values of ϕ_0 no greater than 5.

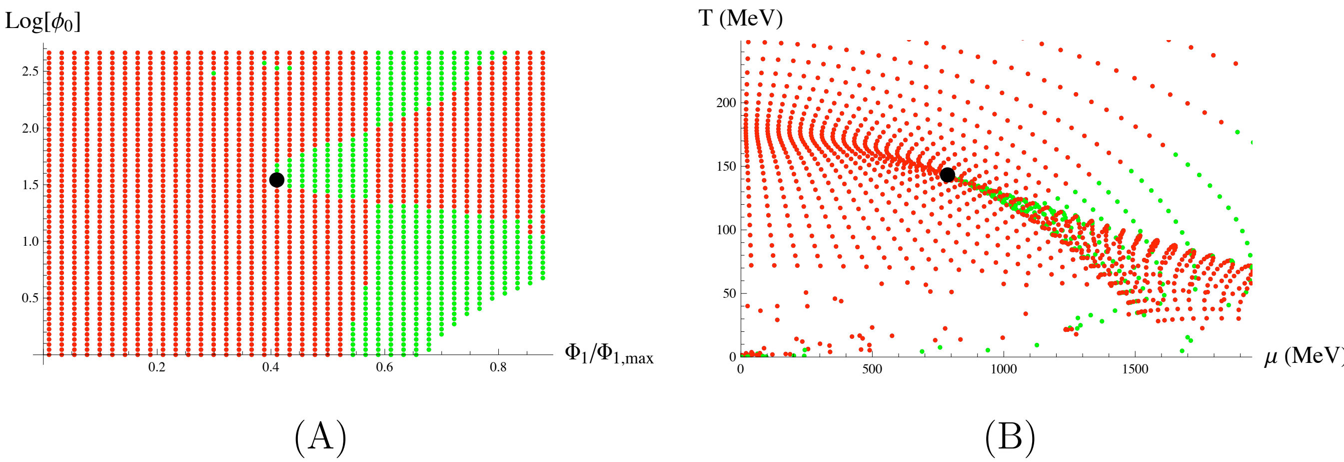

Figure 3.4: Numerically generated black holes. Each dot represents a numerically generated solution. If the Jacobian J defined in 3.72 is positive for this solution, then the dot is red. If $J < 0$, it is green. The bold black circle is the critical endpoint.

Because $V(\phi_0) < 0$ and $f(\phi_0) > 0$, this puts an upper bound on Φ_1:

$$|\Phi_1| < \Phi_{1,\max} \equiv \sqrt{-\frac{2V(\phi_0)}{f(\phi_0)}}\,. \tag{3.71}$$

In practice we scanned black hole solutions from Φ_1 just slightly greater than 0 up to $0.9\Phi_{1,\max}$.

Figure 3.4 shows the results of our numerical scan of the T-μ plane. We examined 61 values of ϕ_0 between 1 and 15, uniformly spaced on a log scale. For each value of ϕ_0 so obtained, we examined 41 evenly spaced values of $\Phi_1/\Phi_{1,\max}$. A small fraction of the values so chosen failed to produce good black hole solutions, generally because A failed to be monotonically increasing, and are simply omitted from the plots.

3.6.2 Locating the critical point

To locate the critical point, we must think a little about what we expect to find in the vicinity of the first-order line. When there are competing phases in a thermodynamic system, only the one minimizing the free energy is the true ground state. However, there is no reason to think our black hole solution-generating method will discover only the true ground state solutions. Due to chiral symmetry not being exact and the presence of the crossover, there is no invariant

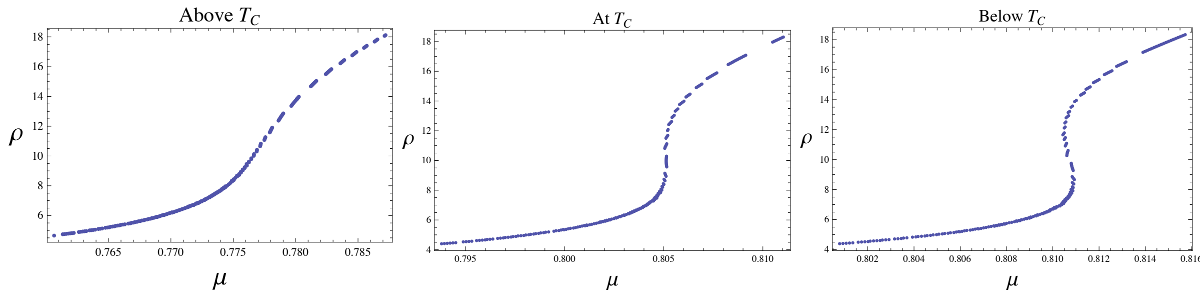

Figure 3.5: The baryon density ρ as a function of chemical potential μ for several values of T near the critical point. For $T > T_c$, $\rho(\mu)$ is single-valued (left), while for $T < T_c$ it is multi-valued (right). At $T = T_c$ the slope is infinite (middle).

distinction between the two sides of the first-order line that could correspond to a difference in topology or other invariant distinction between the phases on the gravity side; the distinct phases will be continuously connected in the space of solutions. Since we are just solving the equations of motion, we expect to find all extrema of the free energy.

In general, extrema of the free energy include not just locally stable minima, but also any thermodynamically unstable saddle points or maxima. Far from the first-order line on the T-μ plane we expect only one solution to the equations of motion; in the vicinity of the first-order line, however, we expect to find ρ and s to be multivalued. Note that this will be true not only on top of the first-order line, but also merely near it, as the free-energetically-unfavored phase will persist for some distance on the phase diagram before ceasing to exist as a solution. The first-order line ends precisely at the (T_c, μ_c) where this multivalued behavior ceases; this is the critical point.

Thus if we consider a constant-T slice of the phase diagram with $T > T_c$ and vary μ, this isotherm will miss the first-order line and the functions $\rho(\mu)$ and $s(\mu)$ will be single-valued (although for T close to T_c they will display crossover-type behavior). But for $T < T_c$, the isotherm will intersect the first order line and we expect $\rho(\mu)$ and $s(\mu)$ to be multivalued near μ_c. The simplest behavior that still increases at both large and small μ is an “S”-shape, and this is what we observe; see figure 3.5. For such behavior there are three solutions at a given μ. Since the slope of the curve is just the quark susceptibility 3.18, we see that two of the solutions have $\chi_2 > 0$ and thus may be thermodynamically stable 3.19; these are the candidate phases. The middle solutions, however, have $\chi_2 < 0$ and must be thermodynamically unstable.[9] Precisely for $T = T_c$ the curve will cease to be multivalued, as the three solutions coalesce into one; the curve $\rho(\mu)$ will have an infinite slope, indicating a divergence in the quark susceptibility at the critical point.

We will locate the critical point by looking for the thermodynamically **unstable** solutions that characterize the vicinity of the first-order line. We can identify the unstable solutions by calculating the Jacobian of the susceptibility matrix 3.15:

$$J \equiv \det \mathcal{S} = \partial(s, \rho)/\partial(T, \mu)\,. \tag{3.72}$$

For a thermodynamically stable black hole, equation 3.19 is satisfied and the Jacobian 3.21 is manifestly positive. If it flips sign to $J < 0$, we have necessarily found a thermodynamically unstable branch. Once we find the thermodynamically unstable black holes, we look to see whether they map to a narrow line-like region on the T-μ plane; the critical point is then the values (T_c, μ_c) where this line ends. We should also be able to see the two stable phases mapping to the same locus on the phase diagram from elsewhere in (ϕ_0, Φ_1).

We can calculate the Jacobian J by finite differences. Since the black holes were scanned on a rectangular grid, we can label them with indices ij, where i determines the value of ϕ_0 and j determines the value of $\Phi_1/\Phi_{1,\mathrm{max}}$. In order to compute J for the black hole labeled ij, we first computed

$$\begin{aligned} J_{ij}^{T\mu} &\equiv \det \begin{pmatrix} T_{i+1,j} - T_{i,j} & T_{i,j+1} - T_{i,j} \\ \mu_{i+1,j} - \mu_{i,j} & \mu_{i,j+1} - \mu_{i,j} \end{pmatrix} \\ J_{ij}^{s\rho} &\equiv \det \begin{pmatrix} s_{i+1,j} - s_{i,j} & s_{i,j+1} - s_{i,j} \\ \rho_{i+1,j} - \rho_{i,j} & \rho_{i,j+1} - \rho_{i,j} \end{pmatrix}. \end{aligned} \tag{3.73}$$

Then $J_{ij}^{s\rho}/J_{ij}^{T\mu}$ is the finite difference approximation to the Jacobian J in 3.72. The results are shown in figure 3.4.

[9] According to the correlated stability conjecture (CSC) [120, 121], such black hole solutions will also have dynamical instabilities, corresponding to the black hole gaining total entropy by locally redistributing charge and energy subject to global conservation of these quantities. In the black hole literature this is known as the Gregory-Laflamme instability [62, 63].

It is clear from figure 3.4A that there is a region of unstable black holes stretching down to $\Phi_1 \approx 0.4\Phi_{1,\text{max}}$. It is this region which we are most interested in, because when mapped to the T-μ plane it becomes a narrow region that ends in a cusp. Moreover, we do indeed find two other sets of black holes with $J > 0$ mapped to the same locus, and hence we identify it as the first-order line. The point of this cusp is then the critical endpoint, which we show as a bold black circle. It occurs at the values

$$(T_c, \mu_c) \approx (143\,\text{MeV}, 783\,\text{MeV})\,. \tag{3.74}$$

We have used the multipliers λ_T and λ_μ from 3.64 and 3.69 to express T and μ in units of MeV. Points at the critical point come from initial conditions in the vicinity of

$$(\phi_0, \Phi_1/\Phi_{1,\text{max}}) \approx (4.84, 0.40)\,. \tag{3.75}$$

Note that the value for ϕ_0 is within the range probed by the $\mu = 0$ solutions described in section 3.5.2—though not by much, if one goes by the values of ϕ over which $f(\phi)$ is meaningfully constrained by lattice data.

In summary, we have identified a candidate critical point and first-order line. As we study it in more detail in the next section, examining the behavior of densities and susceptibilities, this identification will be amply confirmed.

Before moving on, let us consider the other thermodynamically unstable black holes found in our scan. The unstable black holes described so far are associated with a failure of the map $(\phi_0, \Phi_1) \to (T, \mu)$ to be invertible, which is to say a sign change in $J_{ij}^{T\mu}$. Only with such multiple covering can you jump abruptly from one solution to another at the same (T, μ) but different (s, ρ): the *sine qua non* of first-order phase transitions. As one proceeds further to the right in the T-μ plane, one encounters a broader region of unstable black holes immediately above the multiply-covered region. This region is unstable due to a change of sign in $J_{ij}^{s\rho}$, meaning it is the map of $(\phi_0, \Phi_1) \to (s, \rho)$ that is not invertible. This sign change causes black hole instabilities, presumably of the Gregory-Laflamme type [62, 63], but no first-order line. Correspondingly, there are no stable black holes in this region of the phase diagram.[10]

The absence of stable black holes in our model at large μ (roughly, larger than $\mu = 1100\,\mathrm{MeV}$) and T not too big is actually a good thing. It is in approximately this region that one might reasonably expect color superconductivity and/or related phenomena to set in: see for example Figure 7 of [64] and Figure 1 of [89]. Black holes based on the lagrangian 3.1 are not likely to capture such phenomena. However, it is comforting to note that in cases where black hole superconductivity is understood (where the condensate breaks a $U(1)$ gauge symmetry in the bulk), the superconducting instability competes against Gregory-Laflamme instabilities, and one generally must pass beyond minimal supergravity lagrangians to see the superconducting instabilities: see for example [65, 66]. Thus all our findings are at least qualitatively consistent with consensus expectations for the QCD phase diagram.

3.7 Analysis of the Critical Point

Having found the critical point, our final task is to determine its critical exponents. To achieve this, we first construct a large data set which densely populates the critical region. This collection of about 120,000 black holes is generically described by solutions with $\phi_0 \in [4.25, 5.5]$ and $\Phi_1/\Phi_{1,\max} \in [0.35, 0.43]$.

Using these near-critical black holes, we can systematically study the approach of various thermodynamic quantities to criticality. Since the behavior of these quantities is typically expected to be power law in the vicinity of the second order point, it is natural to study them on log-log plots on which critical exponents are trivially related to the slope of the best fit to the data. In practice, we extract this slope by performing a linear regression via a least squares fit. All reported critical exponents in this section have been obtained in this way.

[10] It is interesting to note that $J_{ij}^{s\rho}$ tends to change sign close to $\Phi_1/\Phi_{1,\max} \approx 0.6$ for a fairly wide range of other choices for $f(\phi)$ that we examined numerically.

3.7.1 First-order line and critical density

Despite knowing the location (T_c, μ_c) of the critical point, it remains a challenge to identify the critical density ρ_c.[11] Due to the infinite slope of the curve $\rho(\mu)$ on the critical isotherm, a large number of black holes with very different values of ρ sit very close to the critical point (see the middle plot in figure 3.5).

We can calculate the critical density in the process of determining the exponent β which measures the rate that the discontinuity $\Delta\rho$ across the first-order line goes to zero as the critical point is approached:

$$\Delta\rho \sim (T_c - T)^\beta , \qquad \text{along first order line} . \tag{3.76}$$

In order to determine the discontinuity in ρ for a given $T_f < T_c$, we must identify the μ_f at which the true ground state of the system jumps from the lower branch to the upper branch; this is the μ_f for which the free energy is the same for the two branches. However we have not calculated the free energy, so we cannot identify μ_f in this way. Equivalently, one can use Maxwell's equal-area construction, which states that μ_f should be placed such that the closed regions bounded by the isotherm on either side of the $\mu = \mu_f$ line are of equal area.

We chose a computationally easier procedure which is asymptotically equivalent to the equal-area law as one approaches the critical point. Namely, at a fixed temperature $T = T_f$, we define $\mu_<$ and $\mu_>$ to be the locations of the local minimum and maximum of the isotherm $\rho(\mu)$, and we define μ_f to be the midpoint between them. This in turn determines the mixed-phase densities $\rho_<$ and $\rho_>$ for the point (T_f, μ_f) along the first-order line. This procedure is illustrated in figure 3.6. For points we checked near the critical point, this procedure agrees with the equal-area rule to within a fraction of a percent.

The critical density ρ_c is then most easily obtained as the limit that both $\rho_<$ and $\rho_>$ approach as we near the critical point. The result is

$$\rho_c = 9.9022 . \tag{3.77}$$

[11] Remarks about ρ in this section apply equally well to s.

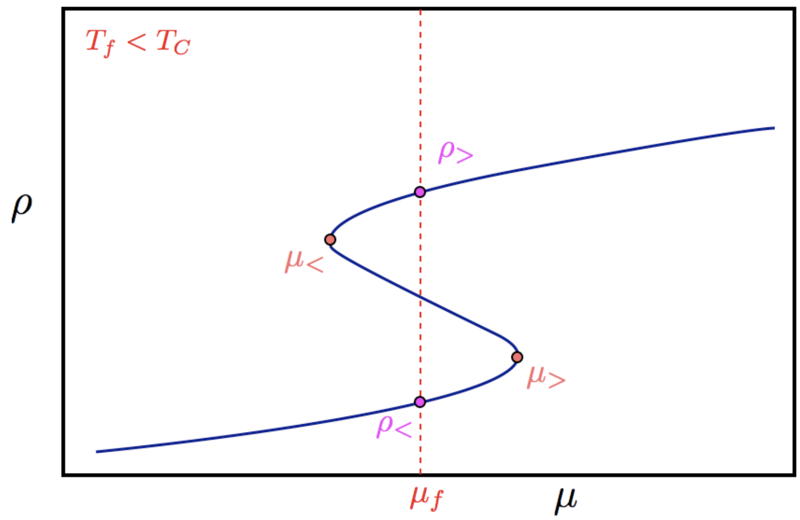

Figure 3.6: Cartoon of $\rho(\mu)$ for an isotherm with $T_f < T_c$, showing multivaluedness near the first-order line. At the location of the line $\mu = \mu_f$ the true minimum of the free energy jumps from the lower to the upper branch and ρ is discontinuous.

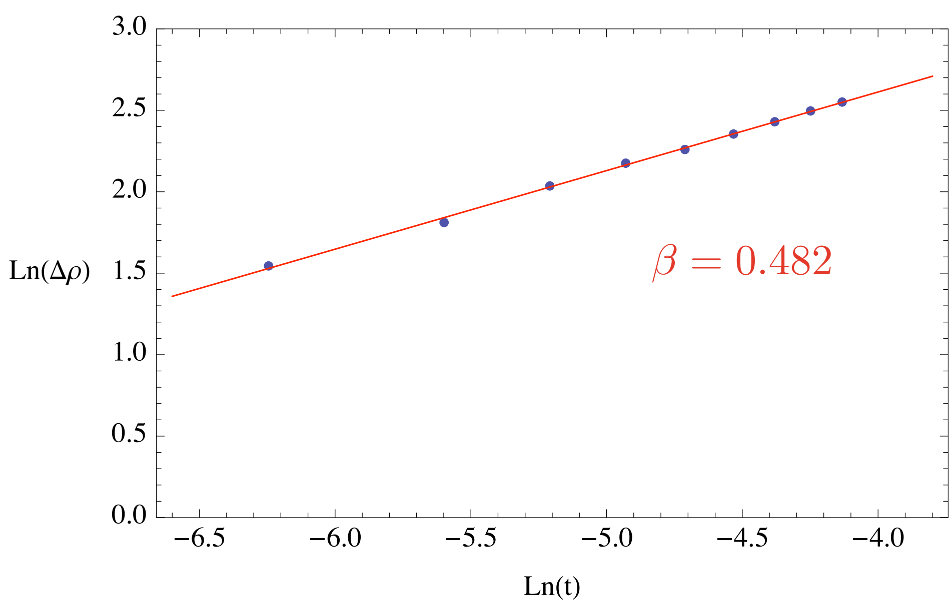

Figure 3.7: The discontinuity in the baryon density as the critical point is approached on a log-log plot. The slope of a best fit line through the data gives us a value $\beta = 0.482$.

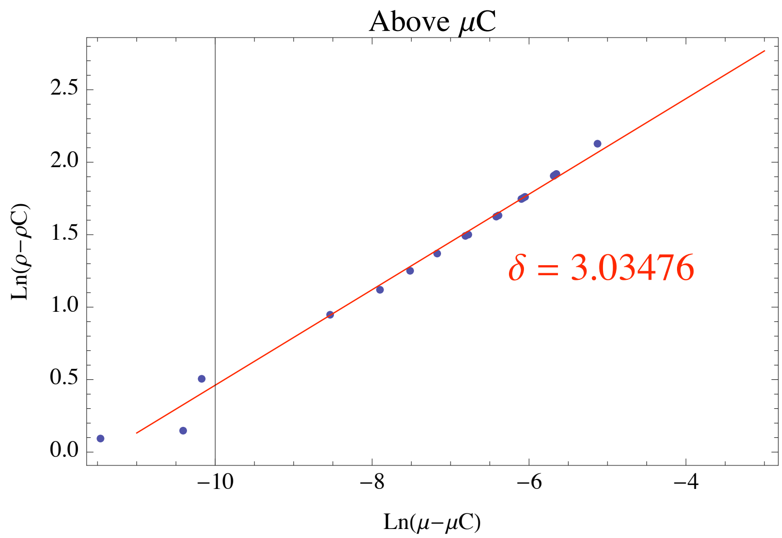

Figure 3.8: The rate at which ρ approaches ρ_c as μ approaches μ_c on the critical isotherm on a log-log plot. The slope gives us a value $\delta = 3.03476$.

Plotting $\Delta\rho \equiv \rho_> - \rho_<$ in a log-log plot with $t \equiv (T - T_c)/T_c$, we obtain

$$\beta \approx 0.482\,. \tag{3.78}$$

In comparison, the exponent in the mean-field case is $\beta_{MF} = 1/2$, and so we have found a result very close to the mean-field value.

3.7.2 Critical isotherm

As discussed in the previous section, the critical isotherm at $T = T_c$ is the curve marking the boundary between single-valued and multi-valued behavior, and correspondingly it has a diverging slope for ρ and s precisely at $\mu = \mu_c$. Using the behavior of ρ on the critical isotherm, we can determine the critical exponent δ, defined as

$$\rho - \rho_c \sim |\mu - \mu_c|^{1/\delta}\,, \qquad \text{for } T = T_c\,. \tag{3.79}$$

Now that we have ρ_c in hand, we plot a number of black holes on a log-log plot near the critical point with $\mu > \mu_c$ in figure 3.8. The points are fit well by a straight line with slope giving $\delta = 3.03476$. We note that the mean field value is $\delta = 3$.

3.7.3 First order axis and susceptibilities

Susceptibilities in general diverge near a critical point. However, it is not required that all possible susceptibilities are divergent. Indeed we find this is the case for α, which is the power law exponent for the specific heat C_ρ along the axis defined by the first order line:

$$C_\rho \sim |T - T_c|^{-\alpha}\,, \qquad \text{along first order axis}\,. \tag{3.80}$$

To avoid the complications of the first-order line itself, we perform this approach from the other side, with $\mu < \mu_c$. A calculational advantage is that the line of constant ρ comes very close to the first order axis [67], so we can simply generate a set of black holes filling out that line, and define C_ρ in terms of finite differences of nearest neighbors.

The result is that C_ρ does not diverge at all along this line, but instead is smooth at values near $C_\rho \approx 10.5$. This corresponds to a vanishing α:

$$\alpha = 0\,. \tag{3.81}$$

In a sense this is the most robust of all our results, since even a weak divergence looks completely different from a lack of divergence; it suggests that the result 3.81 is exact. Moreover, this is again the mean field result; for example in the van der Waals theory of a fluid one has $C_\rho = 3n/2$ with n the number density.[12]

Although we find C_ρ to have no divergence, other quantities do show the expected divergences. The final thermodynamic exponent, γ, is defined by the approach of χ_2 along the same axis,

$$\chi_2 \sim |T - T_c|^{-\gamma}\,, \qquad \text{along first order axis}\,. \tag{3.82}$$

This exponent is the most difficult to calculate. The quantity involves a derivative in the μ-direction, so to calculate the finite difference we must obtain pairs of points with the same T to within a very small tolerance ΔT, which are separated by a larger but still small amount $\Delta\mu$; we then need a sequence of pairs of such points moving along the first-order axis, a direction unrelated to the

[12] Certain systems contain a discontinuity or logarithmic divergence for C_ρ, and are also grouped as $\alpha = 0$; ours is truly smooth, as with the van der Waals field.

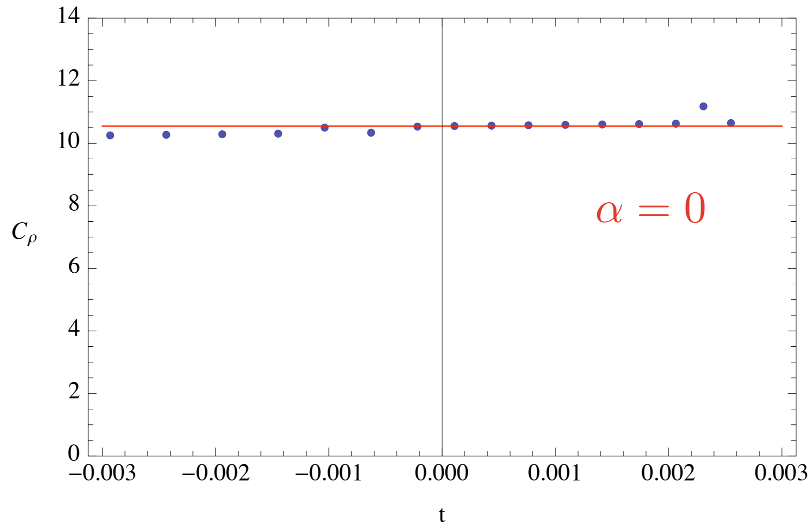

Figure 3.9: The specific heat C_ρ near the critical point along a line of constant ρ, along the first-order axis. There is no divergence, giving $\alpha = 0$.

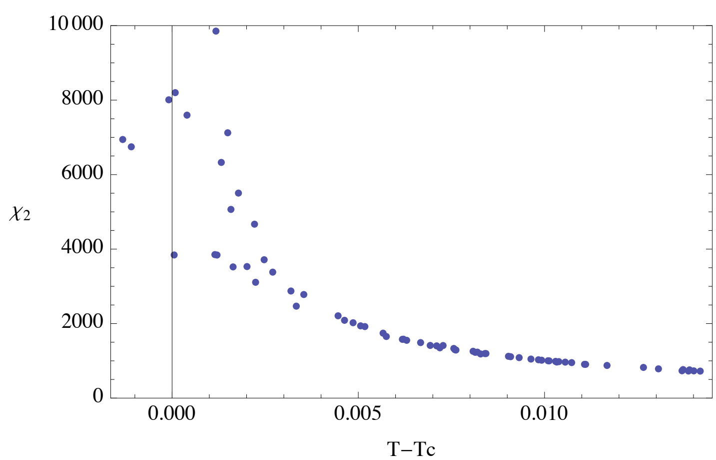

Figure 3.10: The susceptibility χ_2 near the critical point along a line of constant ρ.

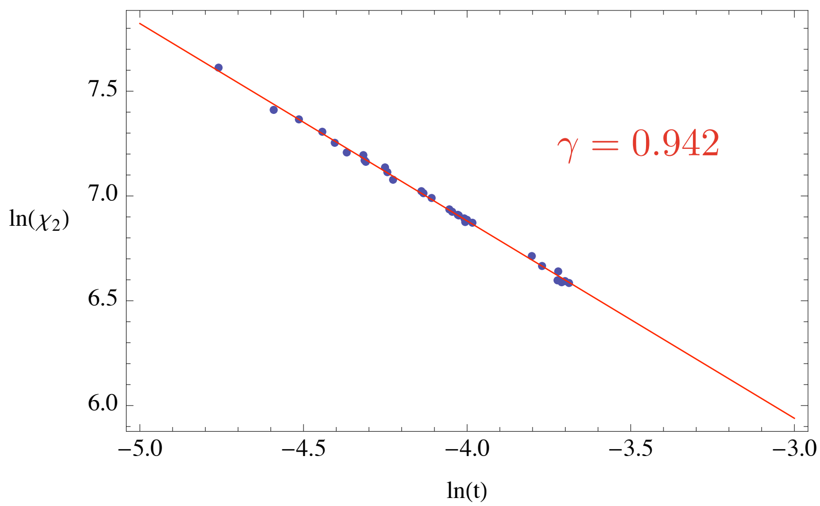

Figure 3.11: The baryon susceptibility χ_2 compared to $t \equiv (T - T_c)/T_c$ as the critical point is approached on a log-log plot. The slope gives us a value $\gamma = 0.942$.

derivative. To find black holes near the axis, we again imposed constant ρ. We then looked for pairs of points with $\Delta\mu < 0.001$ and kept those with $\Delta T/\Delta\mu < 0.002$.

The result is shown in figure 3.10. The black holes for $T - T_c > 0.004$ form a smooth, single-valued curve, but near the critical point numerical errors grow larger and the curve is no longer single-valued. Fitting just the single-valued region, we produce the log-log plot in figure 3.11. The resulting exponent is $\gamma = 0.942$, while the mean field value of γ is $\gamma_{MF} = 1$. Once again our result is consistent with mean field.

3.7.4 Summary and Scaling

In conclusion, we have measured the critical exponents α, β, γ and δ and found them to be consistent with the mean field values. Since the mean field values are themselves consistent with scaling 3.26, it is clear that our results pass this self-consistency check as well.

As an idea of the size of the errors in our measurements, we can choose two exponents, use the scaling laws 3.26 to calculate predictions for the other two, and compare these predictions to our actual results. It is natural to use $\alpha = 0$ as an input, since we obtain it as an apparently exact result. Also inputting $\delta = 3.035$ gives us the results:

Exponent	α	β	γ	δ
Calculated value	0	0.482	0.942	3.035
Scaling prediction from α & δ	0	0.496	1.009	3.035
% Diff.	—	3%	7%	—

Thus our deviations from scaling are in the $3\% - 7\%$ range, giving an idea of the size of the errors in our method.

3.7.5 Other models

We also carried through an analysis of the model with the same potential 3.4 and the gauge kinetic function

$$f(\phi) = e^{-\phi} . \tag{3.83}$$

The phase diagram obtained from this model shares all relevant properties to the one presented here: a first-order line ending in a critical point, and critical exponents consistent with mean field. We omit the details since they are virtually identical to those just discussed. This exponential model has substantially poorer fit to lattice data at $\mu = 0$.

3.8 Discussion

A number of techniques have been employed to predict the location of the QCD critical point. These include lattice calculations that attempt to circumvent the problems of finite μ by a number of different means, including taking a Taylor series expansion around $\mu = 0$, reweighting the contributions to the path integral, or analytically continuing from imaginary chemical potential. There are also calculations in a variety of Nambu–Jona-Lasinio models, along with a number of other methods.

In figure 3.12, we show the location of a number of different calculations of the location of the critical point, along with our result, presented as BH^{10}. A key to the various abbreviations and references is given in the table; for more information see [64, 68]. The variation in prior results is considerable, and our result lies within the parameter space defined by the others. Also included in this plot is an estimate for the chemical freeze-out line [89].

Label	Method	Reference
HB	Hadronic Bootstrap	[69]
LTE	Lattice Taylor Expansion	[70]
LR	Lattice Reweighting	[90], [72]
RM	Random Matrix	[73]
NJL	Nambu–Jona-Lasinio	[93],[94],[95]
CJT	Effective Potential	[77]
LSM	Linear Sigma Model	[94]
CO	Composite Operator	[78], [79]

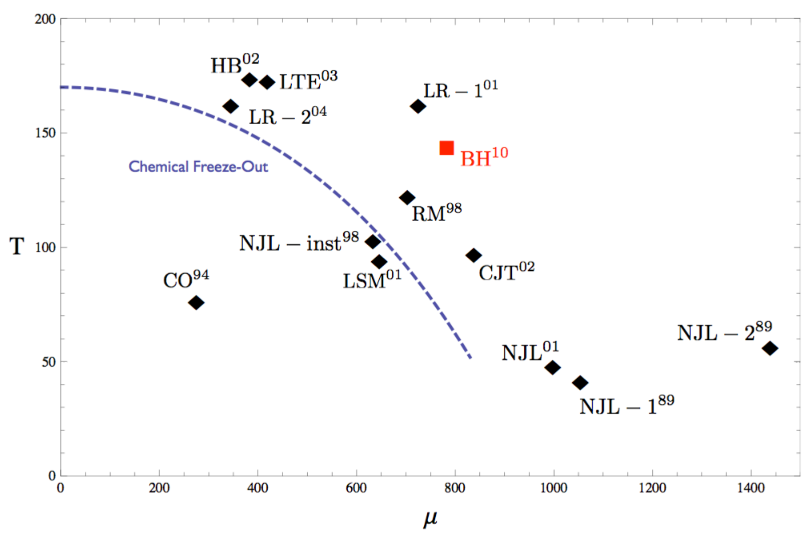

Figure 3.12: Our result for the location of the critical point (BH^{10}) compared to other calculations in the literature, along with the chemical freeze-out curve.

In general, as heavy ion collisions gain center-of-mass energy, the produced medium is characterized by higher T and lower μ. This leads to several issues with the possibility of exploring the region near our prediction, where μ is relatively large. First, assuming the heavy ion collisions attain thermodynamic equilibrium, the value of T that can be reached may be too small by the time one has reached sufficiently large μ. Moreover, at some large μ the center-of-mass energy will become too low to actually thermalize the colliding ions, making a thermodynamic interpretation no longer appropriate. Collisions at RHIC have a minimum energy of 5-7 GeV [89], too high to reach our value of μ_c; LHC is even worse. A more promising possibility is the CBM experiment at the future accelerator center FAIR at GSI, a fixed-target experiment whose intended region of exploration includes the location of our critical point [44].

That said, as we have emphasized our result should be regarded primarily as a proof of principle: it is possible to extract QCD-like phase diagrams from relatively simple holographic duals. This result has substantial promise, precisely because finite chemical potential calculations are so difficult on the lattice; in gravity duals, finite chemical potential simply involves introducing a new field, and possesses no additional qualitative complexity. Of course holographic duals introduce other complications—large N and the fact that they are not precisely QCD, only QCD-like—that must in turn be dealt with.

We have discovered a first-order line and a critical endpoint with mean-field critical exponents. A number of ways to generalize these results are evident. Most obviously, one can study the fluctuations around our classical backgrounds, thereby learning about spectra, transport and the true free energy function. An equally obvious, though potentially difficult, further step is to add $1/N$ corrections to the geometries, hopefully moving the critical point away from mean field. One can also consider studying a larger theory. In particular, the introduction of chiral symmetry in addition to baryon number is straightforward in principle, if more intricate in practice. By enlarging the theory one could also hope to study the color superconducting phases at large μ. We hope to examine these issues in the future.

Chapter 4

Dynamic critical phenomena at a holographic critical point

4.1 Overview

It is interesting to move beyond static phenomena, and to study dynamics. Time-dependent critical behavior includes transport properties, relaxation times and the response to time-dependent perturbations, all necessary for the understanding of a heavy ion collision evolving near the critical point. There are three relevant transport coefficients: the shear and bulk viscosities associated to the traceless and trace perturbations of the energy-momentum tensor, $\bar{\eta}$ and ζ respectively,[1] and the conductivity λ of the $U(1)$ baryon density. The ratio of shear viscosity to entropy density is known to be universal $\bar{\eta}/s = 1/4\pi$ in all two-derivative gravity models [84, 85], but λ and ζ are expected to depend nontrivially on the location in the phase diagram. Moreover, the dynamic critical exponent z controls the phenomenon of critical slowing down, where the equilibration time τ grows with the correlation length ξ as $\tau \sim \xi^z$; this behavior is expected to determine how close to criticality a heavy ion collision can approach in the limited time available before freeze-out and hadronization, as $\xi < (\text{time})^{1/z}$ [100, 101].

Static critical phenomena are sorted into universality classes by properties such as their dimensionality and symmetry of the order parameter. This concept was extended to dynamic critical phenomena by Hohenberg and Halperin [102], who classified various universal "models" based on their conserved quantities, which manifest as hydrodynamic modes, and the Poisson brackets between them and with the order parameter; dynamic universality classes are then determined by

[1] In keeping with the literature, we denote the shear viscosity $\bar{\eta}$ to avoid confusion with the critical exponent η.

these models as well as the static class. Son and Stephanov argued that in QCD, only one combination of the baryon density and the chiral condensate survives as a hydrodynamic mode, and thus having this single conserved mode as well as conserved energy-momentum, the theory should fit into dynamic model H [103].

The response of a fluid to charge inhomogeneities is controlled by the diffusion constant D, associated to the dispersion relation $\omega = -iDk^2$. The diffusion constant is related to the conductivity λ and the charge susceptibility χ by

$$D = \frac{\lambda}{\chi}\,, \tag{4.1}$$

and at a critical point, D tends to zero while χ diverges. The behavior of λ near the critical point, however, depends on the dynamic universality class. Hydrodynamic models neglecting nonlinear interactions predict that λ remains finite at criticality; this is characteristic of Hohenberg and Halperin's model B, where the single hydrodynamic mode is taken to be a conserved density. The only kind of conduction possible in such a model is via diffusion. Model B predicts the dynamic critical exponent

$$z = 4 - \eta\,, \tag{4.2}$$

where η is the usual static exponent giving the anomalous dimension of the density two-point function. In model H, on the other hand, the inclusion of energy and momentum as hydrodynamic modes makes convective conductivity possible, and this new channel naively dominates. In model H, the conductivity λ and shear viscosity $\bar{\eta}$ diverge at the critical point,

$$\lambda \sim |T - T_c|^{x_\lambda}\,, \qquad \bar{\eta} \sim |T - T_c|^{x_\eta}\,, \tag{4.3}$$

with exponents x_λ and x_η which are related to the static exponent η by

$$x_\lambda + x_\eta = 4 - d - \eta\,, \tag{4.4}$$

where d is the spatial dimensionality. In the 3D Ising model η and x_η are close to zero, giving x_λ close to one [103]. The critical exponent z when convection dominates takes the value

$$z = 4 - \eta - x_\lambda\,, \tag{4.5}$$

and is thus moved from $z \approx 4$ in model B to $z \approx 3$ in model H. Note that even in models where λ diverges, χ always diverges faster, so D still goes to zero [102].

The expected behavior of bulk viscosity near the liquid-gas critical point was investigated by Onuki [104], who predicted a divergence also depending on z,

$$\zeta \sim |T - T_c|^{-z\nu+\alpha} \tag{4.6}$$

where $\nu > 0$ and α are static exponents; for several other predictions for bulk viscosity at a critical point, see for example [105].

Work has been done applying the AdS/CFT correspondence to dynamic critical phenomena in various models. Bulk viscosity for the models we consider has been computed at vanishing chemical potential in [46, 97]. Maeda, Natsuume and Okamura calculated the conductivity in the "one-charge black hole" model dual to $\mathcal{N} = 4$ Super-Yang Mills with a chemical potential—hereafter the one-charge $\mathcal{N} = 4$ black hole—and found it to stay finite at the critical point, identifying the result with model B despite the presence of conserved energy and momentum [106]. The natural speculation is that the nonlinear interactions responsible for the convective component in the conductivity in model H are suppressed by the large number of colors N_c, and in [107] Natsuume and Okamura argued that large-N_c counting indeed enhances the diffusive over the convective conductivity, reducing model H to an effective model B. Meanwhile, the bulk viscosity was studied in a mass deformation of the one-charge $\mathcal{N} = 4$ black hole by Buchel [108] and in the $\mathcal{N} = 2^*$ model by Buchel and Pagnutti [109, 11]. In both cases the bulk viscosity was also found to be finite at the critical point, in contradiction with expectations from (4.6). It is natural to speculate that again the large-N_c limit suppresses the divergence in the transport coefficient. The dynamic critical exponent z has also been studied directly, yielding the mean-field model B value $z = 4$ for the deformed one-charge black hole [108] and $z = 0$ for $\mathcal{N} = 2^*$ [110].

Dynamic universality classes depend not just on the conserved quantities and their Poisson brackets, but also on the static universality class. The work described in the previous paragraph shares the list of conserved quantities with QCD, but differs in the static critical exponents. It is natural to wish to extend the study of holographic dynamic critical phenomena to a model that shares the static universality class with QCD as well. In this chapter, we begin the investigation of the dynamic critical phenomena in the QCD-like holographic critical point of [96], by studying finite-ω fluctuations around those black hole backgrounds. With these fluctuations, we are able to calculate the transport coefficients ζ and λ, and the associated diffusion D.

In keeping with the other AdS/CFT cases, we find the transport coefficients remain finite at the critical point, and the diffusion constant goes to zero. Thus these models share the apparent suppression of the convective contribution to transport by the large-N_c limit [107], and behave effectively as model B.

Furthermore, the behavior of λ and ζ as functions of T and μ near the critical point is quite similar to that of the entropy and baryon densities s and ρ: all are smooth approaching the critical point in the T-μ plane along the axis defined by the first-order line, but develop infinite slope when approaching off-axis. Similar behavior arises in the one-charge $\mathcal{N} = 4$ black hole, where the critical exponent controlling all these divergent slopes is the same,

$$\lambda - \lambda_c \sim s - s_c \sim \rho - \rho_c \sim |T - T_c|^{1/\delta} \,, \tag{4.7}$$

with $\delta = 2$; the corresponding exponent in the QCD-like case, $\delta \approx 3$, is consistent with our results for $\lambda - \lambda_c$ and $\zeta - \zeta_c$. This suggests that in the vicinity of the critical point, the deviations of the conductivity and bulk viscosity from their critical values can be thought of as depending smoothly on the deviations of the densities from theirs.

From these results we can estimate the dynamic critical exponent z assuming a mean-field value of η; a precise determination of z and η requires finite-k fluctuations, which we leave for future work. Given the model B behavior and the mean field exponents, using the mean field value $\eta = 0$ in 4.2, we can estimate

$$z \approx 4 \,. \tag{4.8}$$

Another feature of the behavior of the transport coefficients in the phase diagram is worth pointing out. In [96] and [45], the potential and gauge kinetic function in the Lagrangian were only constrained to lattice QCD results over certain ranges of temperature, corresponding to certain values of the scalar field. In principle, one could imagine modifying these functions such that the matched region is not affected, while results change elsewhere; thus the application of these models to QCD should only be trusted in a certain band of temperatures. This is not unreasonable, since the gravity dual picture is only expected to apply in a certain range near the critical temperature where there is no quasiparticle description.

However, phenomena outside the region designed to match QCD may be interesting in their own right. We find that as the temperature decreases, both the bulk viscosity and conductivity begin to rise. In fact, the bulk viscosity has a divergence at a temperature around half the crossover temperature on the T-axis, outside the region matched to QCD, and this divergence extends out into the plane. Unlike the phenomena at the critical point, this divergence in the transport coefficient is not associated with any feature in the thermodynamics of ρ or s. From the gravity point of view, it can be understood as the place where the fluctuation solutions develop a node, but the field theory interpretation is unclear. Whether the conductivity also has a pole at a still lower temperature is outside the range accessible to our numerical solutions. We note that a similar divergence appears for the conductivity of the thermodynamically unstable branch of the one-charge black hole, as the "superstar" limit [111] is approached.

The summary of the remainder of the chapter is as follows. In section 4.2 we discuss the Lagrangian, equations of motion and gauge symmetries of our class of models, and construct the gauge-invariant fluctuations around the black hole backgrounds. The fluctuation equations and the Kubo formulae for extracting the transport coefficients are presented in section 4.3. In section 4.4, we review the one-charge $\mathcal{N} = 4$ black hole solutions and solve for the conductivity both analytically and numerically, checking our method and pointing out several features that will have analogs in the QCD-like black holes; the analytic calculation was previously worked out in [106, 112]. In section 4.5, we present the calculations of the transport coefficients for the QCD-like black holes. We conclude in section 4.6. Results for the conductivity and diffusion of another model, the two-charge $\mathcal{N} = 4$ black hole, are given in the appendix.

4.2 Black hole backgrounds

In this section we review the five-dimensional gravity ansatz that applies both to the QCD-like holographic critical models of [96] and the one-charge $\mathcal{N} = 4$ black hole, present the resulting equations of motion and symmetries, and construct the gauge-invariant fluctuations around these backgrounds with nonzero frequency.

4.2.1 Lagrangian and ansatz

We consider five-dimensional gravitational theories containing a metric $g_{\mu\nu}$, a vector field A_μ and a scalar ϕ, with Lagrangian (3.1). The relevant solutions to these theories are asymptotically AdS black three-brane solutions with radial profiles for the electric potential and scalar field,

$$\begin{aligned} ds^2 &= e^{2A(r)}(-h(r)dt^2 + d\vec{x}^2) + \frac{e^{2B(r)}}{h(r)}dr^2 \,, \\ A_\mu dx^\mu &= \Phi(r)\, dt \,, \qquad \phi = \phi(r) \,, \end{aligned} \tag{4.9}$$

and the equations of motion resulting from this ansatz are presented in (3.27). Asymptotically AdS solutions may be written in coordinates that as $r \to \infty$ approach

$$\begin{aligned} ds^2 &\to e^{2r/L}\left(-dt^2 + d\vec{x}^2\right) + dr^2 \,, \\ \Phi(r) &= \Phi_{(0)} + \Phi_{(2)} e^{-2r/L} + \dots \,, \\ \phi(r) &= \phi_{(4-\Delta)} e^{(\Delta-4)r/L} + \dots + \phi_{(\Delta)} e^{-\Delta r/L} + \dots \,. \end{aligned} \tag{4.10}$$

Black brane backgrounds have a horizon $r = r_H$ defined by the largest solution to the vanishing of the horizon function $h(r_H) \equiv 0$. The temperature T and entropy density s can be calculated as

$$T = \frac{1}{4\pi} h'(r_H) e^{A(r_H) - B(r_H)} \,, \qquad s = \frac{2\pi}{\kappa^2} e^{3A(r_H)} \,, \tag{4.11}$$

while the chemical potential μ and $U(1)$ density ρ can be read off from the near-boundary expansion of $\Phi(r)$,

$$\mu = \frac{\Phi_{(0)}}{L} \,, \qquad \rho = -\frac{\Phi_{(2)}}{\kappa^2} \,. \tag{4.12}$$

4.2.2 Gauge symmetries

The gauge symmetries of the theory are $U(1)$ gauge transformations of the vector field given by $\lambda(x)$, and general coordinate transformations given by $\epsilon^\mu(x)$, with the general transformation of the fields

$$\begin{aligned} \delta A_\mu &= \partial_\mu \lambda + \epsilon^\nu \partial_\nu A_\mu + (\partial_\mu \epsilon^\nu) A_\nu \,, \\ \delta g_{\mu\nu} &= \epsilon^\rho \partial_\rho g_{\mu\nu} + (\partial_\mu \epsilon^\rho) g_{\rho\nu} + (\partial_\nu \epsilon^\rho) g_{\mu\rho} \,, \\ \delta\phi &= \epsilon^\mu \partial_\mu \phi \,. \end{aligned} \tag{4.13}$$

To stay consistent with the ansatz 4.9, one may still make transformations with a general $\epsilon^r(r)$ as well as $\epsilon^0(t)$, $\epsilon^i(\vec{x})$ and $\lambda(t)$ obeying

$$\partial_t \epsilon^0(t) = \text{const}\,, \qquad \partial_i \epsilon_j(\vec{x}) + \partial_j \epsilon_i(\vec{x}) = \text{const} \times \delta_{ij}\,, \qquad \partial_t \lambda(t) = \text{const}\,. \tag{4.14}$$

One may use $\epsilon^r(r)$ to choose the metric function $B(r)$ arbitrarily. In the gauge $B(r) = 0$, which we use for the QCD-like holographic critical black holes, the remaining coordinate transformations 4.14 may be used to set any two of the zero point of $A(r)$ and the overall scales of $h(r)$ and $\Phi(r)$:

$$(r, x^i, t) = \left(\gamma \tilde{r}, \beta \tilde{x}^i, \frac{\beta}{\gamma}\tilde{t}\right) \quad \rightarrow \quad \tilde{h} = \frac{1}{\gamma^2} h\,, \quad \tilde{A} = A + \log\beta\,, \quad \tilde{\Phi} = \frac{\beta}{\gamma}\Phi\,, \tag{4.15}$$

while the gauge transformation λ can fix the zero point of $\Phi(r)$. The remaining transformations are constant shifts of all variables (of which shifts of t and x^i are trivial, while shifts of r will change the form of the various functions), and the manifest $SO(3)$ symmetry acting on x^i.

4.2.3 Fluctuations and gauge invariant quantities

We are interested in studying small fluctuations around the background 4.9 of the form

$$\begin{aligned} ds^2 &= \left[g^0_{\mu\nu} + \Re\{e^{2A(r)} e^{-i\omega t} h_{\mu\nu}(r)\}\right] dx^\mu dx^\nu \,, \\ A_\mu dx^\mu &= \Phi(r)\, dt + \Re\{e^{-i\omega t} a_\mu(r)\} dx^\mu \,, \qquad \phi = \phi(r) + \Re\{e^{-i\omega t}\tilde{\phi}(r)\}\,, \end{aligned} \tag{4.16}$$

where $g^0_{\mu\nu}$ is the background metric, and we have assumed plane-wave dependence in the time direction. This ansatz preserves the $SO(3)$ rotating the spatial directions together. From here on, we will omit the instruction to take the real part and work directly with complexified perturbations, on the understanding that appropriate superpositions of complexified perturbations will be real.

Certain combinations of the fluctuations will be gauge degrees of freedom. These correspond to gauge transformations at linear order in the small parameter associated to the fluctuations; gauge transformations at zeroth order act on the background. Gauge transformations preserving the ansatz 4.16 for the time dependence of the fluctuations also take a plane wave form,

$$\epsilon^\mu(t,\vec{x},r) = e^{-i\omega t}\xi^\mu(r)\,, \qquad \lambda(t,\vec{x},r) = e^{-i\omega t}\eta(r)\,. \tag{4.17}$$

We can then calculate the transformation of the fluctuations $h_{\mu\nu}$, a_μ, $\tilde{\phi}$ under the gauge transformations. Here we record only the results for modes with no index in the r-direction; all independent fluctuating modes come from this set of fields. For the metric we have,

$$\begin{aligned} \delta h_{tt} &= -(h' + 2A'h)\xi^r + 2i\omega h\xi^0\,, \\ \delta h_{ti} &= -i\omega\delta_{ij}\xi^j\,, \\ \delta h_{ij} &= 2A'\xi^r\delta_{ij}\,, \end{aligned} \tag{4.18}$$

for the gauge field,

$$\begin{aligned} \delta a_t &= -i\omega\eta + \xi^r\Phi' - i\omega\Phi\xi^0\,, \\ \delta a_i &= 0\,, \end{aligned} \tag{4.19}$$

and for the scalar,

$$\delta\tilde{\phi} = \xi^r\phi'\,. \tag{4.20}$$

We would like to construct gauge-invariant combinations corresponding to the fluctuating modes of the theory. We expect a total of nine such fluctuations: five modes from the graviton, three from the gauge field and one from the scalar. We immediately see eight such gauge invariant combinations: the three a_i, and the five traceless components of h_{ij}. The trace of the spatial part of the graviton transforms as

$$\delta\left(\frac{1}{3}\left(h_{xx} + h_{yy} + h_{zz}\right)\right) = 2A'\xi^r\,, \tag{4.21}$$

and so we can construct the ninth gauge invariant mode involving the scalar fluctuation,

$$\mathcal{S} \equiv \tilde{\phi} - \frac{\phi'}{2A'}\frac{1}{3}\left(h_{xx} + h_{yy} + h_{zz}\right) \,. \tag{4.22}$$

Thus the nontrivial profile for the background scalar field $\phi = \phi(r)$ couples the scalar fluctuations to fluctuations of the graviton trace; in the AdS limit, this reduces to just the scalar fluctuation $\mathcal{S} \to \tilde{\phi}$ and the graviton trace becomes a pure gauge mode. For a nonzero scalar profile, this is the AdS/CFT encoding of the running coupling that breaks scale invariance producing a nonzero trace of the energy-momentum tensor.

While $\mathcal{S}$ is a natural definition for the fluctuation since it has a smooth AdS limit and shares its possible asymptotic behaviors with ϕ, it will be useful for us to consider the rescaled mode

$$\begin{aligned} \mathcal{H} &\equiv -\frac{2A'}{\phi'}\mathcal{S} \\ &= \frac{1}{3}(h_{xx} + h_{yy} + h_{zz}) - \frac{2A'}{\phi'}\tilde{\phi}\,. \end{aligned} \tag{4.23}$$

This normalization is the natural one for thinking of the mode as the graviton trace; for $\phi' \neq 0$ one may pick a gauge where $\tilde{\phi} = 0$, where $\mathcal{H}$ is the trace precisely.

We see the fields organize themselves under $SO(3)$ as a singlet (the scalar $\mathcal{S}$ or $\mathcal{H}$), a triplet (the gauge field a_i) and a quintuplet (the traceless graviton h_{ij}), and since they are in different representations they cannot mix at the linearized level. Thus we expect each of these modes to satisfy a decoupled fluctuation equation. Note this would not hold for a nonzero spatial momentum; instead, a smaller $SO(2)$ symmetry group would organize the perturbations.

4.3 Fluctuation equations and transport coefficients

The fluctuation equations of the nine modes $\mathcal{H}$, a_i and h_{ij} can be obtained by linearizing the Einstein, Maxwell and Klein-Gordon equations around the background 4.9. In general, the various equations that result will also contain the auxiliary quantities a_r, $h_{\mu r}$. By taking linear combinations of the Einstein and Maxwell equations, these can be eliminated, giving us nine differential equations in nine unknowns.

The coefficients of the fluctuation equations include the background fields A, B, h, Φ and ϕ and their derivatives. These fields obey the background equations of motion, which act as constraints on these coefficients. To exhaust the constraints, we use the various background equations 3.27 to eliminate the second derivatives A'', Φ'', h'' and ϕ''; in addition, the zero-energy constraint 3.32 can be used to eliminate the potential $V(\phi)$, although derivatives of the potential will still appear. In this way we achieve a unique presentation for each coefficient with no hidden constraints.

Each fluctuation equation can be used to calculate a transport coefficient via a Kubo formula. These are associated to the imaginary part of the corresponding Green's function, which comes from the "conserved flux" $\mathcal{F}$ for each equation. For a differential equation of the form

$$y''(r) + p(r)y'(r) + q(r)y(r) = 0\,, \tag{4.24}$$

Abel's identity guarantees that for two solutions $y_1(r)$, $y_2(r)$, the quantity

$$\mathcal{F} \equiv \exp\Big(\int p(r)dr\Big)\, W(y_1, y_2)\,, \tag{4.25}$$

is independent of r, where $W(y_1, y_2) \equiv y_1 y_2' - y_2 y_1'$ is the Wronskian of the two solutions. As long as $p(r)$, $q(r)$ are real, for some complex solution $y(r)$ its conjugate $y^*(r)$ is also a solution. Taking $y_1 = y$ and $y_2 = y^*$, our expression for the conserved flux becomes

$$\mathcal{F} \equiv \exp\Big(\int p(r)dr\Big)\, \mathrm{Im}\,(y^* y')\,, \tag{4.26}$$

up to an overall factor.

4.3.1 Near-horizon behavior and boundary conditions

Noting that h has a zero at the horizon, $h = h'(r_H)(r - r_H) + \ldots$, while A and its derivatives are regular there, all the fluctuation equations considered in this chapter have the same limit near the horizon,

$$X'' + \frac{1}{r - r_H} X' + \frac{\omega^2 e^{2B(r_H) - 2A(r_H)}}{h'(r_H)^2 (r - r_H)^2} X = 0\,, \tag{4.27}$$

where X is any of Z, a, $\mathcal{S}$ or $\mathcal{H}$ (see the following subsections), and we have assumed that the gauge degree of freedom B is chosen so it and its derivatives do not diverge at the horizon. Near the horizon, one may expand

$$X(r) = (r - r_H)^\alpha (x_0 + x_1(r - r_H) + \ldots)\,, \tag{4.28}$$

where we must choose the exponent α to be

$$\alpha = \pm i\omega \frac{e^{B(r_H) - A(r_H)}}{h'(r_H)}\,. \tag{4.29}$$

In solving the fluctuation equations we must impose two boundary conditions. The first is the requirement of infalling boundary conditions at the horizon: this corresponds to solving for retarded Green's functions, in accord with the usual prescription for calculating transport coefficients. This simply involves imposing that only the negative sign solution in 4.29 contributes.

The second boundary condition must be imposed not at the horizon, but at the boundary. Each mode has two solutions near the boundary, one falling off more quickly and corresponding to a VEV deformation of the dual field theory, and the other falling off more slowly and corresponding to turning on a source. Our prescription will be to normalize the coefficient of the "source" mode to unity.

Assuming we have imposed infalling boundary conditions, a part of the conserved flux 4.26 simplifies,

$$h\,\mathrm{Im}(X^* X') = -\omega |x_0|^2 e^{B(r_H) - A(r_H)}\,, \tag{4.30}$$

where we used the fact that α is pure imaginary. One can evaluate the conserved flux at any r, but since one boundary condition is at the horizon and the other at the boundary, one must in general solve for the mode everywhere in order to do so. As we shall see, in some cases it is possible to do this analytically in the $\omega \to 0$ limit; in general, we shall solve the fluctuation equations numerically.

4.3.2 Traceless graviton and shear viscosity

This case is well-known, and the outcome, $\bar{\eta}/s = 1/4\pi$, is guaranteed by the general arguments of [84, 85]. However, it is useful to go through an explicit calculation as a warmup for the more difficult conductivity and bulk viscosity cases, to be treated next.

Letting Z be any of the traceless h_{ij}, the corresponding fluctuation equation is the massless scalar equation,

$$Z'' + \left(4A' - B' + \frac{h'}{h}\right) Z' + \frac{e^{2B-2A}}{h^2}\,\omega^2 Z = 0\,. \tag{4.31}$$

The behavior of Z near the boundary is

$$Z = Z_{(0)} + \ldots + Z_{(4)} e^{-4r/L} + \ldots\,, \tag{4.32}$$

and so the proper boundary condition is simply to take $Z_{(0)} = 1$. The associated conserved flux from Abel's identity is

$$\mathcal{F}_Z = h e^{4A-B}\,\mathrm{Im}\,(Z^* Z')\,, \tag{4.33}$$

and the Kubo formula for the corresponding transport coefficient, the shear viscosity, is

$$\bar{\eta} = -\frac{1}{2\kappa^2} \lim_{\omega \to 0} \frac{1}{\omega} \mathcal{F}_Z\,. \tag{4.34}$$

The simplicity of the equation 4.31 in the $\omega \to 0$ limit allows one to solve for the shear viscosity analytically; we take our discussion from [97]. In the $\omega \to 0$ limit the term with no derivatives vanishes, and we are left with

$$\partial_r(\log Z') = -\partial_r(4A - B + \log h)\,, \tag{4.35}$$

which has the solution

$$Z = a_0 + b_0 \int_r^\infty dr\, \frac{e^{-4A+B}}{h}\,. \tag{4.36}$$

The second term is technically not allowed at strict $\omega = 0$ due to a logarithmic divergence; it may be kept for very small ω, but for us it is enough to note that matching to the near-horizon expansion

$$Z(r) \approx z_0 (r - r_H)^\alpha = z_0(1 + \alpha \log(r - r_H) + \ldots)\,, \tag{4.37}$$

we have $z_0 = a_0$; however as $r \to \infty$ we see $a_0 = Z_{(0)}$. Thus the boundary condition $Z_{(0)} = 1$ imposes $z_0 = 1$ near the horizon. Using 4.30 and 4.33, one can then evaluate $\bar{\eta}$ at the horizon,

$$\bar{\eta} = \frac{1}{2\kappa^2} e^{3A(r_H)}\,, \tag{4.38}$$

which using 4.11 implies for the shear viscosity to entropy density ratio the familiar universal result,

$$\frac{\bar{\eta}}{s} = \frac{1}{4\pi}\,. \tag{4.39}$$

The other transport coefficients we consider will not be universal in this way; from a practical standpoint, imposing the boundary condition at infinity will not impose a universal constraint on the near-horizon behavior. A similar technique to the one reviewed here will, however, be useful in calculating the conductivity of the one-charge $\mathcal{N} = 4$ black hole of the next section.

4.3.3 Gauge field, conductivity and diffusion

Because of $SO(3)$ symmetry, we can treat each of the fluctuations a_i separately: they cannot mix at linear order. For notational simplicity, we will drop the index i altogether and use a to denote one of the components of a_i: for example, $a = a_1$ to compute the conductivity in the x^1 direction. The fluctuation equation is

$$a'' + \left(2A' - B' + \frac{h'}{h} + \frac{\phi' f'(\phi)}{f}\right) a' + \frac{e^{-2A}}{h}\left(\frac{e^{2B}}{h}\,\omega^2 - \, f(\phi)\Phi'^2\right) a = 0\,, \tag{4.40}$$

and the associated conserved flux is

$$\mathcal{F}_a = h f(\phi) e^{2A-B}\,\mathrm{Im}\,(a^* a')\,. \tag{4.41}$$

Near the boundary the gauge field fluctuation behaves as

$$a = a_{(0)} + a_{(2)} e^{-2r/L} + \ldots\,, \tag{4.42}$$

so the appropriate boundary condition is simply $a_{(0)} = 1$. The Kubo formula for this mode determines the (zero-frequency) conductivity λ,

$$\lambda = -\frac{L^2}{2\kappa^2} \lim_{\omega\to 0} \frac{1}{\omega} \mathcal{F}_a\,. \tag{4.43}$$

This quantity is related to the frequency-dependent complex conductivity, defined as

$$\sigma \equiv -\frac{i}{\omega}\frac{L}{\kappa^2}\frac{a_{(2)}}{a_{(0)}}\,. \tag{4.44}$$

by

$$\lambda = \lim_{\omega\to 0} \Re\sigma(\omega) \tag{4.45}$$

which follows from 4.41 and 4.44 using the boundary condition. The diffusion constant D is related to the conductivity by

$$\lambda = D\chi\,, \tag{4.46}$$

where the susceptibility is

$$\chi \equiv \left(\frac{\partial\rho}{\partial\mu}\right)_T\,, \tag{4.47}$$

leading to the the Nernst-Einstein relation,

$$D\chi = \lim_{\omega\to 0} \Re\sigma(\omega)\,. \tag{4.48}$$

Unlike the shear viscosity, the conductivity does not take a universal value; notice that the equation 4.40 still has a zero-derivative term at $\omega = 0$. For the example of the next section, however, we will be able to solve the $\omega \to 0$ limit and find an analytic solution for the conductivity.

4.3.4 Scalar fluctuation and bulk viscosity

Finally the scalar equation is

$$\mathcal{S}'' + \left(4A' - B' + \frac{h'}{h}\right)\mathcal{S}' + \left(\frac{e^{2B-2A}}{h^2}\omega^2 + \Sigma(r)\right)\mathcal{S} = 0\,, \tag{4.49}$$

where $\Sigma(r)$ is determined by the background:

$$\begin{aligned}\Sigma(r) \qquad &\equiv \tfrac{e^{-2A}}{18fh^2A'^2}\Big(- 18hA'^2f'^2\Phi'^2 - e^{2A}fh^2\phi'^4 + 6fhA'\phi'\Big[- 2e^{2A+2B}V' \\ &+ e^{2A}h'\phi' + f'\Phi'^2\Big] + 3fA'^2\left[8e^{2A}h^2\phi'^2 + 3h\Phi'^2f'' - 6e^{2A+2B}hV''\right]\Big)\,.\end{aligned} \tag{4.50}$$

The associated conserved flux is

$$\mathcal{F}_\mathcal{S} = he^{4A-B}\,\mathrm{Im}\left(\mathcal{S}^*\mathcal{S}'\right), \tag{4.51}$$

and one may in principle calculate the bulk viscosity ζ from this flux using the formula

$$\zeta = -\frac{2}{9\kappa^2}\lim_{\omega\to 0}\frac{1}{\omega}\mathcal{F}_\mathcal{S}\,, \tag{4.52}$$

with $\mathcal{S}$ suitably normalized. Since a gauge may be chosen where $\mathcal{S} = \tilde{\phi}$, it is evident that $\mathcal{S}$ has the same asymptotic behavior as the scalar ϕ itself,

$$\mathcal{S}(r) = \mathcal{S}_{(4-\Delta)} e^{r(\Delta-4)/L} + \ldots + \mathcal{S}_{(\Delta)} e^{-r\Delta/L} + \ldots . \tag{4.53}$$

Thus to calculate 4.51, one must properly normalize the coefficient $\mathcal{S}_{(4-\Delta)}$ of the dying exponential. This is not as straightforward numerically as normalizing an asymptotic constant.

Since the bulk viscosity is a quantity extracted from the trace of the energy-momentum tensor, and the energy-momentum tensor couples to the graviton, it is the mode $\mathcal{H}$ that we more naturally wish to canonically normalize. The scaling of $\mathcal{H}$ depends on $\phi(r)$ via 4.23. If the background scalar profile includes the "source" term $\phi_{(4-\Delta)}$, we have $A'/\phi' \sim e^{r(4-\Delta)/L}$ and we end up with the $\mathcal{H}$ scaling

$$\mathcal{H}(r) = \mathcal{H}_{(0)} + \ldots + \mathcal{H}_{(4-2\Delta)} e^{r(4-2\Delta)/L} + \ldots , \tag{4.54}$$

and the suitable boundary condition to calculate the bulk viscosity is $\mathcal{H}_{(0)} = 1$, an easier prescription to implement.[2]

The fluctuation equation for $\mathcal{H}$ simplifies most when we use the background equations of motion to eliminate V' and ϕ'^2 in favor of ϕ'' and A'':

$$\mathcal{H}'' + \left(4A' - B' + \frac{h'}{h} + \frac{2\phi''}{\phi'} - \frac{2A''}{A'}\right)\mathcal{H}' + \left(\frac{e^{2B-2A}}{h^2}\omega^2 + \Sigma_{\mathcal{H}}(r)\right)\mathcal{H} = 0 , \tag{4.55}$$

with

$$\Sigma_{\mathcal{H}} = \frac{h'}{h}\left(\frac{A''}{A'} - \frac{\phi''}{\phi'}\right) + \frac{e^{-2A}}{h\phi'}\left(3A'f' - f\phi'\right)\Phi'^2 . \tag{4.56}$$

One can check that the boundary behavior as described above does indeed result from the asymptotic expansion of 4.55, as it must. The coefficient of the first-derivative term is again explicitly integrable, and it is then easy to use Abel's identity to show that the conserved flux is

$$\mathcal{F}_{\mathcal{H}} = \frac{e^{4A-B} h \phi'^2}{4A'^2} \mathrm{Im}\left(\mathcal{H}^* \mathcal{H}'\right) , \tag{4.57}$$

[2] The asymptotic scaling of $\mathcal{H}$ is different when the background scalar profile only contains the VEV term $\phi_{(\Delta)}$ but no source. However, in this case the conformal invariance of the dual field theory is not explicitly broken, and the bulk viscosity is identically zero.

where we chose the normalization so that this conserved flux coincides exactly with $\mathcal{F}_\mathcal{S}$ 4.51 when one substitutes 4.23:

$$\mathcal{F}_\mathcal{H} = \mathcal{F}_\mathcal{S}\Big(\mathcal{S} \to -\frac{\phi'\mathcal{H}}{2A'}\Big) . \tag{4.58}$$

Thus the bulk viscosity may most easily be calculated as

$$\zeta = -\frac{2}{9\kappa^2} \lim_{\omega \to 0} \frac{1}{\omega} \mathcal{F}_\mathcal{H} , \tag{4.59}$$

with the boundary condition $\mathcal{H}_{(0)} = 1$.

4.3.5 Large-N_c counting

The various Kubo formulae are all proportional to the five-dimensional gravitational constant $1/\kappa^2$, since they all come ultimately from evaluating the five-dimensional action. The gravitational constant can be expressed in terms of the AdS radius L and the underlying string coupling g_s and Regge slope α' when an explicit string theory construction is specified. For $AdS_5 \times S^5$, the result is

$$\frac{1}{\kappa^2} = \frac{L^5}{64\pi^4 g_s^2 \alpha'^2} , \tag{4.60}$$

while the AdS radius is

$$L^4 = 4\pi g_s N_c \alpha'^2 , \tag{4.61}$$

with N_c the number of colors in the dual gauge theory (the five-form flux from the gravity point of view). Field theory quantities should not involve α', which drops out of the combination

$$\frac{L^3}{\kappa^2} = \frac{N_c^2}{4\pi^2} , \tag{4.62}$$

and all the Kubo formulae indeed result in this combination on dimensional grounds. As a result, all three transport coefficients go like N_c^2 in the large-N_c limit defined by the dual gauge theory.

For AdS/CFT models not based on a known string theory construction, the precise coefficient in 4.62 is not determined. However, the N_c^2 dependence is expected to remain the same for any gravity dual of a four-dimensional gauge theory. For the QCD-like holographic critical models of section 4.5, we will use the formula 4.62 with the understanding that the overall normalization is not truly determined, but the N_c^2 factor is expected to be robust. Note too that the factor 4.62 cancels out of ζ/s and D, and so will only be relevant for us in λ/T.

4.4 One-charge $\mathcal{N}=4$ black hole

Before discussing our primary interest, the numerical QCD-like critical black holes, we first consider a family of black hole backgrounds where the thermodynamics are known analytically, which we call the one-charge $\mathcal{N}=4$ black hole [161, 187, 169, 116, 179, 167]. These geometries are known solutions of string theory, coming most simply from a truncation of the maximally supersymmetric gauged supergravity in five dimensions, which is in turn a truncation of the dimensional reduction of type IIB string theory on $AdS_5 \times S^5$. The dual field theory configurations should be thought of as states in $\mathcal{N}=4$ super-Yang-Mills theory with a temperature and a chemical potential for a $U(1)$ subgroup of the $SO(6)$ R-symmetry. In the appendix, we discuss a second family, the two-charge $\mathcal{N}=4$ black hole, which does not display finite-temperature critical phenomena.

Since the temperature and chemical potential are the only massive parameters, dimensionless quantities can only depend on their ratio; for this reason the phase diagram is not truly two-dimensional, but is more properly thought of as depending on this single ratio. The phase diagram has the form of a semi-infinite line, ending on a critical point.

Because the conformal invariance of the theory is not broken explicitly, the bulk viscosity is identically zero. The conductivity and associated diffusion have been calculated by [106, 112]. We reproduce the calculation for two reasons. First, since it is analytically solvable, it allows us to check our numerical methods against a known analytic solution; and second, it exhibits several features that will persist to the QCD-like black holes.

In this section, in keeping with the literature, we use μ to denote a parameter in the solutions, and thus use Ω for the chemical potential. Also, it is inconvenient to set $B(r)=0$ for these solutions, so for this section (and the appendix) only we employ a radial coordinate where AdS space is related to that given in 4.10 as $\exp(r_{\text{there}}/L) = r_{\text{here}}/L$.

4.4.1 Thermodynamics and phase diagram of the one-charge $\mathcal{N}=4$ black hole

The one-charge $\mathcal{N}=4$ black hole is a solution to the Lagrangian 3.1 with the potential and gauge kinetic function,

$$V(\phi) = -\frac{1}{L^2}\left(8e^{\frac{\phi}{\sqrt{6}}} + 4e^{-\sqrt{\frac{2}{3}}\phi}\right), \quad f(\phi) = e^{-2\sqrt{\frac{2}{3}}\phi}. \tag{4.63}$$

The solution takes the form

$$\begin{aligned} A(r) &= \log\frac{r}{L} + \frac{1}{6}\log\left(1+\frac{Q^2}{r^2}\right), \quad B(r) = -\log\frac{r}{L} - \frac{1}{3}\log\left(1+\frac{Q^2}{r^2}\right), \\ h(r) &= 1 - \frac{\mu L^2}{r^2(r^2+Q^2)}, \quad \phi(r) = -\sqrt{\frac{2}{3}}\log\left(1+\frac{Q^2}{r^2}\right), \quad \Phi(r) = \frac{\sqrt{\mu}Q}{r^2+Q^2} - \frac{\sqrt{\mu}Q}{r_H^2+Q^2}, \end{aligned} \tag{4.64}$$

and is characterized by the charge parameter Q, mass parameter μ and the asymptotic AdS scale L. The horizon is at

$$r_H = \sqrt{\frac{1}{2}\left(\sqrt{Q^4+4\mu L^2} - Q^2\right)}, \tag{4.65}$$

and in what follows we will generally trade the parameter μ for r_H. The temperature and chemical potential can be expressed as

$$T = \frac{Q^2+2r_H^2}{2\pi L^2\sqrt{Q^2+r_H^2}}, \qquad \Omega = \frac{Qr_H}{L^2\sqrt{Q^2+r_H^2}}, \tag{4.66}$$

For fixed Q and L, μ is only required to be nonnegative; the limit $\mu \to 0$ corresponds to $r_H \to 0$ but the temperature approaches

$$T(\mu \to 0) \to \frac{Q}{2\pi L^2}. \tag{4.67}$$

This value is properly thought of as the **limiting** temperature of a sequence of honest black holes with nonzero values of μ. The solution with strictly $\mu = 0$ is not a black hole, as the horizon function is trivial $h(r) = 1$ and no horizon exists. The $\mu = 0$ solution is supersymmetric and has been dubbed the "superstar" by Myers and Tafjord [111].

Choosing Q to be positive along with r_H, T and Ω are in general multivalued as functions of these parameters. The transformation

$$r_H \to \frac{Q}{2}\frac{\sqrt{Q^2+4r_H^2}}{\sqrt{Q^2+r_H^2}}, \qquad Q \to r_H\frac{\sqrt{Q^2+4r_H^2}}{\sqrt{Q^2+r_H^2}}, \tag{4.68}$$

maps pairs (r_H, Q) to physically distinct pairs with the same (T, Ω). The transformation takes

$$\frac{Q^2}{2r_H^2} \rightarrow \frac{2r_H^2}{Q^2}\,, \tag{4.69}$$

which defines a fixed locus,

$$Q = \sqrt{2}r_H \quad \rightarrow \quad \pi T = \sqrt{2}\Omega\,. \tag{4.70}$$

Since dimensionless quantities like s/T^3 and χ/T^2 will be functions only of the dimensionless ratio Ω/T, we should properly think of this system as a one-dimensional phase diagram with this locus interpreted as a fixed point $\Omega/T = \pi/\sqrt{2}$, rather than a fixed line. The models of the next section add another massive parameter, with explicitly breaks conformal invariance and leads to a true two-dimensional phase diagram.

We notice that in general,

$$\pi^2 T^2 - 2\Omega^2 = \frac{(Q^2 - 2r_H^2)^2}{4L^4(Q^2 + r_H^2)} \geq 0\,, \tag{4.71}$$

which establishes the minimum value of T for a given Ω lies at the fixed point,

$$T \geq \frac{\sqrt{2}\Omega}{\pi}\,. \tag{4.72}$$

Thus for $\pi T < \sqrt{2}\Omega$ there are no corresponding black holes, at the fixed point $\pi T = \sqrt{2}\Omega$ there is one, and for $\pi T > \sqrt{2}\Omega$ there are two. The limit $\Omega \to 0$ produces two configurations dual under the transformation 4.68: the superstar with $r_H = 0$, $Q \neq 0$, and an uncharged black hole with $Q = 0$, $r_H \neq 0$.

Black holes on the two branches with the same (T, Ω) will not have the same values of other thermodynamic quantities, and so are physically distinct. The entropy and charge density in terms of Q and r_H are

$$s = \frac{2\pi r_H^2}{\kappa^2 L^3}\sqrt{Q^2 + r_H^2}\,, \qquad \rho = \frac{Q r_H}{\kappa^2 L^3}\sqrt{Q^2 + r_H^2}\,, \tag{4.73}$$

which in terms of T and Ω can be written

$$s = \frac{N_c^2 T^3}{16\pi}(3\pi \mp y)^2(\pi \pm y)\,, \qquad \rho = \frac{N_c^2 T^2 \Omega}{16\pi^2}(3\pi \mp y)^2\,, \tag{4.74}$$

where the top sign corresponds to the branch with $\sqrt{2}r_H > Q$, the bottom sign to the branch with $\sqrt{2}r_H < Q$, and where we have defined

$$y \equiv \sqrt{\pi^2 - 2\tilde{\Omega}^2}\,, \tag{4.75}$$

with $\tilde{\Omega} \equiv \Omega/T$. Note that the positivity of the quantity inside the square root follows from 4.72.

The quantities s and ρ are the T and Ω derivatives of the pressure,

$$p = \frac{N_c^2 T^4}{16\pi^2}\left(\pi^4 + 5\pi^2\tilde{\Omega}^2 - \frac{\tilde{\Omega}^4}{2} \pm \pi y^3\right)\,, \tag{4.76}$$

We note that the free energy density is $f = -p$, so for fixed (T, Ω) the $\sqrt{2}r_H > Q$ branch has a lower free energy and hence is thermodynamically preferred in the canonical ensemble.

The $U(1)$ susceptibility for the two branches is

$$\chi = \frac{N_c^2 T^2}{8\pi^2}\left(5\pi^2 - 3\tilde{\Omega}^2 \mp 3\pi y \pm \frac{6\pi\tilde{\Omega}^2}{y}\right)\,, \tag{4.77}$$

which diverges along the fixed line for $y = 0$. The heat capacity and off-diagonal susceptibility diverge as well. Thus the fixed point is a second-order phase transition. The determinant of the matrix of susceptibilities $\mathcal{S}$ is

$$\det\mathcal{S} = \frac{3N_c^4 T^4}{64\pi}\left(4\pi^4 - 22\pi^2\tilde{\Omega}^2 + \tilde{\Omega}^4 \pm 4\pi^3 y \pm \frac{46\pi^3\tilde{\Omega}^2 - 11\pi\tilde{\Omega}^4}{y}\right)\,, \tag{4.78}$$

and while this is always positive for the thermodynamically preferred branch $\sqrt{2}r_H > Q$, it is always negative for the other; thus the non-preferred branch is thermodynamically unstable as well.

The exponents for this critical point have been calculated. The fundamental relation is the approach of the density to the critical density, which for fixed T takes the form:

$$\rho - \rho_c \sim |\Omega - \Omega_c|^{1/2} \equiv |\Omega - \Omega_c|^{1/\delta}\,, \tag{4.79}$$

defining the critical exponent

$$\delta = 2\,. \tag{4.80}$$

An analogous relation holds for the approach to T_c with fixed Ω, as well as for the entropy. The divergence of the conductivity χ (as well as the heat capacity C_Ω) follows from (4.79),

$$\chi \sim |\Omega - \Omega_c|^{-1/2} \equiv |\Omega - \Omega_c|^{-\epsilon}\,, \tag{4.81}$$

where the exponent[3] $\epsilon \equiv 1 - 1/\delta = 1/2$.

4.4.2 Conductivity and diffusion of the one-charge $\mathcal{N} = 4$ black hole

We may now turn to solving for the conductivity. First we consider the gauge field fluctuation equation 4.40. This can be solved exactly at $\omega = 0$, allowing an analytic determination of the conductivity and the associated diffusion constant using similar techniques to those used for the shear viscosity. We find the $\omega = 0$ solutions

$$a(r) = C_1 \frac{Q^2 + 2r^2}{(Q^2+2)(Q^2+r^2)} + C_2\, a_2(r)\,, \tag{4.82}$$

where $a_2(r)$ is a more complicated expression including $\log(r - r_H)$ whose explicit expression is unenlightening. In order to determine C_1 and C_2, one may match the zero-frequency solution 4.82 to the near-horizon solution

$$a(r) = (r - r_H)^\alpha\,, \tag{4.83}$$

where the exponent α from 4.29 corresponding to infalling boundary conditions is

$$\alpha = -\frac{i\omega L^2 \sqrt{Q^2 + r_H^2}}{2Q^2 + 4r_H^2}\,. \tag{4.84}$$

Then looking at the near-boundary behavior, we can determine the series 4.42 and solve for the frequency-dependent conductivity 4.44. For small ω we find the result

$$\sigma = \frac{iQ^2}{2\omega\kappa^2 L} + \frac{L(Q^2 + 2r_H^2)^2}{8r_H^2\kappa^2\sqrt{Q^2 + r_H^2}} + \mathcal{O}(\omega)\,, \tag{4.85}$$

which in terms of T and Ω can be written

$$\frac{\sigma}{T} = \frac{N_c^2}{4\pi^2}\left[\frac{i}{2\tilde{\omega}}\left(2\pi^2 - \tilde{\Omega}^2 \mp 2\pi y\right) + \frac{\pi^2}{\pi \pm y} + \mathcal{O}(\omega)\right]\,. \tag{4.86}$$

where $\tilde{\Omega} = \Omega/T$ and $\tilde{\omega} = \omega/T$. The $1/\omega$ pole in $\mathrm{Im}\,\sigma$ indicates by the Kramers-Kronig relations a delta-function contribution to the real part, $\mathrm{Re}\,\sigma \propto \delta(\omega)$, not visible in our calculation. This

[3] In the literature for critical phenomena, the well-known exponent labels α, β and γ are often associated to behavior approaching the critical point along the axis defined by the first-order line. Since there is no first-order transition in this model, we avoid these exponent names. ϵ encodes the approach of χ to the critical point off the first-order axis.

infinite contribution is characteristic of a translationally-invariant charged system [119]. Setting aside the delta-function, we have the zero-frequency conductivity [106]

$$\lambda = \frac{N_c^2 T}{4(\pi \pm y)} \,. \tag{4.87}$$

We also calculated this conductivity using the numerical methods that will be employed in the next section, and find excellent agreement.

Since $y \to 0$ at the critical point, the conductivity λ approaches the constant

$$\lambda_c \equiv \frac{N_c^2 T_c}{4\pi} \,. \tag{4.88}$$

The conductivity not diverging is a sign of the large-N_c domination of diffusive conduction (characteristic of model B) over convective conduction (model H) [106, 107]. However, the slope of λ diverges as the critical point is approached. One has

$$\lambda - \lambda_c \sim (T - T_c)^{1/2} \,. \tag{4.89}$$

We note that the exponent is $1/\delta$; this transport coefficient has the same critical behavior as the thermodynamic quantities s and ρ. We will find an analogous phenomenon for the QCD-like black holes.

The diffusion $D \equiv \lambda/\chi$ is given by

$$D = \frac{4\pi^2}{T} \frac{1}{(\pi \pm y)(3\pi \mp y)(3\pi \mp y \pm 4\tilde{\Omega}^2/y)} \,. \tag{4.90}$$

Since the conductivity is constant at the critical point, while the susceptibility diverges, the diffusion goes to zero. On the stable branch at large temperature, D asymptotes to its AdS value $D \to 1/2\pi T$. Because χ on the unstable branch is negative close to the critical point and passes through zero, the diffusion on the unstable branch is negative and diverges before returning from positive infinity.

Away from the critical point, an entirely distinct phenomenon occurs in the superstar limit. Since as $y(\Omega \to 0) \to \pi$, the conductivity ratio λ/T approaches zero at the charged black hole (the far end of the stable branch) and approaches infinity in the superstar limit (the far end of the

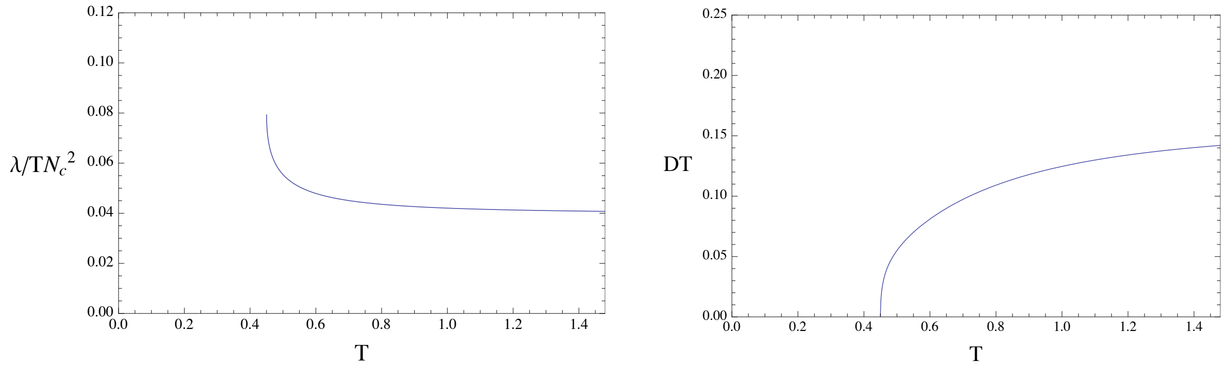

Figure 4.1: The conductivity over temperature and diffusion times temperature for the one-charge black hole with $\Omega = 1$, for the stable branch only. λ/T approaches a finite value with an infinite slope at the critical point, while DT goes to zero.

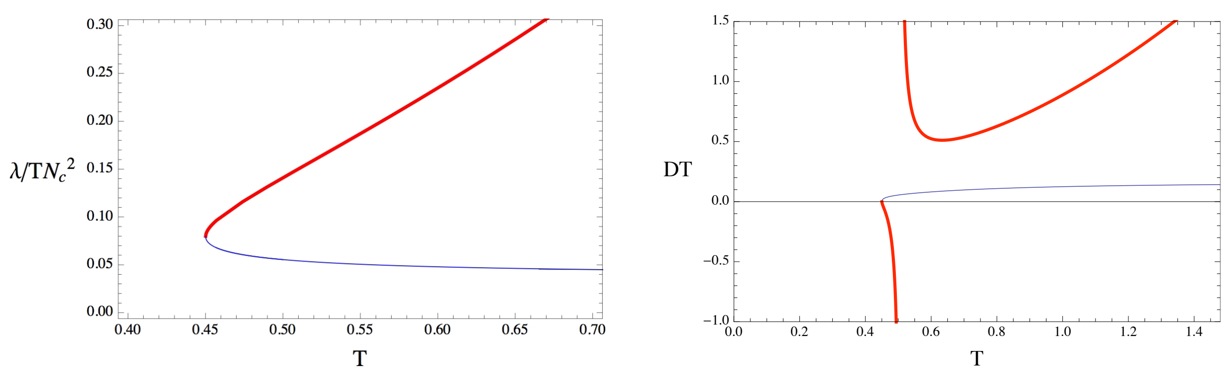

Figure 4.2: The conductivity over temperature and diffusion times temperature for the one-charge black hole with $\Omega = 1$, for both branches; the unstable branch is the thick red line. The approach to infinity at large T is the superstar divergence.

unstable branch). The rate of approach to infinity in the superstar limit becomes

$$\lambda \sim \frac{1}{\Omega^2}\,. \tag{4.91}$$

We will find a similar divergence in the bulk viscosity of the holographic critical black holes of the next section, away from the critical point and the region expected to be related to QCD.

4.5 QCD-like holographic critical black holes

We now turn to our primary interest, studying the transport coefficients of the class of solutions designed to emulate the thermodynamic and phase structure of QCD [96]. These black holes are the solutions to the Lagrangian ansatz 3.1 with the potential 3.4 and the gauge kinetic function 3.5 familiar from the previous chapter. The black hole solutions are of the form 4.9. In this calculation too, the gauge $B(r) = 0$ was chosen, and the residual coordinate transformations 4.15 and the freedom to shift r were used to set

$$A(r_H) = 0\,, \quad \Phi(r_H) = 0\,, \quad h'(r_H) = 1/L\,, \quad r_H = 0\,. \tag{4.92}$$

The solutions were characterized by two initial conditions at the horizon, $\phi_0 \equiv \phi(r_H)$ and $\Phi_1 \equiv \Phi'(r_H)$; the ensemble of black holes was generated by numerically integrating the equations 3.27 from the horizon to the boundary for a large set of distinct (ϕ_0, Φ_1), and the thermodynamic quantities of temperature T, entropy density s, chemical potential μ and baryon density ρ were obtained for each.

Again, the functions 3.4 and 3.5 have been chosen so that the thermodynamics of the $\mu = 0$ black holes reproduce lattice results for the equation of state [45] and the quark susceptibility [96], building into the model the rapid crossover that connects the hadron phase to the quark-gluon phase in physical QCD with massive quarks; see figure 3.3. Normalizations for the scales of T and μ were also derived from matching to the lattice results, allowing the thermodynamic quantities to be expressed in MeV.

The potential 3.4 leads to the scalar mass,

$$m_\phi^2 L^2 \approx -0.293\,, \tag{4.93}$$

with implies a dual operator that is barely on the relevant side of marginal,

$$\Delta_\phi \approx 3.93\,, \tag{4.94}$$

designed to emulate the slow running of the QCD coupling constant somewhat above the confinement scale. The profile of the scalar in the background includes a "source" term that explicitly breaks conformal invariance.

At nonzero μ for this ensemble of black holes, the crossover sharpens into a line of first-order phase transitions ending at a critical point, as is expected for QCD. The region of the first-order line is characterized by the existence of two distinct phases, realized as distinct black hole solutions at the same point in the phase diagram, as well as a third black hole corresponding to the thermodynamically unstable state lying in between the stable phases in the Maxwell construction.

The first-order line ends on the critical point. For the static critical exponents defined as

$$\begin{aligned} C_\rho \equiv T\left(\frac{\partial s}{\partial T}\right)_\rho &\sim |T-T_c|^{-\alpha}\,, && \text{along first order axis} \\ \Delta\rho &\sim (T_c-T)^{\beta}\,, && \text{along first order line} \\ \chi \equiv \left(\frac{\partial \rho}{\partial \mu}\right)_T &\sim |T-T_c|^{-\gamma}\,, && \text{along first order axis} \\ \rho-\rho_c &\sim |\mu-\mu_c|^{1/\delta}\,, && \text{for } T=T_c\,, \end{aligned} \tag{4.95}$$

this critical point was found numerically to have

$$\alpha = 0\,, \qquad \beta \approx 0.482\,, \qquad \gamma \approx 0.942\,, \qquad \delta \approx 3.035\,, \tag{4.96}$$

with accuracies consistent with the Ising mean field values $(\alpha,\beta,\gamma,\delta) = (0,1/2,1,3)$. Matching the temperature and chemical potential scales to that of the lattice data, the location of the critical point was found to be

$$T_c = 143\,\mathrm{MeV} \qquad \mu_c = 783\,\mathrm{MeV}\,. \tag{4.97}$$

While these results generate a large phase diagram, the applicability to QCD is expected to be limited to a band surrounding the crossover and extending out into the plane, for two reasons. First of all, the potential 3.4 and gauge kinetic function 3.5 were only matched to lattice data over a finite range. In principle, one can imagine varying the functions so as to keep matching the data in the range required, while changing the results elsewhere. The potential $V(\phi)$ was only matched up to about $\phi_0 \approx 7.5$, corresponding to $T_{\rm min} \approx 135\,\text{MeV}$ at $\mu = 0$; the crossover is at $T_c \approx 175\,\text{MeV}$ on the T-axis. Moreover, AdS/CFT is only expected to provide a good description of QCD in the region where no quasiparticle description is available; both above and below the crossover such a description is possible, with hadrons at lower T and quarks and gluons at higher T. Thus we expect our geometries to be reasonable potential models for QCD only near the crossover; and we hypothesize that this applicability extends along with the crossover out into the T-μ plane to the critical point.

4.5.1 Boundary conditions

To calculate the correct transport coefficients (or thermodynamics for that matter) for these black holes, a technical detail must be taken into account. The numerical integration beginning at the horizon produces solutions that asymptote to AdS space, but in general in coordinates that do not match standard AdS coordinates. In the gauge $B(r) = 0$, one usually uses the AdS coordinates 4.10, with $A(r) \to r/L$ and $h(r) \to 1 + \mathcal{O}(e^{-4r/L})$; however with the coordinate choices 4.92 used for the numerical solution, the horizon function in general approaches a non-unit value $h \to h_0^{\rm far}$, and the warp factor goes like $A(r) \to r/(\sqrt{h_0^{\rm far}}L) + A_0^{\rm far}$. To calculate thermodynamic and hydrodynamic quantities using the usual formulae, it is necessary to pass to a new set of coordinates that takes the usual AdS form, with unit normalization for the horizon function and $A \sim r/L$; this can be done by making a different rescaling 4.15.

Moreover, the scalar field generically approaches $\phi \to \phi_A e^{-\nu A(r)}$, with $\nu \equiv 4 - \Delta_\phi \approx 0.07$. It is useful to rescale the leading perturbation to the scalar to a standard magnitude $\phi_A = 1$, which can be achieved by adding a constant to r. Fixing the value of ϕ_A is useful because turning on this perturbation corresponds to deforming the ultraviolet theory with an almost-marginal relevant operator, playing the role of the running coupling, and hence changing the theory. We want every point on the phase diagram to correspond to the same theory, not different theories, and hence we make ϕ_A identical in all of them. Put another way, there are three massive parameters in the theory, T, μ and Λ, where Λ is the scale associated with the scalar. Normalizing $\phi_A = 1$ corresponds to measuring T and μ in units of Λ. The explicit breaking of conformal invariance coming from Λ permits a non-zero bulk viscosity to be present.

The desired coordinates are achieved by the transformation

$$\tilde{t} = \phi_A^{1/\nu}\sqrt{h_0^{\rm far}}\, t\,, \qquad \tilde{\vec{x}} = \phi_A^{1/\nu}\vec{x}\,, \qquad \frac{\tilde{r}}{L} = \frac{r}{\sqrt{h_0^{\rm far}}L} + A_0^{\rm far} - \log(\phi_A^{1/\nu})\,, \tag{4.98}$$

which is a combination of a scale transformation associated to $\phi_A^{1/\nu}$ and a time dilation by $\sqrt{h_0^{\rm far}}$ as well as a shift of r, implying the relation of the functions,

$$\tilde{A}(\tilde{r}) = A(r) - \log(\phi_A^{1/\nu}) \qquad \tilde{h}(\tilde{r}) = \frac{1}{h_0^{\rm far}}\, h(r) \qquad \tilde{\Phi}(\tilde{r}) = \frac{1}{\phi_A^{1/\nu}\sqrt{h_0^{\rm far}}}\,\Phi(r)\,. \tag{4.99}$$

Thermodynamic and hydrodynamic quantities are naturally calculated in terms of the tilded coordinates because of their standard near-AdS form. The black hole solutions exist in the untilded variables, but as we now show it is possible to compute certain ratios directly in the untilded coordinates. One may also use the thermodynamic formulae 4.11, 4.12 in the untilded variables to calculate "horizon" quantities T_H, μ_H, s_H and ρ_H. The true entropy and temperature are related to their "horizon" counterparts as

$$T = \frac{1}{\phi_A^{1/\nu}\sqrt{h_0^{\rm far}}}\, T_H\,, \qquad s = \frac{1}{\phi_A^{3/\nu}}\, s_H\,, \tag{4.100}$$

where the horizon quantities are constants independent of the black hole considered,

$$T_H = \frac{1}{4\pi L}\,, \qquad s_H = \frac{2\pi}{\kappa^2}\,. \tag{4.101}$$

Transforming from one set of coordinates to the other, and using $\omega = \phi_A^{1/\nu}\sqrt{h_0^{\rm far}}\tilde{\omega}$, we have[4]

$$\bar{\eta} = \frac{1}{\phi_A^{3/\nu}}\,\bar{\eta}_H\,, \qquad \lambda = \frac{1}{\phi_A^{1/\nu}}\,\lambda_H\,, \qquad \zeta = \frac{1}{\phi_A^{3/\nu}}\,\zeta_H\,. \tag{4.102}$$

[4] Although under this rescaling one has $\tilde{a} = a/\phi_A^{1/\nu}$, we assume the gauge field fluctuation is asymptotically normalized to one in both coordinate systems before being plugged into the Kubo formulae.

Thus, we can assemble the invariants

$$\frac{\bar{\eta}_H}{s_H} = \frac{\bar{\eta}}{s}\,, \qquad \frac{\lambda_H}{s_H^{1/3}} = \frac{\lambda}{s^{1/3}}\,, \qquad \frac{\zeta_H}{s_H} = \frac{\zeta}{s}\,, \tag{4.103}$$

and thus these ratios can be calculated directly in the untilded variables.

With the gauge choices $B(r) = 0$ and 4.92, the value of the exponent α characterizing the near-boundary behavior of the fluctuation equations is simply

$$\alpha = \pm iL\,\omega\,. \tag{4.104}$$

As usual, one should choose the minus sign to impose infalling boundary conditions at the horizon. The boundary conditions at the boundary are that a and $\mathcal{H}$ approach unity. As mentioned previously, if one employed $\mathcal{S}$ instead of $\mathcal{H}$, it would be the coefficient of the $e^{-\nu r}$ term that had to be properly normalized; this is numerically more difficult. The results outlined in the following subsections were obtained using the $\mathcal{H}$ equation, but the $\mathcal{S}$ method was checked as well, and while the $\mathcal{S}$ calculation developed numerical pathologies in certain (low-T) regions of the phase diagram, the two methods agreed well in the regions where both appeared reliable.

4.5.2 Bulk viscosity for the QCD-like holographic critical black holes

The computation of the bulk viscosity for the QCD-like black hole solutions is a straightforward application of the Kubo formula 4.59. To construct the mode solutions to the $\mathcal{H}$ fluctuation equation 4.55 we used a near-horizon series expansion to seed a numerical integration routine which propagates the mode solution out to close to the boundary.

Because the flux 4.57 satisfies Abel's identity, it must be independent of the radial location at which it is evaluated; ascertaining that this holds is a check that the fluctuations obtained indeed satisfy 4.55. After verifying that this remains true in practice, we then evaluated the flux at a radial location r_T where the numerical solutions are particularly robust. The black hole solutions are defined from $r \sim 10^{-6}$ near the horizon out to $r \sim 10$, and we used a value around $r_T \sim 10^{-4}$. With the fluctuation in hand, we normalized it to one asymptotically and inserted it into 4.59 and used 4.100 and 4.103 to calculate the bulk viscosity over entropy density ratio ζ/s.[5]

The results of this calculation, when carried out for many points on the T-μ plane, are shown in figure 4.3 up to $\mu = \mu_c$; in all figures in this section we have used the normalization of [96] to express T and μ in MeV. Two features are immediately apparent. One is the propagation of a "bump" on the T-axis at the location of the crossover, out into the plane towards the critical point. As the bump moves into the plane, it becomes increasingly asymmetrical as the slope on the lower-T side becomes more vertical. Precisely at the critical point, this slope diverges. Constant-μ plots of ζ/s for both $\mu = 0$ and $\mu = \mu_c$ are given in figure 4.4. The result at vanishing μ was obtained previously in [97]. For $\mu > \mu_c$, the peak "tips over" and the plot of ζ/s becomes multivalued.

The first and more important conclusion from this critical behavior is that the bulk viscosity remains finite at the critical point; it does not diverge as is predicted in a number of models such as that of Onuki [104], given in equation 4.6; see also [105].

Moreover, the way in which the quantity stays finite is interesting. Approaching the critical point along the "crest" of the peak turns out to be equivalent to approaching along the axis defined by the first-order line (but on the other side of the critical point); along this path, the value of ζ/s scarcely changes at all. On the other hand, approaching the critical point from a direction other than the first-order axis, for example constant $\mu = \mu_c$ as depicted on the right of figure 4.4, ζ/s develops a divergent slope; the same is true for constant T or any other direction of approach, save only the first-order axis, where no such divergent slope is seen.

The bulk viscosity is not the only quantity with this property. It is common for thermodynamic functions to behave differently depending on whether the approach to the critical point is on the first-order axis or not. In [96] it was found that the thermodynamic densities s and ρ also behave smoothly approaching the critical point along the first-order axis, but have divergent slope approaching off-axis. Since the derivatives of these densities are the specific heat and susceptibilities, these properties are characterized by various static critical exponents: the smooth approach along the first-order axis corresponds to the vanishing $\alpha = 0$, while the divergent slope

[5] Since $\bar{\eta}/s$ is a constant, ζ/s is simply proportional to $\zeta/\bar{\eta}$.

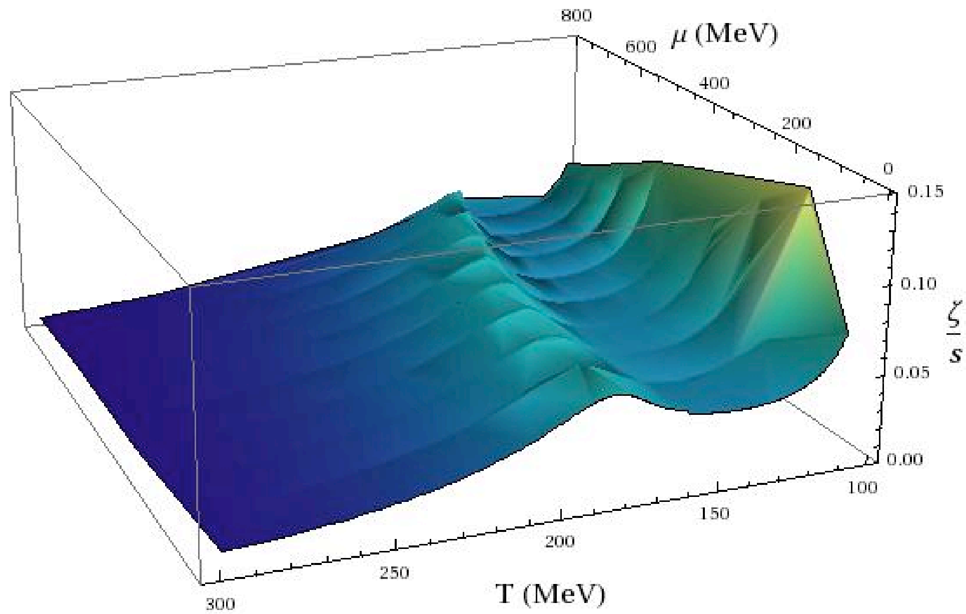

Figure 4.3: The bulk viscosity over entropy density over the T-μ plane for the QCD-like black hole solutions.

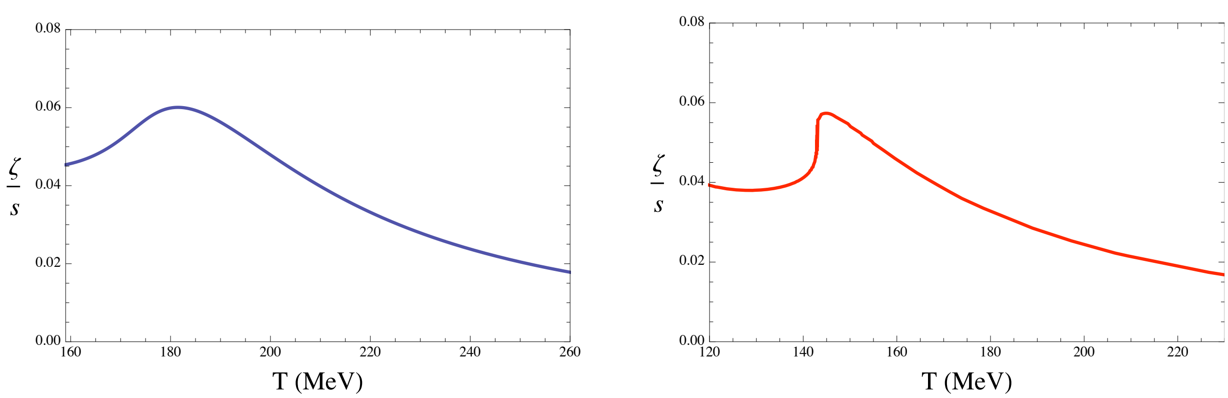

Figure 4.4: The bulk viscosity over entropy density at zero chemical potential and at $\mu = \mu_c$ for the QCD-like black hole solutions; the "bump" at left evolves into the peak with singular slope on one side as μ is increased.

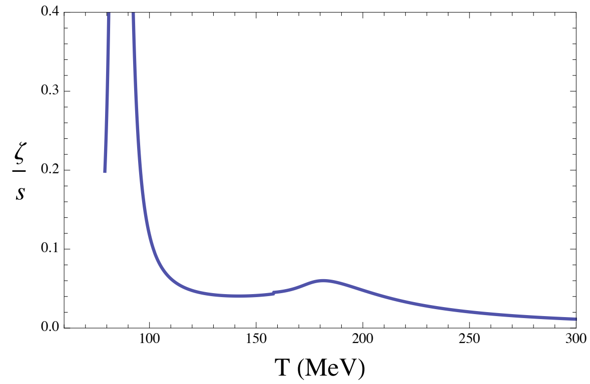

Figure 4.5: The bulk viscosity over entropy density at zero chemical potential down to lower temperatures, showing the divergence.

approaching off the axis is encoded in the value of $\delta \approx 3$, giving an approach of the susceptibility **off** the first-order axis as

$$\chi \sim |\mu - \mu_c|^{-\epsilon} \sim |T - T_c|^{-\epsilon}\,, \qquad \text{off first order axis}\,, \tag{4.105}$$

with

$$\epsilon \equiv 1 - \frac{1}{\delta} \approx 2/3\,. \tag{4.106}$$

A natural guess is then that this behavior can be explained by the hypothesis that the bulk viscosity is a smooth function of the two densities: $\zeta = \zeta(s, \rho)$. Let us characterize the divergent slope of ζ by an exponent δ_ζ:

$$\zeta - \zeta_c \sim |\mu - \mu_c|^{1/\delta_\zeta} \sim |T - T_c|^{1/\delta_\zeta}\,. \tag{4.107}$$

Then we would expect $\delta_\zeta = \delta$. We analyzed the results of numerics and found an exponent consistent with this interpretation, although the strong sensitivity to the precise value of ζ_c, which is difficult to determine due to the infinite slope, gave an uncertainty in the exponent in the range of $0.1 < 1/\delta_\zeta < 0.7$. A similar argument can be carried through more precisely for the zero-frequency conductivity λ of the one-charge $\mathcal{N} = 4$ black hole. In this case, the result 4.89 shows that $\delta_\lambda = 2$, in agreement with $\delta = 2$ for the one-charge model.

The second salient feature of the ζ/s on the phase diagram is the strong rise at colder temperatures and smaller chemical potential. This behavior is shown for zero chemical potential in figure 4.5, which shows the same thing as the left-hand-side of figure 4.4 but including lower values of T. The bulk viscosity actually diverges at a temperature T_*, which on the T-axis is at $T_*(\mu = 0) \approx 86$ MeV, before becoming finite again at smaller temperatures; this divergence extends from the T-axis out along a curve into the finite chemical potential region of the phase diagram. The divergence is power law, with

$$\frac{\zeta}{s} \sim (T - T_*)^{-2} \, . \tag{4.108}$$

Notably, the thermodynamic densities s and ρ and their derivatives do nothing special at this locus.

From the gravity point of view, this divergence can be understood as related to a formation of a node in the mode solution for $\mathcal{H}(r)$. For $T > T_*$, the fluctuation $\mathcal{H}(r)$ never crosses zero as it asymptotes to a constant value at the boundary. For $T < T_*$ on the other hand, the solutions have a single zero before asymptoting to a constant. As $T \to T_*$ from below, this node moves out towards the boundary, and precisely at $T = T_*$ the solution goes to zero at infinity; that is, the leading constant $\mathcal{H}_{(0)}$ in the asymptotic expansion of $\mathcal{H}$ 4.54 vanishes. Since the AdS/CFT prescription is to normalize this constant to unity, the scaling required to accomplish this normalization leads to the divergence.

A reasonable expectation is that for $T < T_*$, there is a perturbative instability in the black hole. Because the thermodynamics is perfectly well-defined and stable in the vicinity of $T = T_*$, such an instability, if present, would be a decisive counter-example to the correlated stability conjecture of [120, 121].

On the field theory side, however, it is unclear what this divergence means, and what the conjectured instability would be for $T < T_*$. Importantly, this particular feature is not a prediction for QCD-like systems, since it lies well outside the range that was matched to lattice QCD data; $T_* \approx 86$ MeV is well below the lower bound of $T_{\min} \approx 135$ MeV where the matching to lattice QCD ended. (In fact, the value of the temperature where ζ/s begins to rise towards the divergence is close to $T_{\min}$.) Instead one should view this phenomenon as an indication of what features are generally possible in gauge/gravity transport.

Interestingly, this divergence is reminiscent of the superstar divergence in the conductivity for the one-charge $\mathcal{N} = 4$ black hole 4.91. In both cases, the transport coefficient has a double pole in the thermodynamic variable as the divergence is approached.

4.5.3 Conductivity and diffusion for the QCD-like holographic critical black holes

Utilizing a numerical algorithm identical in spirit to that employed for the computation of the bulk viscosity, it was also possible to construct solutions to the fluctuation equation for $a(r)$ 4.40 and subsequently evaluate the conductivity Kubo formula 4.43. The results of this calculation are displayed in figure 4.6, where the dimensionless ratio λ/T is plotted over the T-μ plane. Unlike the ratio ζ/s, this quantity grows in the larger-T region of the diagram. Note that as mentioned in section 4.3.5, the overall normalization for this ratio is not known due to the lack of a string theory embedding, but the N_c^2 dependence should be general, so we plot λ/TN_c^2 using 4.62 as a concrete choice.

Once again, the most salient attribute is the propagation of the crossover feature out to the critical point, which is the sudden rise of λ/T. Cuts at $\mu = 0$ and $\mu = \mu_c$ are displayed in figure 4.7. As with the bulk viscosity, the conductivity attains a finite value at the critical point; and also like the bulk viscosity, the slope of the rise increases as the critical point is approached, until it diverges, except along the first-order axis. Thus it is again natural to hypothesize that $\lambda = \lambda(s, \rho)$, and that off the first-order axis the conductivity approaches its critical value with exponent $1/\delta_\lambda$

$$\lambda - \lambda_c \sim |\mu - \mu_c|^{1/\delta_\lambda} \sim |T - T_c|^{1/\delta_\lambda} \,, \tag{4.109}$$

with $\delta_\lambda = \delta$.

As described in the introduction, the finiteness of the critical conductivity is reminiscent of dynamic critical model B rather than model H [102], matches the result for the one-charge $\mathcal{N} = 4$ models (see equation 4.88 and [106, 112]), and is consistent with the interpretation of a large-N_c enhancement of diffusive conductivity over convective conductivity [107].

We may also consider the baryon diffusion $D_B \equiv \lambda/\chi$. Since the conductivity diverges at

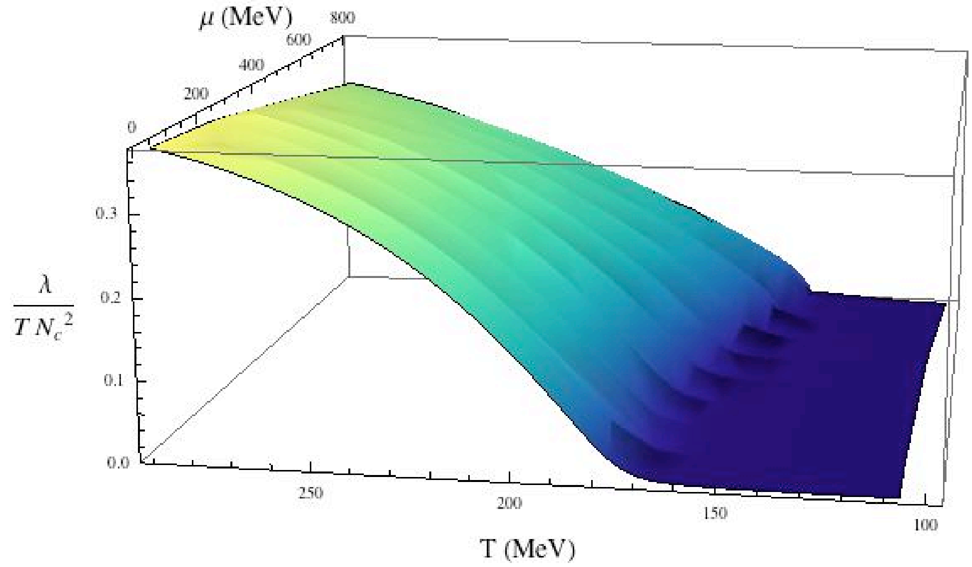

Figure 4.6: The conductivity over temperature over the T-μ plane for the QCD-like black hole solutions.

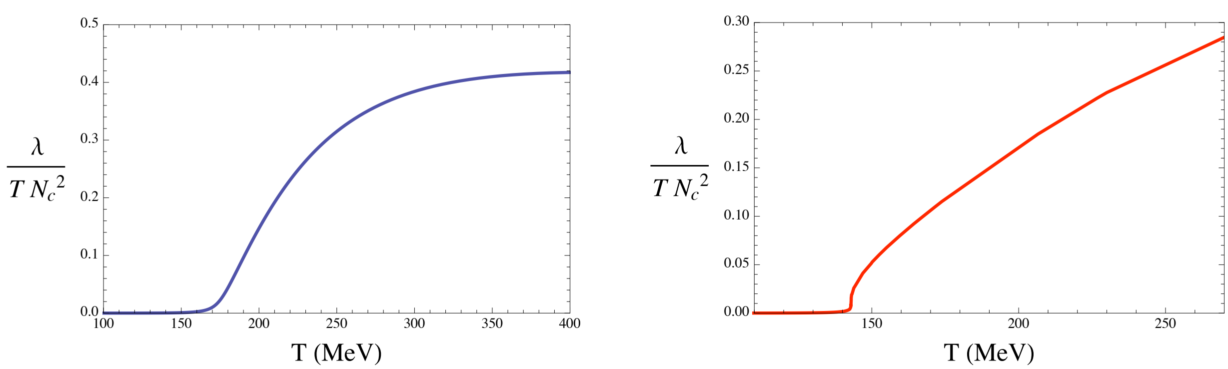

Figure 4.7: Conductivity over temperature at zero chemical potential and at $\mu = \mu_c$ for the QCD-like black hole solutions; the smooth rise on the left evolves to the singular jump on the right as μ is increased.

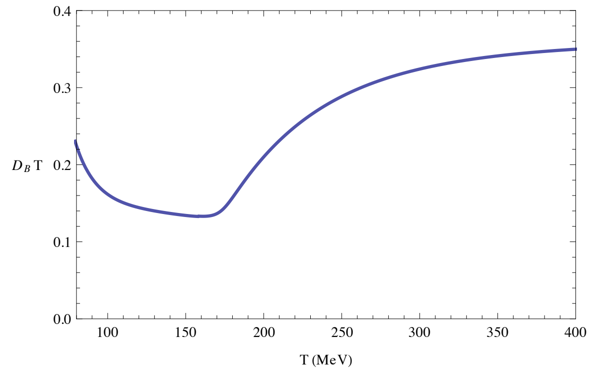

Figure 4.8: Baryon diffusion at zero chemical potential for the QCD-like black hole solutions.

the critical point, the finite critical conductivity implies vanishing baryon diffusion. In [96], the behavior of the baryon susceptibility was studied as the second order point was approached along the first order line axis, and along directions off this axis. From 4.96 and 4.105, one has that on and off the axis the susceptibility diverges with critical exponents $\gamma \approx 1$ and $\epsilon \approx 2/3$, respectively. Thus, we find the rates of approach to zero for the diffusion

$$D_B \sim |T - T_c|^{\gamma} \sim |T - T_c| \,, \qquad \text{along first order axis} \,, \tag{4.110}$$

and

$$D_B \sim |T - T_c|^{\epsilon} \sim |T - T_c|^{2/3} \,, \qquad \text{off first order axis} \,. \tag{4.111}$$

In figure 4.8, the conductivity divided by temperature is plotted for vanishing chemical potential. In this region of the phase diagram, the baryon susceptibility is particularly easy to compute, as it can be explicitly related to the background metric and scalar [96]. As a result, it is straightforward to extract the baryon diffusion along the T-axis. The diffusion also experiences a rise at low temperature, but we are unable to determine whether or not this rise culminates in a divergence (as is the case for the bulk viscosity) as it manifests in a numerically unreliable region of the phase diagram.

4.6 Discussion

The primary lesson so far of the study holographic critical phenomena has been the suppression of fluctuations and convective transport by large N_c. The models considered here have a thermodynamic crossover designed to emulate QCD, and correspondingly a critical point arises in the T-μ phase diagram. However, rather than exact 3D Ising static critical exponents, we found mean field Ising critical exponents; and rather than divergences in the transport coefficients, we here find finite critical behavior. (In fact, one can view the famous constancy of the shear viscosity over entropy density, which holds throughout the phase diagram, as being the first example of this phenomenon, since mode-coupling theories predict a weak divergence.) These results can be explained by the hypothesis that large-N_c suppresses quantum corrections as well as convective transport [107].

Physical QCD of course has $N_c = 3$, but large-N_c counting is still a useful way of looking at the theory for a number of phenomena. Understanding better the extent to which the suppression phenomena that emerge from the AdS/CFT duals apply to real QCD is the primary outstanding question: in other words, could large-N_c-suppression in real QCD significantly push the behavior of physical quantities toward mean field and model B expectations, except very close to the critical point? Understanding both the nonzero-momentum fluctuations and the finite-N_c corrections to these models is essential for making further progress, and we hope to report on these issues in the future.

Chapter 5

Charged Schrödinger Black Holes

5.1 Overview

A series of beautiful experiments on cold atoms at unitarity [122] and other non-relativistic critical systems has led to intense study of non-relativistic conformal field theories (NRCFTs) [123]. Since these systems are generally strongly non-perturbative, making progress with traditional tools has proven difficult. In an attempt to provide a strong-coupling expansion, Son [124] and Balasubramanian and McGreevy [125] proposed a new application of gauge-gravity duality to NRCFTs in which the usual AdS_{d+1} space, whose isometry group is the relativistic conformal group in d space-time dimensions, is replaced by the Sch_{d+2} geometry,

$$ds^2 = -\frac{dt^2}{r^4} + \frac{2dtd\xi + d\vec{x}^2 + dr^2}{r^2}\,,$$

whose isometry group is the non-relativistic conformal group in d space-time dimensions – the so-called Schrödinger group. In this construction, ξ is a compact null circle, with the particle number of the NRCFT identified with momentum along this Discrete Light Cone Quantization (DLCQ) direction, $N = i\partial_\xi$. Using a simple generalization of the usual AdS/CFT dictionary, one can show that this gravitational dual does indeed reproduce the correlation functions of a NRCFT at zero temperature and chemical potential.

Of course, a non-relativistic system at zero temperature and zero density is a somewhat degenerate system. Meanwhile, the Sch_{d+2} geometry above has a null singularity in the IR region near $r \to \infty$. To improve the situation, one can turn on a non-zero temperature and chemical potential. In the gravity solution, this corresponds to hiding the erstwhile null singularity behind a warm fuzzy black hole horizon at finite r [126, 127, 128]. Using the previously-conjectured dictionary, these gravity systems generate boundary correlation functions which transform like those of an NRCFT at finite temperature and density, which pass some rather non-trivial checks [129], and which lead to the prediction that the dual NRCFT has a viscosity to entropy ratio which saturates the KSS bound [130]. The evidence is thus strong that these systems describe some NRCFT living on the boundary.

Our main interest, however, is not in the symmetric phase of these systems, but rather in superfluid phases in which the particle-number $U(1)$ is spontaneously broken by the particle condensate. In the relativistic context, such condensates have been studied in some detail by Gubser [131] and by Hartnoll, Herzog and Horowitz [132] and others, where charged black holes were shown to be unstable to the spontaneous emission of charge into a trapped layer above their horizons – a near-horizon superfluid. Rotation is readily incorporated by studying charged rotating black holes [133]. Relatedly, in the context of fermions, the study of fermi condensates involves a very similar structure, with a sharp fermi surface appearing in the zero temperature extremal limit of a charged black hole [134]. It would be very interesting to extend these construction to the non-relativistic regime.

We are thus led to search for more general charged rotating asymptotically Schrödinger black holes. In this chapter, we will construct precisely such black hole solutions in IIB supergravity. As in the original example, we will derive these solutions from charged, rotating AdS solutions by the application of a solution generating technique, the null Melvin twist. Also as in the original example, these black holes will inherit many of their properties from AdS space. However, they will enjoy a number of novel features. First, these solutions will boast extremal limits with AdS_2 near-horizon geometries, a very powerful constraint on the IR physics. Secondly, unlike the AdS case, the radius of curvature of the near-horizon region will be independent of the radius of curvature of the asymptotic geometry, but will instead be controlled by the NR density of the boundary CFT. Third, these solutions will allow us to explicitly break rotation invariance in the boundary solution with either rotation or additional fields.

In constructing these solutions explicitly, several bits of technology will be quite useful. First, we obtain a closed-form expression for a general melvinization, including RR forms, which simplifies our computations. Secondly, we determine the dimensionally reduced five-dimensional action associated to the Melvinized solutions. The Melvin map on five dimensional solutions is shown to slightly modify the metric, preserve the initial massless gauge field, and introduce a massive gauge field corresponding to the Killing vector in the direction of the number operator isometry.

This chapter is organized as follows. In Section 2, we present the closed-form expression for the null Melvin twist, restrict the general form to solutions of 5d gauged supergravity, and discuss the 5d effective action after Melvinization. Section 3 addresses general properties of black holes which arise from Melvinization, including their thermodynamics and near-horizon geometries. Section 4 works out two examples, the charged RN-Sch$_5$ black hole and the charged-rotating Kerr-Newman-Sch$_5$ black hole, including a brief discussion of their thermodynamics and near horizon geometries. We conclude in Section 5.

5.2 The Null Melvin Twist

The Null Melvin Twist [135, 136] is a simple solution generating technique for IIB supergravity. The idea is to act with a series of symmetry operations which preserve, point by point, the satisfaction of the equations of motion, but which do not necessarily respect global properties of the solution. The result is a new and generally inequivalent solution which, however, inherits some of the structure of the original background. This process of "Melvinization" has been used successfully to construct (up to now uncharged, unrotating) black holes with asymptotic Schrödinger symmetry from AdS black holes in type IIB supergravity. With an eye toward extremal solutions with Schrödinger asymptotics, we would like to apply this technique to AdS black holes carrying charge and rotation.

For this technique to work, the initial solution must admit one timelike and two spacelike isometries, ∂_τ, ∂_y and ∂_χ. One then performs a boost of rapidity γ in the τ-y plane followed by a

T-duality along y, and then twists $d\chi \to d\chi + \alpha dy$; this is followed by another T-duality along y and a boost of rapidity $-\gamma$ in the τ-y plane. Finally one takes a double-scaling limit with

$$\alpha \to 0\,, \quad \gamma \to \infty\,, \qquad \beta \equiv \alpha \cosh\gamma \;\; \text{fixed}\,. \tag{5.1}$$

The "Melvinized" solution is characterized by the new constant β; the original solution is recovered in the limit $\beta \to 0$. By construction, the end result is again a solution of 10d IIB supergravity.

While the procedure is completely straightforward in principle, intermediate steps can be messy. For simplicity, we begin this section with a closed-form expression for the Melvinization of a broad class of initial solutions, then specialize to 10d solutions corresponding to general AdS_5 black holes. We use the result as an ansatz for a dimensional redution to five dimensions and present the reduced 5d action. We will use these results to discuss the thermodynamics of Melvinized black holes in the next section, then discuss some simple examples in the subsequent section.

5.2.1 General Melvin map

We consider a type IIB supergravity background with the requisite three isometries, a self-dual five form F_5, constant dilaton and all other fields vanishing. These assumptions can be relaxed straightforwardly, but will suffice for our purposes.

Letting a, b run over the isometry directions τ, y, χ, with $x^{i=3\ldots9}$ the remaining seven coordinates, the initial background may be written as,

$$ds^2 \;=\; \mathrm{g}_{ab}\, e^a e^b + \mathcal{G}_{ij}\, dx^i dx^j\,, \tag{5.2}$$

$$F_5 = *F_5 \;=\; F_5^0\,, \tag{5.3}$$

$$\Phi \;=\; \Phi_0\,, \tag{5.4}$$

where the one-forms e^a, given by

$$e^\tau \equiv d\tau + A^\tau{}_i(x)dx^i, \qquad e^y \equiv dy + A^y{}_i(x)dx^i, \qquad e^\chi \equiv d\chi + A^\chi{}_i(x)dx^i\,, \tag{5.5}$$

are defined so that all cross terms between the three-dimensional part of the metric spanned by τ,

y, χ and the other seven directions x^i are absorbed into it; however, they do not contain the cross terms between τ, y and χ themselves, which are realized by off-diagonal elements in g_{ab}.

In writing down the Melvinized solution, it is useful to decompose the 5-form F_5^0 into all possible tensors relative to e^τ, e^y and e^χ and single out two terms in particular:

$$F_5^0 \equiv e^\tau \wedge e^y \wedge e^\chi \wedge a_2 + \frac{1}{2}(e^y - e^\tau) \wedge e^\chi \wedge b_3 + \dots\,, \tag{5.6}$$

where a_2 and b_3 are a 2-form and a 3-form with indices in the x^i directions; all other possible terms consistent with self-duality can be present as well, but these two play a special role in the results.

We now perform the Melvinization as described. A compact and convenient presentation of the T-duality rules is given in appendix B.2. After some character-building labor, we find the result

$$ds^{2\prime} = \frac{\beta^2||\mathrm{g}_{ab}||}{K}(e^\tau + e^y)^2 + \frac{1}{K}\,\mathrm{g}_{ab}\,e^a e^b + \mathcal{G}_{ij}\,dx^i dx^j\,, \tag{5.7}$$

$$B_2{}' = B'_{ab}\,e^a \wedge e^b\,, \tag{5.8}$$

$$F_3{}' = \beta\left[(e^\tau + e^y) \wedge a_2 + b_3\right]\,, \tag{5.9}$$

$$F_5{}' = F_5^0 + B'_2 \wedge F'_3\,, \tag{5.10}$$

$$\Phi' = \Phi_0 - \frac{1}{2}\log K\,, \tag{5.11}$$

where $||\mathrm{g}_{ab}||$ is the determinant of the initial metric in the τ-y-χ directions, and

$$K = 1 + \beta^2(\mathrm{g}_{\chi\chi}(\mathrm{g}_{\tau\tau} + \mathrm{g}_{yy} - 2\mathrm{g}_{\tau y}) - (\mathrm{g}_{y\chi} - \mathrm{g}_{\tau\chi})^2)\,, \tag{5.12}$$

$$B'_{\tau y} = \frac{\beta}{K}(\mathrm{g}_{\tau\chi}(\mathrm{g}_{yy} - \mathrm{g}_{\tau y}) + \mathrm{g}_{y\chi}(\mathrm{g}_{\tau\tau} - \mathrm{g}_{\tau y}))\,, \tag{5.13}$$

$$B'_{\tau\chi} = \frac{\beta}{K}(\mathrm{g}_{\tau\chi}(\mathrm{g}_{y\chi} - \mathrm{g}_{\tau\chi}) + \mathrm{g}_{\chi\chi}(\mathrm{g}_{\tau\tau} - \mathrm{g}_{\tau y}))\,, \tag{5.14}$$

$$B'_{y\chi} = \frac{\beta}{K}(\mathrm{g}_{y\chi}(\mathrm{g}_{y\chi} - \mathrm{g}_{\tau\chi}) + \mathrm{g}_{\chi\chi}(\mathrm{g}_{\tau y} - \mathrm{g}_{yy}))\,. \tag{5.15}$$

Note that the only change in the metric is the squashing of the (τ, y, χ) part by $1/K$ and the addition of a single new term in the $(\tau + y)$-direction. In addition a B-field is generated, as well as a varying dilaton.

We also see that the RR flux now includes not only a 5-form but also, in general, a 3-form. The RR 3-form is non-vanishing only if the five-form terms written explicitly in (5.6) are nonzero.

For all the explicit examples considered in this note, τ and y will be part of a noncompact five-dimensional geometry, M, and χ will be on a compact Sasaki-Einstein space; when these two factors of the geometry are orthogonal in the metric and $F_5^0 = (1+*)\mathrm{vol}_M$, as is the case for the uncharged, non-rotating black hole examples of [128, 127, 126], it is easy to see F_3 vanishes. In general, however, F_3 is nonzero, as will be the case for the charged examples we study in the following sections.

5.2.2 Light Cone Coordinates

The form of the solution simplifies considerably if we rotate initial and final solutions to a light-cone frame defined by,

$$t = \beta(\tau + y)\,, \qquad \xi = \frac{1}{2\beta}(y - \tau)\,.$$

In the asymptotically Schrödinger examples of interest in the following sections, this is also the physically useful choice, as ∂_t becomes the canonically normalized generator of time translations in the asymptotic region. Note that this transformation is unimodular, so we don't have to worry about Jacobians.

In light cone frame, the new term in the metric becomes diagonal, and the Melvinized solution takes the simpler form,

$$ds^{2\prime} = \frac{||\mathrm{g}_{ab}||}{K} e^t e^t + \frac{1}{K}\,\mathrm{g}_{ab}\,e^a e^b + \mathcal{G}_{ij}\,dx^i dx^j\,, \tag{5.16}$$

$$B_2' = \frac{\sqrt{|\mathrm{g}|}}{K}\,*_{\mathrm{g}} e^t\,, \tag{5.17}$$

$$F_3' = i_\chi i_\xi F_5^0\,, \tag{5.18}$$

$$F_5' = F_5^0 + B_2' \wedge F_3'\,, \tag{5.19}$$

$$\Phi' = \Phi_0 - \frac{1}{2}\log K\,, \tag{5.20}$$

where i is the inclusion acting as $i_X(e^X \wedge Y) \equiv Y$, and

$$K = 1 + (g_{\chi\chi} g_{\xi\xi} - g_{\xi\chi}^2)\,.$$

The components of B take a simple form in terms of minors,

$$B_{t\xi} = \frac{1}{K}(g_{\xi\xi}g_{t\chi} - g_{t\xi}g_{\xi\chi})\,, \qquad B_{t\chi} = \frac{1}{K}(g_{\chi\xi}g_{t\chi} - g_{t\xi}g_{\chi\chi})\,, \qquad B_{\xi\chi} = \frac{1}{K}(g_{\xi\chi}^2 - g_{\xi\xi}g_{\chi\chi})\,.$$

Note that all factors of β have been absorbed by the change of coordinates.

5.2.3 Melvinizing Solutions of 5d Gauged Supergravity

Melvin maps ten-dimensional solutions to ten-dimensional solutions. In using Melvin to build Schrödinger black holes, we will generally begin with a five-dimensional AdS black hole, lift it to ten dimensions, Melvinize, and then reduce back to five dimensions. It is therefore convenient to write down a formula circumventing the side-trip to ten dimensions, and simply mapping one five-dimensional geometry into another. In this subsection we choose a 10d ansatz corresponding to 5d gauged supergravity and construct a five to five map.

Suppose our initial metric solution takes the Kaluza-Klein form [137, 138],

$$ds_{10}^2 \quad = \quad ds_5^2(M) + ds^2(X) + (\eta + A_q)^2\,, \tag{5.21}$$

where M is a five-dimensional Lorentzian spacetime on which the isometries ∂_t and ∂_ξ act, X is a compact Kähler-Einstein 4-manifold, $\eta \equiv d\chi + \mathcal{A}$ defines a Sasaki-Einstein fibration Y over X, and A_q is a 1-form on M. For example if $X = \mathbb{P}^2$, η is then the Hopf fiber on S^5; see appendix B.1 for more details. We can always cast the 5d metric in the form,

$$ds_5^2(M) = G_{\alpha\beta}\, e^\alpha e^\beta + G_{mn} dx^m dx^n\,, \tag{5.22}$$

with α, β running over only t, ξ and m, n over the remaining three spatial dimensions, where $e^t \equiv dt + A^t_m dx^m$ and $e^\xi \equiv d\xi + A^\xi_m dx^m$ contain the cross terms between the t, ξ directions and the other three, but not each other. (One may equally well use the coordinates τ, y, for which analogous statements hold.) Additionally, the 1-form A_q can be written as

$$A_q = A_{q(\alpha)} e^\alpha + A_{q(m)} dx^m\,. \tag{5.23}$$

We assume as before a constant dilaton, self-dual five-form F_5^0 and no other fields. The 5-form that supports the metric (5.21) has the form [137, 138, 127]

$$\begin{aligned} F_5^0 &= -4\mathrm{vol}_M + \frac{1}{2}(\eta + A_q)\wedge d\mathcal{A}\wedge d\mathcal{A} \\ &\quad + \frac{1}{2} *_5 F_q \wedge d\mathcal{A} - \frac{1}{2}F_q\wedge(\eta + A_q)\wedge d\mathcal{A}\,, \end{aligned} \tag{5.24}$$

where each line is self-dual by itself; the top line contains the volume form on M and its Hodge dual, and the second line contains a factor of $F_q \equiv dA_q$. The Bianchi identity $dF_5^0 = 0$ implies

$$d *_5 F_q = F_q \wedge F_q\,, \tag{5.25}$$

which must be satisfied by any initial solution. Solutions of the form (5.21), (5.24) include the various charged, rotating AdS_5 black holes which we will study. The dimensional reduction of this ansatz is precisely minimal gauged supergravity in five dimensions,

$$2\kappa_5^2\, S_5 = \int \mathrm{vol}_M(R^{(5)} + 12) - \frac{3}{2}\int F_q\wedge *_5F_q + \int A_q\wedge F_q\wedge F_q\,, \tag{5.26}$$

where the canonically normalized gauge field is $A \equiv \sqrt{3}A_q$, and the pre-Melvinized 5D metric and gauge field A_q are solutions to the equation of motion coming from this action.

We can now apply the Melvin machine to this 10d solution. Using e^t and e^ξ (or e^τ and e^y) from (5.22) and defining $e^\chi \equiv \eta + A_{q(m)}dx^m$ to be our 1-forms (5.5), we find the resulting 10d solution,

$$ds_{10}^{2\,\prime} = ds_5^2(M)' + ds_X^2 + e^{2V}(\eta + A_q)^2\,, \tag{5.27}$$

$$F_5' = F_5^0 + B_2'\wedge F_3'\,, \tag{5.28}$$

$$F_3' = f\wedge d\eta\,, \tag{5.29}$$

$$B_2' = A_M\wedge(\eta + A_q)\,, \tag{5.30}$$

$$\Phi' = \Phi_0 - \frac{1}{2}\log K\,, \tag{5.31}$$

where the new five-dimensional metric takes the form

$$ds_5^2(M)' = \frac{||G_{\alpha\beta}||}{K}e^te^t + \frac{1}{K}G_{\alpha\beta}\,e^\alpha e^\beta + G_{mn}\,dx^m dx^n\,, \tag{5.32}$$

with $||G_{\alpha\beta}|| \equiv G_{tt}G_{\xi\xi} - G_{t\xi}^2 = G_{\tau\tau}G_{yy} - G_{\tau y}^2$, and

$$K = e^{-2V} = 1 + G_{\xi\xi}\,, \tag{5.33}$$

and where we have defined 1-forms A_M and f on M:

$$A_M = -e^{2V}G_{\xi\alpha}e^{\alpha}\,, \qquad f = -\frac{1}{2}dA_{q(\xi)}\,. \tag{5.34}$$

Importantly, the vector A_q does not change.

In the original τ-y coordinates, this takes the equivalently simple form,

$$\begin{aligned} ds_5^2(M)' &= \frac{\beta^2||G_{\alpha\beta}||}{K}(e^{\tau}+e^{y})^2 + \frac{1}{K}G_{\alpha\beta}\,e^{\alpha}e^{\beta} + G_{mn}\,dx^m dx^n\,, && (5.35)\\ K &= e^{-2V} = 1 + \beta^2(G_{\tau\tau} + G_{yy} - 2G_{\tau y})\,, && (5.36)\\ A_M &= -\beta e^{2V}(G_{y\alpha} - G_{\tau\alpha})e^{\alpha}\,, \qquad f = -\frac{\beta}{2}d(A_{q(y)} - A_{q(\tau)})\,, && (5.37) \end{aligned}$$

where now α, β run over τ and y.

Notice that the Melvinized 5D metric does not involve A_q or any other data, but only components of the original 5D metric tensor. In the case where $G_{t\xi} = 0$, one can see that

$$G'_{tt} = \frac{1}{K}(G_{tt} + G_{tt}G_{\xi\xi}) = G_{tt}\,, \qquad (G_{t\xi} = 0)\,, \tag{5.38}$$

and hence only the $G'_{\xi\xi} = G_{\xi\xi}/(1 + G_{\xi\xi})$ component changes in this case. The generalization of this observation to $G_{t\xi} \neq 0$ can be found in appendix B.3.

The metric also determines the new vector field A_M, while the gauge field A_q fixes f. The nature of the vector A_M can be understood more easily if we raise its index, with either the pre-Melvinized or post-Melvinized 5D metric. Either way we find it points purely in the ξ-direction:

$$G'^{\mu\nu}(A_M)_{\nu} = -\delta^{\mu}_{\xi} = e^{-2V}G^{\mu\nu}(A_M)_{\nu}\,. \tag{5.39}$$

In particular, this implies that A_M is (minus) the ξ-Killing vector with respect to the Melvinized metric.

We now turn to dimensionally reducing the 10D type IIB supergravity action to five dimensions using (5.27)-(5.31) as an ansatz for the fields; see Appendix C for further details. Since $V = \Phi$

in our solution, the simplest dimension reduction involves setting them equal and keeping only this single scalar field.[1] We find the (string frame) result,

$$
\begin{aligned}
2\kappa_5^2\, S_5 \;=\; & \int \mathrm{vol}_M e^{-\Phi}\left[R'^{(5)} + 16 - 4e^{2\Phi}\right] - \frac{1}{2}\int e^{\Phi} F_q \wedge *_5' F_q \\
& - \int e^{-\Phi}(F_q - 2f\wedge A_M)\wedge *_5'(F_q - 2f\wedge A_M) + \int A_q \wedge F_q \wedge F_q - \frac{1}{2}\int 8e^{\Phi} f \wedge *_5' f \\
& - \frac{1}{2}\int \left[e^{-\Phi}(A_M\wedge F_q)\wedge *_5'(A_M \wedge F_q) + e^{-3\Phi} F_M \wedge *_5' F_M + 8e^{-\Phi} A_M \wedge *_5' A_M\right],
\end{aligned} \tag{5.40}
$$

with $2\kappa_5^2 \equiv 2\kappa_{10}^2/\mathrm{vol}(S^5)$. Thus upon KK reduction on Y, the five-dimensional effective dynamics includes the metric $ds_5^{2\prime}$; a massless vector A_q, which was present in the 10D metric before the Melvin map acted; a massive vector A_M coming from B_2 of the type that is by now standard in Schrödinger-type backgrounds; and a scalar Φ. Upon setting $\Phi = V$ the kinetic term for the combined field vanishes, but it will reappear in Einstein frame.

Note that f, the field characterizing F_3, is completely fixed by the vectors A_M and A_q and is not an independent mode. The field equation for f involves no derivatives, consistent with what we obtain from reducing the ten-dimensional F_3 equation of motion. Varying (5.40) with respect to f, we obtain

$$
f = -\frac{1}{2}e^{-2\Phi} *_5' \Big(A_M \wedge *_5'(F_q - 2f\wedge A_M)\Big), \tag{5.41}
$$

$$
= -\frac{1}{2}e^{-2\Phi} *_5 (A_M \wedge *_5 F_q), \tag{5.42}
$$

where in the second line we used the results (B.34), (B.30) and (B.29); evaluating the Hodge stars and using that A_M is a Killing vector for ξ (5.39) gives us precisely the expression (5.34) for f.

To pass to five-dimensional Einstein frame, we define

$$
G^E_{\mu\nu} \equiv e^{-2\Phi/3} G_{\mu\nu}\,. \tag{5.43}
$$

[1] We have set $\Phi_0 = 0$ for convenience; it can easily be restored if necessary.

This leads to the 5D Einstein frame action,

$$
\begin{aligned}
2\kappa_5^2\, S_{5,E} \;=\; & \int \mathrm{vol}_M^E \left[R'^{(5)}_E - \frac{4}{3}\partial_\mu \Phi \partial^{\mu'_E}\Phi + 16 e^{2\Phi/3} - 4 e^{8\Phi/3} \right] - \frac{1}{2}\int e^{4\Phi/3} F_q \wedge *'_E F_q \\
& - \int e^{-2\Phi/3} (F_q - 2f\wedge A_M) \wedge *'_E (F_q - 2f \wedge A_M) \\
& + \int A_q \wedge F_q \wedge F_q - \frac{1}{2}\int 8 e^{2\Phi} f \wedge *'_E f \\
& - \frac{1}{2}\int \left[e^{-4\Phi/3}(A_M\wedge F_q)\wedge *'_E (A_M \wedge F_q) + e^{-8\Phi/3} F_M \wedge *'_E F_M + 8 A_M \wedge *'_E A_M \right].
\end{aligned}
\tag{5.44}
$$

The limit of the action in either frame (5.40) or (5.44) where $A_M = \Phi = f = 0$ is simply minimal gauged supergravity (5.26).

5.3 Properties of Melvinized Black Holes

In this section, we study the general properties of generic Schrödinger black holes which arise by Melvinization, including their thermodynamics, extremal limits and near-horizon geometries.

It was shown in [127, 128, 126] that Melvinizing the Schwarzschild-AdS_5 black hole leads to a special asymptotically Schrödinger black hole whose odd thermodynamic properties are a consequence of its origin.[2] As we shall see, a number of features of the charged and rotating asymptotically Schrödinger black holes derived via Melvinization are similarly inherited from their pre-Melvin progenitors– in particular, their temperature, entropy, chemical potential and properties of the near-horizon geometry.

Consider a black hole metric of the class in (5.22), with the particular form

$$
ds_5^2(M) = G_{\tau\tau}(e^\tau)^2 + 2G_{y\tau} e^y e^\tau + G_{yy}(e^y)^2 + G_{rr} dr^2 + G_{ij} dx^i dx^j\,, \tag{5.45}
$$

where we choose Schwarzschild-like coordinates where $G^{rr} \to 0$ at the horizon $r = r_+$. We use τ and y, rather than t and ξ, as the more natural coordinates near the horizon. The Melvinized

[2] This unusual thermodynamics, which we will recapitulate below, was shown to similarly follow from DLCQ in the dual field theory in an interesting paper by Barbon and Fuertes[144]; see also [143] for a discussion of the more lenient constraints of Schrödinger symmetry on the thermodynamic potentials.

solution is obtained from (5.35), and passing to Einstein frame produces an extra factor of $K^{1/3}$:

$$\begin{aligned} ds_5^2(M)' &= \frac{1}{K^{2/3}}\Big(G_{\tau\tau}(e^\tau)^2 + 2G_{y\tau}e^y e^\tau + G_{yy}(e^y)^2 + \beta^2(G_{\tau\tau}G_{yy} - G_{y\tau}^2)(e^\tau + e^y)^2\Big) \\ &\quad + K^{1/3}G_{rr}dr^2 + K^{1/3}G_{ij}dx^i dx^j\,, \end{aligned} \tag{5.46}$$

where as before

$$K = 1 + \beta^2(G_{\tau\tau} + G_{yy} - 2G_{y\tau})\,. \tag{5.47}$$

In general K is finite and nonzero at the horizon; as long as this holds, the horizon still exists at the same radius $G'^{rr}(r = r_+) = 0$ after the Melvin map is performed. We will now enumerate a number of thermodynamic properties related to this horizon.

For simplicity, here we will consider the class of black holes where $e^\tau = d\tau$. This restricts the only possible rotation of the hole to be along the y-direction, which encompasses our examples. There is no reason this analysis cannot be generalized.

The divergence of $G_{rr} \to \infty$ at the horizon is in general accompanied by a corresponding zero in the determinant of G, so that the volume element remains finite at the coordinate singularity. When $G_{\tau y} = 0$, it is $G_{\tau\tau} \to 0$ that provides this zero; when $G_{\tau y}$ is nonzero, $G_{\tau\tau}$ vanishes at the stationary limit surface, which may not coincide with the horizon, and instead the determinant of the τ-y metric vanishes at the horizon. To emphasize this we can write the metric in the non-coordinate form

$$\begin{aligned} ds_5^2(M) &= \mathcal{G}_{\tau\tau}d\tau^2 + \mathcal{G}_{yy}\Big(e^y + \frac{G_{\tau y}}{G_{yy}}d\tau\Big)^2 + G_{rr}dr^2 + G_{ij}dx^i dx^j\,, \\ \mathcal{G}_{\tau\tau} &\equiv \frac{G_{\tau\tau}G_{yy} - G_{\tau y}^2}{G_{yy}}\,, \qquad \mathcal{G}_{yy} \equiv G_{yy}\,. \end{aligned} \tag{5.48}$$

In general at the horizon $\mathcal{G}_{\tau\tau} \to 0$, and we shall assume this is the case in what follows.

5.3.1 Entropy

The entropy of the black hole is simply proportional to the area of the horizon, $S = A/4G_5$, integrated at constant τ and $r = r_+$. For the unMelvinized solution, this reads

$$S = \frac{1}{4G_5}\int \sqrt{G_3} = \frac{1}{4G_5}\int \sqrt{G_{yy}\det(G_{ij})}\,. \tag{5.49}$$

In the Melvin case we get

$$S' = \frac{1}{4G_5}\int\sqrt{G_3'} = \frac{1}{4G}\int\sqrt{K^{-2/3}(G_{yy}+\beta^2(G_{\tau\tau}G_{yy}-G_{\tau y}^2))\det(K^{1/3}G_{ij})}\,, \tag{5.50}$$

$$= \frac{1}{4G_5}\int\sqrt{G_{yy}\det(G_{ij})} = S\,, \tag{5.51}$$

where we used $G_{\tau\tau}G_{yy}-G_{\tau y}^2 = 0$ at the horizon, and found the factors of K to cancel. Thus the area of the horizon, and consequently its entropy, is unchanged by the Melvin map.

5.3.2 Temperature and Chemical Potential

The temperature is most easily calculated by analytically continuing to imaginary time and verifying that the region near the horizon in the τ-r plane is free of conical singularities. This is conveniently done with the metric in the form (5.48), and we find

$$T = \lim_{r\to r_+}\frac{1}{2\pi\sqrt{G_{rr}}}\frac{d}{dr}\sqrt{\mathcal{G}_{\tau\tau}}\,. \tag{5.52}$$

Under the Melvin map, the relevant quantities transform like (in Einstein frame),

$$\mathcal{G}'_{\tau\tau} = K^{1/3}\frac{\mathcal{G}_{\tau\tau}}{1+\beta^2\mathcal{G}_{\tau\tau}}\,, \qquad G'_{rr} = K^{1/3}G_{rr}\,, \tag{5.53}$$

and using the vanishing $\mathcal{G}_{\tau\tau}(r\to r_+)\to 0$ at the horizon,

$$\frac{d}{dr}\sqrt{\mathcal{G}'_{\tau\tau}} = K^{1/3}\left(\frac{d}{dr}\sqrt{\mathcal{G}_{\tau\tau}}\right)(1+\mathcal{O}(\mathcal{G}_{\tau\tau}))\,, \tag{5.54}$$

where we assumed the regularity of dK/dr at the horizon, implying

$$T' = \lim_{r\to r_+}\frac{1}{2\pi\sqrt{G'_{rr}}}\frac{d}{dr}\sqrt{\mathcal{G}'_{\tau\tau}} = T\,, \tag{5.55}$$

and thus the temperature is unchanged by the Melvin map.

This result assumes the temperature is defined with respect to the same Killing generator of the event horizon both before and after the Melvin transformation. One does have to take into account the change from using $i\partial_\tau$ as the asymptotic time coordinate, as is suitable for an AdS black hole, to using $i\partial_t$ as the asymptotic time coordinate as suits the Schrödinger cases.

In our class of solutions, the generator of the Killing horizons can take the form

$$\begin{aligned} \chi &= \partial_\tau + \Omega_H \partial_y && (5.56) \\ &= \beta(1+\Omega_H)\partial_t - \frac{1}{2\beta}(1-\Omega_H)\partial_\xi\,, && (5.57) \end{aligned}$$

where Ω_H parameterizes rotation in the y-direction; χ has unit coefficient with respect to the τ-coordinate. To switch to a generator suited to the t-coordinate, we define

$$\chi_t \equiv \frac{1}{\beta(1+\Omega_H)}\chi = \partial_t - \frac{1}{2\beta^2}\frac{1-\Omega_H}{1+\Omega_H}\partial_\xi\,. \tag{5.58}$$

Since the temperature may be defined as $T \equiv \kappa/(2\pi)$ where the surface gravity κ is

$$\kappa^2 \equiv -\frac{1}{2}(\nabla_\mu \chi_\nu)(\nabla^\mu \chi^\nu)\,, \tag{5.59}$$

we see that the shift in coordinates to the Schrödinger time t produces a rescaling of the temperature,

$$T_t = \frac{T_\tau}{\beta(1+\Omega_H)}\,. \tag{5.60}$$

We can also read the chemical potential off the expression (5.58). Since $i\partial_t$ corresponds to the Hamiltonian H while $i\partial_\xi$ is the number operator N, we obtain the chemical potential from the identification $\chi_t \sim H + \mu N$ for the grand canonical ensemble,

$$\mu = \frac{1}{2\beta^2}\frac{\Omega_H - 1}{\Omega_H + 1}\,. \tag{5.61}$$

5.3.3 Near-horizon limit

One of our main goals in studying charged and rotating asymptotically Schrödinger black holes is to find extremal examples with scale-invariant near-horizon geometries, or throats. Quite apart from just being unusually simple, such extremal black holes have become important tools in the application of gauge-gravity duality in a number of contexts, most notably in the holographic description of (non-)fermi liquids [134].[3]

[3] The reason throats are important is easy to see. When the near-horizon region has a scaling invariance (for example, the near-horizon AdS_2 symmetry of the extremal RN-AdS_4 black holes), taking a scaling limit allows one to consistently decouple the modes near the horizon from the modes near the boundary. Since the horizon and boundary are holographically related to IR and UV physics, this means that at least some aspects of UV and IR physics may be studied independently of each other, a powerful statement of universality. This view is elegantly presented in [139] and by Liu in a talk at the KITP on July 7, 2009.

A number of extremal black holes are known to have near-horizon AdS_2 regions. We now show that if this is the case for the pre-Melvin extremal metric, the Melvinized result also has an AdS_2 region, albeit with a different radius of curvature. Recall that the AdS portion of the near-horizon limit of the original AdS_5 black hole came from the $\mathcal{G}_{\tau\tau}d\tau^2 + G_{rr}dr^2$ portion of the metric. Under the Melvin map above, this sector becomes,

$$\mathcal{G}_{\tau\tau}d\tau^2 + G_{rr}dr^2 \quad \rightarrow \quad K^{1/3}\left(\mathcal{G}_{\tau\tau}(1+\mathcal{O}(\mathcal{G}_{\tau\tau}))d\tau^2 + G_{rr}dr^2\right) . \tag{5.62}$$

The near-horizon geometry is thus simply rescaled by a factor of $K^{1/3}$ common to both terms. In the case of an extremal black hole with a near-horizon AdS_2 region, the Melvinized Schrödinger version will have an analogous AdS_2 region, with the AdS radius rescaled by the factor $K^{1/6}$.

Due to the different scalings of the y direction from the x and z directions under Melvin, the remaining three-dimensional space is in general squashed by a factor of K. In the planar limit, this is a completely trivial rescaling of the flat spatial section. When the spatial section is S^3, however, the net result is a squashing of the S^3.

One interesting consequence of this result is that the radius of curvature of the near-horizon region is now independent of that of the asymptotic region – explicitly, K depends on β^2, which can be tuned independently. That the radius of curvature of the extremal throat depends explicitly on the density of non-relativistic excitations in the boundary theory is an interesting result, and may play in important role in understanding holography in this spacetime.

5.4 Examples: Schrödinger black holes with charge

In this section, we apply our Melvin map to a pair of five-dimensional AdS black holes, and explicitly write down the resulting backgrounds. We also discuss thermodynamic properties, and find the results consistent with the previous section where we showed they are unchanged by Melvin, modulo the coordinate transformations needed for asymptotically Schrödinger solutions. First we consider a charged AdS black hole in the Poincaré patch; this will give us the simplest charged Schrödinger black hole. Then we examine the more complicated case of a charged black hole in global coordinates, rotating along the Hopf fiber of the global S^3; this includes as a limiting case the chargeless rotating black hole.

5.4.1 Charged Schrödinger black hole

As a first application of our results, we can construct the first charged black hole with asymptotic Schrödinger symmetries, which we call RN-Sch$_5$ for Reissner-Nordstrom-Schrödinger in five dimensions.

Our pre-Melvinized solution is a five-dimensional RN-AdS$_5$ black hole. This solution is associated to a ten-dimensional solution of D3-branes rotating around the Hopf direction χ of the S^5 [137, 138]. The five-dimensional metric and gauge field are

$$ds^2 = \frac{1}{r^2}\left[-\frac{f}{H^2}d\tau^2 + H\left(\frac{dr^2}{f} + d\vec{x}^2\right)\right]\,, \qquad A_q = \frac{qr^2}{Hr_H^2}d\tau\,, \tag{5.63}$$

where q is the charge, and

$$f \equiv H^3 - \frac{r^4}{r_H^4}\,, \qquad H \equiv 1 + q^2 r^2\,. \tag{5.64}$$

Note that r_H is the location of the horizon in the *un*charged geometry; it is related to the mass parameter m by $r_H^4 = 1/2m$. In what follows we use r_+ to denote the true horizon radius. This background is a solution to the action (5.26) for five-dimensional minimal gauged supergravity, and lifts to a ten-dimensional solution of type IIB supergravity described by (5.21), (5.24) with $X = \mathbb{P}^2$ and $\eta = \eta^{(5)}$ the Hopf fiber generating the map $S^1 \to S^5 \to \mathbb{P}^2$; see appendix B.1 for more details.

We now turn the Melvinization crank as outlined in the section 5.2, with $e^\tau = d\tau$ and $e^y = dy$; the directions x, y, z are all equivalent and so the choice of Melvin direction is arbitrary. We arrive at the five dimensional charged Schrödinger solution in Einstein frame:

$$ds^2 = \frac{K^{1/3}}{r^2}\left[-\frac{f}{H^2K}d\tau^2 - \frac{f\beta^2}{r^2HK}(d\tau + dy)^2 + \frac{H}{K}dy^2 + H\left(\frac{dr^2}{f} + dx^2 + dz^2\right)\right]\,, \tag{5.65}$$

with

$$K = 1 + \frac{\beta^2 r^2}{H^2 r_H^4}\,. \tag{5.66}$$

The overall factor of $K^{1/3}$ is absent in string frame. For the special case $q = 0$, (5.65) is precisely the uncharged Schrödinger geometry previously studied in [128, 127, 126].

Entropy The entropy S associated with (5.65) is easily computed via the Beckenstein-Hawking result $S = A/4G_5$ where A is the area of the horizon, and G_5 is the gravitational constant in five dimensions. Performing this calulation, we find for the entropy density,

$$s \equiv \frac{S}{V_{x,y,z}} = \frac{1}{4G_5\, r_H^2 r_+} = \frac{H(r_+)^{3/2}}{4G_5 r_+^3} \tag{5.67}$$

where $V_{x,y,z}$ is the (infinite) horizon volume. Again, in the limit $q \to 0$ ($r_+ \to r_H$), this result agrees with those obtained in [128, 127, 126]. Furthermore, it is manifestly independent of β, demonstrating that it was not changed by the Melvin procedure, consistent with our general argument in the previous section.

Temperature and Chemical Potential The corresponding Hawking temperature is readily calculated from the relation $T = \kappa/2\pi$ where κ is the surface gravity of the horizon (5.59). As discussed in the previous section, to obtain the temperature associated with the asymptotic Schrödinger Hamiltonian $H = i\partial_t$ we should take the generator the horizon to be $\chi_t = \partial_\tau/\beta$; we have $\Omega_H = 0$ in this nonrotating case. We then find

$$T = \frac{\left|f'(r_+)\right|}{4\pi\beta}\left(\frac{r_H}{r_+}\right)^2 = \frac{\sqrt{H(r_+)}}{2\pi\beta\, r_+}\Big|H(r_+) - 3\Big|\,. \tag{5.68}$$

Notice that the temperature vanishes when $H(r_+) = 3$, which implies the geometry becomes extremal when

$$q = \frac{\sqrt{2}}{r_+}\,. \tag{5.69}$$

We will use this fact in the following section. The temperature corresponding to the asymptotic τ-coordinate is βT, which is manifestly β-independent and thus unchanged by Melvin.

Because χ_t takes the form

$$\chi_t = \frac{1}{\beta}\partial_\tau = \partial_t - \frac{1}{2\beta^2}\partial_\xi\,, \tag{5.70}$$

we can read off the chemical potential for for ξ-translations as

$$\mu = -\frac{1}{2\beta^2}\,, \tag{5.71}$$

consistent with the previous section.

On Shell Action A straightforward, if tedious, application of familiar techniques from holographic renormalization allows us to construct a renormalized on-shell action for this solution. Dispensing with the technicalities, the result is,

$$S_5 = -\frac{1}{16\kappa_5}\int dx^4 \frac{H[r_+]^3(1-2q^2\beta^2)}{r_+^4}\,. \tag{5.72}$$

Continuing to periodically identified euclidean time then gives the on-shell Euclidean action,

$$S_E = -\frac{\pi\beta V}{8\kappa_5}\frac{H[r_+]^{5/2}(1-2q^2\beta^2)}{r_+^3\,|H(r_+)-3|}\,. \tag{5.73}$$

which we would like to identify as the action of a saddle-point approximation to the full grand-canonical partition function.

The Extremal, Near-Horizon Limit Near the horizon of an extremal Reissner-Nordstrom black hole, the geometry becomes a direct product space with one factor AdS_2. We expect an analogous limit for the extremal version of (5.65). To obtain this, we define the deviation from the horizon ζ,

$$\zeta \equiv \frac{r}{r_+} - 1\,, \tag{5.74}$$

and expand the metric (5.65) in the extremal limit (5.69) in powers of ζ. The horizon in the extremal case is located at

$$r_+ = 27^{1/4}\,r_H = \left(\frac{27}{2m}\right)^{1/4}\,. \tag{5.75}$$

Shifting τ to absorb the cross term with y, rescaling the coordinates and inverting $\zeta = 1/\rho$, we find the near-horizon result

$$ds^2 = \frac{L^2}{\rho^2}\left(d\tau^2 + d\rho^2\right) + dx^2 + dy^2 + dz^2\,. \tag{5.76}$$

Lo and behold, the limiting form is $\mathrm{AdS}_2 \times \mathbb{R}^3$, with AdS radius

$$L^2 = \frac{K(r_+)^{1/3}}{12} = \frac{\left(1 + 3\beta^2/r_+^2\right)^{1/3}}{12}\,, \tag{5.77}$$

which as anticipated, depends on β.

5.4.2 Charged, Hopf-rotating Schrödinger black hole

We now turn to a more complicated example, a charged AdS black hole that is also rotating. In five dimensions there are two independent rotation parameters, in the literature usually termed a and b; we focus on the case where $b = a$, corresponding to rotation along the Hopf fiber of the S^3 of global AdS. The uncharged version of this solution was written in [140], while the charged version, which is a solution to minimal gauged supergravity (5.26) was formulated in [141]. The solution reads in our conventions

$$\begin{aligned} ds^2 &= -\frac{q + \sigma^2(1+\rho^2/L^2)}{\sigma^2\Delta} d\tau^2 + \frac{f + q\sigma^2\Delta}{\sigma^4\Delta^2}\left(d\tau - a\,\eta^{(3)}\right)^2 \\ &\quad + \frac{\sigma^2}{\Delta_\rho} d\rho^2 + \frac{\sigma^2}{\Delta}\left[ds^2_{\mathbb{P}^1} + \left(1 + \frac{q\,a^2}{\sigma^4}\right)(\eta^{(3)})^2\right]\,, \end{aligned} \tag{5.78}$$

$$A_q = \frac{q}{\sigma^2\Delta}\left(d\tau - a\,\eta^{(3)}\right)\,, \tag{5.79}$$

where $\eta^{(3)}$ is the vertical 1-form along the Hopf fibre of the S^3, as described in appendix B.1, and

$$\begin{aligned} \Delta &= 1 - a^2/L^2\,, \qquad \sigma^2 = \rho^2 + a^2\,, \qquad f = 2m\,\sigma^2 + 2q\,a^2\sigma^2/L^2 - q^2\,, \\ \Delta_\rho &= \frac{q^2 + 2qa^2 + \sigma^4(1+\rho^2/L^2) - 2m\rho^2}{\rho^2}\,. \end{aligned} \tag{5.80}$$

In the limit $a \to 0$ this solution becomes the RN-AdS_5 black hole in global coordinates, while for $q \to 0$ it reduces to the uncharged AdS-Kerr black hole rotating along the Hopf fiber.

This solution is readily Melvinized. We take $e^\tau = d\tau$, $e^\psi = 2\eta^{(3)} = d\psi + \cos\theta d\phi$, where ψ takes the place of y as the T-duality direction; we are thus choosing the Hopf direction for the y-isometry. The resulting Melvinized Kerr-Newman-Sch_5 metric is then

$$\begin{aligned} ds^2 &= -\frac{q + \sigma^2(1+\rho^2/L^2)}{K\sigma^2\Delta} d\tau^2 + \frac{f + q\sigma^2\Delta}{K\sigma^4\Delta^2}\left(d\tau - a\,\eta^{(3)}\right)^2 + \frac{\sigma^2}{K\Delta}\left(1 + \frac{q\,a^2}{\sigma^4}\right)(\eta^{(3)})^2 \\ &\quad - \frac{\beta^2\rho^2\,\Delta_\rho}{4\Delta^2\sigma^2 K}(d\tau + 2\eta^{(3)})^2 + \frac{\sigma^2}{\Delta_\rho} d\rho^2 + \frac{\sigma^2}{\Delta} ds^2_{\mathbb{P}^1}\,, \end{aligned} \tag{5.81}$$

where

$$K = 1 + \beta^2 \left(\frac{f(2+a)^2}{4\Delta^2\sigma^4} + \frac{a(2+a)q}{2\Delta\sigma^2} + \frac{\sigma^2 - 4(1+\rho^2/L^2)}{4\Delta} \right) . \tag{5.82}$$

Entropy, Temperature and Chemical Potential The entropy density associated with this geometry is found to be

$$s = \frac{\sigma_+^4 + a^2 q}{4G_5\,\Delta^2\,\rho_+} \tag{5.83}$$

which, as expected, is independent of β and hence identical to that obtained from the 5D un-Melvinized metric. As a result, it agrees with [141].

To determine the temperature and chemical potential, it is necessary to compute the null generator of the horizon for this geometry. Because the metric is stationary but not static, the generator will be of the form $\chi \propto \partial_\tau + \Omega_H \partial_\psi$ where Ω_H is the angular velocity of a test particle at location ρ_+. By considering a photon emitted in the ψ direction at fixed ρ, θ, and ϕ, it is easy to show that,

$$\Omega_H = \frac{2a\left(\sigma_+^2\left(1+\rho_+^2\right)+q\right)}{\sigma_+^4 + a^2 q} . \tag{5.84}$$

This too is unchanged by Melvinization. As is by now familiar, to use our null generator for asymptotically Schrödinger thermodynamics, one must normalize it such that the coefficient of ∂_t is one. As in (5.58), this amounts to a scaling by $1/\beta(1+\Omega_H)$:

$$\chi_t = \partial_t + \frac{1}{2\beta^2}\left(\frac{\Omega_H - 1}{\Omega_H + 1}\right)\partial_\xi , \tag{5.85}$$

from which we easily read off the chemical potential

$$\mu = \frac{1}{2\beta^2}\left(\frac{\Omega_H - 1}{\Omega_H + 1}\right) . \tag{5.86}$$

We note that the rotation of the original AdS black hole has been converted into a rescaling of the chemical potential for the corresponding Schrödinger geometry. In particular, there is no spatial rotation associated to the $(2+1)$-dimensional field theory dual spacetime. Such a rotation could be obtained by considering the Melvin map on an AdS black hole with two independent angular momenta.

The temperature must also be identical to that of the un-Melvinized $5d$ geometry [141], up to a rescaling introduced by the properly normalized null generator, and we find

$$T = \frac{1}{2\pi\beta}\frac{\rho_+^4\left(1+2\sigma_+^2\right)-(a^2+q)^2}{\rho_+\left(1+\Omega_H\right)\left(\sigma_+^4+a^2q\right)}\,. \tag{5.87}$$

<u>**The Extremal, Near Horizon Limit**</u> From (5.87), it is easy to see that the geometry becomes extremal when

$$q = -a^2 \pm \rho_+^2\sqrt{1+2\sigma_+^2}\,. \tag{5.88}$$

Using this fact, we can again study the near horizon limit of the extremal solution, whose horizon is located at

$$\rho_+ = \frac{1}{\sqrt{3}}\left[\sqrt{1+6m+a^2(a^2-2)}-1-2a^2\right]^{1/2}\,. \tag{5.89}$$

As before, we scale the radial coordinate like $\rho/\rho_+ = 1+\zeta$ and expand about $\zeta = 0$. Although the details are tedious, we again find all geometries satisfying (5.88) decompose into a direct product space with one factor AdS$_2$. Computationally, it is easiest to work with the metric written in the form (5.48), in which case $\mathcal{G}_{\tau\tau} \propto r^2$ and $g_{\rho\rho} \propto r^{-2}$ near the horizon, with all other components $\mathcal{O}(r^0)$.

5.5 Discussion

In this chapter we have obtained a general expression for the action of the null Melvin twist, constructed a series of charged and rotating asymptotically Schrödinger black hole solutions of type IIB supergravity, found a 5d truncation of the 10d IIB theory adapted to these solutions, and examined some of the salient features of their geometry and thermodynamics. Along the way we discovered that these spacetimes inherit extremal limits from their parent AdS spaces, but that some of their features – like the radii of curvature of the near-horizon regions – are not inherited, leading to a potentially interesting class of new solutions. The fact that these systems are explicitly embedded in IIB string theory allows us to identify the boundary CFT as the $_\beta$DLCQ of the pre-Melvin boundary theory. Such a theory is by construction a non-relativistic conformal field theory.

Whatever this boundary system is, however, it is decidedly not a good description of fermions at unitarity. First, the thermodynamics of this system is wrong. For example, while the pressure is positive, it scales with a negative power of the chemical potential, $\mathcal{P} \sim T^4/\mu^2$; positivity of the number density $N = \partial\mathcal{P}/\partial\mu$ then requires that the chemical potential is negative. Notably, this scaling is not a consequence of NR conformal symmetry, as the conformal algebra requires only that $\mathcal{P} \sim T^{\frac{d+2}{2}} g(\mu/T)$, as elegantly explained in [143]. Rather, this odd thermodynamics is a direct consequence of the identification of particle number with a DLCQ momentum, $N = i\partial_\xi$, as powerfully argued in [144], who found that the curious scalings follow from the summation over the infinite tower of KK modes.

Secondly, and importantly, while the system certainly has a finite density of non-relativistic excitations, it is not in a superfluid phase, since the $U(1)$ conjugate to the particle number – here, ξ-translation invariance – is manifestly **un**-broken. It is certainly possible that this geometry is secretly a subleading saddle, with a ξ-momentum violating solution dominating entropically; unfortunately, no such solution is presently known.

Eventually, one would like to find solutions that dispense with the ξ-translation symmetry entirely, for example by breaking it explicitly even in the asymptotic regime, or by KK-reducing on a finite-density geometry in which the ξ-circle is spacelike and lifting the KK modes by moving out along a Coulomb branch, as was done for example in the DLCQ of M-theory. This is an important direction for future work.[4]

All that said, even if these systems are not fermions at unitarity, they are NRCFTs and deserve study in their own right. The solutions presented and explored in this chapter open the door to a number of physically interesting questions, such as the study of superfluids and fermi surfaces in field theories which are microscopically non-relativistic. We will return to these questions in the future.

[4] We thank J. McGreevy and D. Son for illuminating discussions on this topic.

Chapter 6

Fermi Surfaces in Maximal Gauged Supergravity

6.1 Overview

Since the first work on obtaining Fermi surfaces [145, 146, 147] in the framework of the gauge-string duality [1, 148, 149], examples have generally been obtained through the "bottom-up" approach of writing down an effective Lagrangian in the gravity theory and then determining its consequences; an investigation of fermion behavior for general dimension, mass and charges was carried out in [150]. While this method is extremely useful, it is naturally of interest to understand what analogous phenomena, if any, can be obtained from a known string theory or supergravity construction. Previous top-down approaches to Fermi surfaces include [151, 152], which studied fermions realized on probe branes, and [153, 154, 155], which studied the gravitino in the gravity multiplet of minimal supergravity and found no Fermi surface singularity.

In this chapter, we study spin-1/2 fermions in both four-dimensional and five-dimensional maximally supersymmetric gauged supergravity and find Fermi surfaces. We proceed through three steps for each case. First, we recall how one identifies a subset of the fields of the gauged supergravity into which one can embed an extremal Reissner-Nordström anti-de Sitter (RNAdS) black hole; this is nontrivial since turning on a generic gauge field will source unwanted scalars as well. Second, we isolate particular charged fermions and derive their linearized fluctuation equations. Third, we solve these equations in the extremal RNAdS background with suitable infalling boundary conditions, identify a Fermi surface by finding the momentum at which the "source" term vanishes, and obtain the corresponding scaling exponent at the Fermi momentum.

In both cases, we find a scaling exponent $0 < \nu_{k_F} < 1/2$, which indicates non-Fermi liquid behavior. A generic exponent in this range leads to excitations whose width Γ is comparable to their energy ω_*, resulting in no well-defined quasi-particles close to the Fermi surface. In both of our examples, we find at least some excitations with the width more than ten times smaller than the energy, for small energies. Thus, though quasi-particles do not become parametrically well defined at low energies (as is the case in Landau theory), they are fairly well defined.

6.2 Fermi surfaces from four-dimensional supergravity

Gauged $\mathcal{N} = 8$ supergravity in four dimensions [156] has gauge group $SO(8)$, embedded inside the global symmetry group $E_{7(7)}$; the 70 scalar fields of the theory live in an $E_{7(7)}/SU(8)$ coset. The maximally supersymmetric vacuum corresponds to the compactification of 11-dimensional supergravity on $AdS_4 \times S^7$, and is dual to the strongly coupled $d = 3$, $\mathcal{N} = 8$ theory living on the worldvolume of a stack of M2-branes.

To embed a charged black hole in this theory, we restrict to a consistent truncation considered in [157] which includes the metric, the four Cartan gauge fields $A_{\mu ij} \equiv A_{\mu[ij]}$ with $ij = 12, 34, 56, 78$, and three scalar fields. Within this abelian truncation, a general gauge field configuration acts as a source for the scalars; however, [157] showed that turning on $A_{\mu 12}$ alone is consistent with the scalar fields being zero (the constant value attained in the maximally supersymmetric AdS_4 vacuum) everywhere.[1] Thus if we take

$$a_\mu \equiv A_{\mu 12}\,, \tag{6.1}$$

we may build our geometry out of the fields in the effective Lagrangian,

$$e^{-1}\mathcal{L} = -\frac{1}{2}R - \frac{1}{4}f_{\mu\nu}f^{\mu\nu} + 6g^2\,, \tag{6.2}$$

where $f_{\mu\nu} \equiv \partial_\mu a_\nu - \partial_\nu a_\mu$ and the gauge coupling is related to the AdS_4 scale by $g = 1/(\sqrt{2}L)$; note that we use the mostly-minus metric conventions of [156]. The extremal RNAdS solution in

[1] For comparison with the $D = 5$ case, and to understand the dual field theory operators, it is useful to note that choosing only $A_{\mu 12}$ non-zero is related by an $SO(8)$ triality transformation to a presentation where all four Cartan gauge fields are turned on equally.

$D = d + 1$ dimensions is

$$ds^2 = \frac{r^2}{L^2}(f dt^2 - d\vec{x}^2) - \frac{L^2}{r^2}\frac{dr^2}{f}\,, \tag{6.3}$$
$$a_\mu dx^\mu = \mu\left(1 - \left(\frac{r_0}{r}\right)^{d-2}\right) dt\,,$$

with the horizon function

$$f = 1 + \frac{d}{d-2}\left(\frac{r_0}{r}\right)^{2d-2} - \frac{2(d-1)}{(d-2)}\left(\frac{r_0}{r}\right)^{d}\,, \tag{6.4}$$

where r_0 is the horizon radius $f(r_0) \equiv 0$, and the chemical potential for the $d = 3$ action (6.2) is

$$\mu = \frac{\sqrt{6} r_0}{L}\,, \tag{6.5}$$

corresponding in the notation of [150] to $g_F = \sqrt{2}L$.

We now consider the spin-1/2 fermions of $D = 4$, $\mathcal{N} = 8$ gauged supergravity: there are 56 Majorana spinors $\chi_{ijk} = \chi_{[ijk]}$ where $i, j = 1 \ldots 8$. The gauging of the supergravity couples the fermions to the gauge fields via the composite connection, which for vanishing scalars leads to the gauge covariant derivative[2]

$$D_\mu \chi_{ijk} = \nabla_\mu \chi_{ijk} + 3g A_\mu{}^m{}_{[i}\, \chi_{jk]m}\,. \tag{6.6}$$

With our gauge field (6.1) turned on, the 56 fermions divide into three sectors: 6 containing both the indices 1 and 2, 20 containing neither, and 30 containing just one of them. It is easy to see that only the last sector is charged under a_μ.

The terms in the $\mathcal{N} = 8$ Lagrangian that contribute to the quadratic fermion action are

$$e^{-1}\mathcal{L}_{1/2} = -\frac{1}{12}\bar{\chi}^{ijk}(\gamma^\mu D_\mu - \overleftarrow{D}_\mu \gamma^\mu)\chi_{ijk} \tag{6.7}$$
$$-\frac{1}{2}\left(F^+_{\mu\nu ij} S^{ij,kl} O^{+\mu\nu kl} + \text{h.c.}\right)\,,$$

where $S^{ij,kl} = \delta^{[i}_j \delta^{k]}_l$ when the scalars vanish, and $O^{+\mu\nu ij}$ is bilinear in the χ_{ijk} and the gravitini $\psi_{\rho i}$:

$$O^{+\mu\nu ij} \equiv -\frac{\sqrt{2}}{144}\epsilon^{ijklmnpq}\bar{\chi}_{klm}\sigma^{\mu\nu}\chi_{npq} \tag{6.8}$$
$$-\frac{1}{2}\bar{\psi}_{\rho k}\sigma^{\mu\nu}\gamma^\rho\chi^{ijk} + (\psi_\rho^2 \text{ term})\,.$$

[2] Usually one must carefully distinguish between $SO(8)$ indices and the indices of the local $SU(8)$ symmetry, but when the scalars vanish, a description can be found where there is no difference between them.

Note there are no elementary mass terms for the spin-1/2 fermions. It is easy to see that the Pauli-type terms in the presence of the gauge field couple the first sector of neutral fermions to the gravitini and generate an effective mass term for the second neutral sector, but do not affect the charged spin-1/2 fields. Thus the 15 complex fermions of the form $\chi \sim \chi_{1jk} + i\chi_{2jk}$ with $j, k = 3, \ldots 8$ all satisfy the simple Dirac equation,

$$\gamma^\mu \left(\nabla_\mu - iqa_\mu\right) \chi = 0\,, \tag{6.9}$$

with $q = g = 1/(\sqrt{2}L)$.; their conjugates have charge $-q$.

We now consider the solutions to this equation. The near-boundary behavior is controlled by the (vanishing) mass and is (see for example [158]),

$$\chi_+ \quad \sim \quad Ar^{-3/2} + Br^{-5/2}\,, \tag{6.10}$$

$$\chi_- \quad \sim \quad Cr^{-5/2} + Dr^{-3/2}\,, \tag{6.11}$$

where $\chi_\pm$ are eigenvectors of γ^r; A is the source term and D is the response, while B and C are determined by the other two. The near-horizon behavior is

$$\chi \sim (r - r_0)^{-1/2 \pm \nu_k}\,, \tag{6.12}$$

where ν_k is the scaling exponent [150],

$$\begin{aligned} \nu_k &= \sqrt{\frac{k^2 L^4}{6r_0^2} - \frac{1}{12}} \\ &= \frac{1}{2\sqrt{3}}\sqrt{6\left(\frac{k}{\mu\, q}\right)^2 - 1}\,, \end{aligned} \tag{6.13}$$

which controls the IR behavior of the Green's function. An "oscillatory region" with imaginary ν_k thus exists for $|k| < r_0/(\sqrt{2}L^2) = \mu q/\sqrt{6}$.

To find a Fermi surface we set $\omega = 0$ and impose regular boundary conditions at the horizon by choosing the plus in (6.12), and search for values of the spatial momentum k outside the oscillatory region where the source term A vanishes. This case has in fact been treated by [150], with $m = 0$ and $qg_F = 1$; the Green's function is plotted near the Fermi momentum in their figure 4. Also, an analytic treatment of this class of fermions was made in [159], in which k_F can be determined through a relation involving hypergeometric functions. Setting $L = r_0 = 1$, we verify that there is a Fermi surface at $k_F \approx 0.9185$, or $\frac{k_F}{\mu q} \approx 0.5305$, at which value the scaling exponent becomes

$$\nu_{k_F} \approx 0.2393\,. \tag{6.14}$$

The conjugate fermions with charge $-q$ see the Fermi surface at $k_F \approx -0.9185$, with the same ν_{k_F}.

It is argued in [150] that $\delta_{k_F} \equiv \frac{1}{2} + \nu_{k_F}$ is the conformal dimension of the dual operator in the auxiliary AdS_2 theory controlling the IR dynamics, and for $\nu_{k_F} < 1/2$ this operator represents a relevant deformation, leading to non-Fermi liquid behavior. For $\nu_{k_F} < 1/2$ there is no Fermi velocity; in the notation of [150], the retarded Green's function near the Fermi surface (that is, for small ω as well as small $k_\perp \equiv k - k_F$) takes the form

$$G_R = \frac{h_1}{k_\perp - h_2 e^{i\gamma_F}\omega^{2\nu_{k_F}}}\,. \tag{6.15}$$

As developed in [150], the real positive constants h_1 and h_2 encode ultraviolet data, but the phase $e^{i\gamma_F}$ is entirely determined by the behavior of an $AdS_2 \times R^2$ Green's function relating to the near-horizon behavior of the spinors. Since $h_2 e^{i\gamma_F}$ provides both the leading real and imaginary parts in the dispersion relation, the width of would-be quasiparticles is generically of the same order as the excitation energy, making them not well-defined.

It is interesting to note, however, that for some of our excitations the widths are relatively small. For negative q, we find $\gamma_F \approx 0.163$. Expressing the fermionic quasinormal frequency lying closest to the Fermi surface as $\omega_{\mathrm{QNM}} = \omega_* - i\Gamma$, we find for particles ($k_\perp > 0$):

$$\frac{\Gamma}{\omega_*} = \tan\frac{\gamma_F}{2\nu_{k_F}} \approx \frac{1}{2.8}\,, \qquad k_\perp > 0\,, \tag{6.16}$$

while for holes ($k_\perp < 0$),

$$\frac{\Gamma}{\omega_*} = \tan\frac{\gamma_F - \pi}{2\nu_{k_F}} \approx \frac{1}{16.8}\,, \qquad k_\perp < 0\,, \tag{6.17}$$

manifesting a particle-hole asymmetry characteristic of $\nu_{k_F} < 1/2$ models [150]. We see there are almost well-defined quasiparticles in the latter case, in the sense that (6.17) indicates a small ratio of width to excitation energy. The positive q fermion sees the Fermi surface with particles and holes exchanged.

The residue Z of the poles goes to zero as

$$Z \sim (k_\perp)^{\frac{1}{2\nu_{k_F}}-1} \approx k_\perp^{1.089}\,, \tag{6.18}$$

and the dispersion relation goes like

$$\omega_* \sim (k_\perp)^{\frac{1}{2\nu_{k_F}}} \approx k_\perp^{2.089}\,. \tag{6.19}$$

6.3 Fermi surfaces from five-dimensional supergravity

We turn now to the case of five dimensions. Five-dimensional $\mathcal{N} = 8$ gauged supergravity [160] features an $SO(6)$ gauge group and 40 scalars living in the coset $E_{6(6)}/USp(8)$. The maximally supersymmetric vacuum corresponds to the compactification of 10-dimensional type IIB supergravity on $AdS_5 \times S^5$, and is dual to $d = 4$, $\mathcal{N} = 4$ super-Yang-Mills theory.

As with the four-dimensional case, we embed an extremal RNAdS black hole by appealing to a known consistent truncation, in this case the so-called STU model [161], which contains the three Cartan gauge fields $A_{\mu 12}$, $A_{\mu 34}$ and $A_{\mu 56}$ as well as a pair of scalars. While generic gauge fields will turn on the scalars, the scalar-free choice is the diagonal

$$a_\mu \equiv A_{\mu 12} = A_{\mu 34} = A_{\mu 56}\,, \tag{6.20}$$

which provides us with the consistently truncated Lagrangian,

$$e^{-1}\mathcal{L} = -\frac{1}{4}R - \frac{3}{4}f_{\mu\nu}f^{\mu\nu} + \frac{3g^2}{4}\,, \tag{6.21}$$

with $g = 2/L$. The RNAdS solution is again given by (6.3), (6.4) with $d = 4$ and

$$\mu = \frac{r_0}{\sqrt{2}L}\,, \tag{6.22}$$

matching the notation of [150] with $g_F = L/\sqrt{3}$.

We turn now to the Fermi fields. There are 48 spin-1/2 fermions $\chi_{abc} = \chi_{[abc]|}$ where $a, b, c = 1 \ldots 8$ are $USp(8)$ indices and $[\ldots]|$ denotes antisymmetrization with the symplectic trace removed.

For several reasons, these fields are more involved to deal with than the four-dimensional case. First, they obey the symplectic Majorana condition, a condition particular to five dimensions relating one field to the complex conjugate of another via the $USp(8)$ symplectic metric Ω_{ab}. Second, the embedding of $SO(6)$ into $USp(8)$ is less straightforward than the elementary embedding of $SO(8)$ into $SU(8)$ that occurs in four dimensions, necessitating the introduction of $SO(6)$ gamma matrices as Clebsch-Gordan coefficients. Third, the fermions have elementary mass terms, as well as Pauli terms that do not decouple. Evaluating the composite connection and the various tensors living in the group space, we find the spin-1/2 quadratic action to be

$$\begin{aligned}
e^{-1}\mathcal{L}_{1/2} = \frac{i}{12}\bar{\chi}^{abc}\gamma^{\mu}\nabla_{\mu}\chi_{abc} \\
+\frac{ig}{16}\bar{\chi}^{abc}\delta_{cd}\Omega^{de}\chi_{abe} - \frac{ig}{8}\bar{\chi}^{abc}\gamma^{\mu}a_{\mu}\tilde{\Gamma}^{cd}\chi_{abd} \\
+\frac{i}{16}f_{\mu\nu}\tilde{\Gamma}^{ab}\left(\sqrt{2}\bar{\psi}^{c}_{\rho}\gamma^{\mu\nu}\gamma^{\rho}\chi_{abc} + \bar{\chi}_{a}{}^{cd}\gamma^{\mu\nu}\chi_{bcd}\right) ,
\end{aligned} \tag{6.23}$$

where $\tilde{\Gamma} \equiv \Gamma_{12} + \Gamma_{34} + \Gamma_{56}$ and the $\Gamma_{IJ} \equiv [\Gamma_I, \Gamma_J]/2$ are elements of the $SO(6)$ Clifford algebra.

Under the decomposition of $USp(8)$ to $SO(6)$, the 48 fermions organize themselves into complex symplectic Majorana pairs in the $\mathbf{20} + \mathbf{4}$, while the gravitini are in the $\mathbf{4}$. In terms of the $U(1) \subset SO(6)$ defined by the gauge field a_μ (6.20), one can analyze the weight vectors to see that the $\mathbf{20}$ contains 3 elements with charge 5/2, 8 elements with charge 3/2 and 9 elements with charge 1/2, while the $\mathbf{4}$ contains an element of charge 3/2 and three of charge 1/2. (Here and below we indicate the charge magnitude, since each symplectic Majorana pair contains excitations of both signs of the charge.) Thus the three complex fermions with charge 5/2 cannot mix with the gravitini; it is these that we will study.

We were able to find simultaneous eigenvectors of the kinetic, mass, gauge and Pauli operators corresponding to these three complex fermions; each obeys the same decoupled Dirac equation,[3]

$$\left(i\gamma^{\mu}\nabla_{\mu} \pm \frac{5}{L}\gamma^{\mu}a_{\mu} \mp \frac{1}{2L} + \frac{i}{4}f_{\mu\nu}\gamma^{\mu\nu}\right)\chi = 0\,, \tag{6.24}$$

where the lower set of signs is for the conjugate excitation in the symplectic Majorana pair. In

[3] One may transform this equation into the mostly-plus metric signature more common in the contemporary literature with the replacement $\gamma^{\mu} \to -i\gamma^{\mu}$.

solving the conjugate equation one may for convenience switch the sign of the gamma matrices, effectively flipping the signs of both m and the Pauli term; the conjugate then has the same mass but opposite signs in both couplings to the gauge field, and is thus equivalent to studying the original fluctuation in the the background of an oppositely-charged black hole.

Considering solutions to this equation for either sign charge, the near-boundary scaling is controlled by the mass $mL = 1/2$ and takes the form,

$$\begin{aligned} \chi_+ &\sim Ar^{-3/2} + Br^{-7/2}\,, \\ \chi_- &\sim Cr^{-5/2}\log r + Dr^{-5/2}\,, \end{aligned} \tag{6.25}$$

for spinors $\chi_\pm$ that are eigenvectors of γ^r, where again A is the source and D the response.

Pauli couplings were considered in [162], and generalize the formulas of [150] for the near-horizon behavior of the solutions by shifting the momentum $k \to \tilde{k}$, where in our case

$$\tilde{k} \equiv k \mp \frac{r_0}{\sqrt{2}L^2}\,, \tag{6.26}$$

where the different signs correspond to different eigenvectors of $\gamma^r\gamma^t\vec{k}\cdot\vec{\gamma}$; each of χ_+ and χ_-, with two components each, contains one component with each sign shift.

This leads to near horizon behavior of the form (6.12) with

$$\begin{aligned} \nu_k &= \frac{1}{6}\sqrt{\frac{3\tilde{k}^2L^4}{r_0^2} - \frac{47}{4}}\,, \\ &= \frac{\sqrt{47}}{12}\sqrt{\frac{150}{47}\left(\frac{\tilde{k}}{\mu q}\right)^2 - 1}\,. \end{aligned} \tag{6.27}$$

The oscillatory region of imaginary ν_k thus occurs for $|\tilde{k}| < \sqrt{47/12}(r_0/L^2) = \sqrt{47/150}(\mu q)$.

Selecting infalling boundary conditions and again taking $L = r_0 = 1$ for simplicity, we find Fermi surfaces with

$$\tilde{k}_F \approx \pm 2.00000\,, \tag{6.28}$$

or $\tilde{k}_F/(\mu q) \approx \pm 0.56569$. (Note the values of k_F will have opposite signs for different components due to (6.26).) The precision of this result is suggestive that the $\tilde{k}_F$ values are ± 2 exactly; notice that the Fermi surfaces are barely outside the oscillatory region. The corresponding value of ν_k is then exactly

$$\nu_{k_F} = \frac{1}{12} \,. \tag{6.29}$$

Thus these Fermi surfaces also have $\nu_{k_F} < 1/2$, meaning again we have a non-Fermi liquid.

Again the retarded Green's function takes the form (6.15). For negative q we have $\gamma_F \approx 0.0126$, whose small size makes $e^{i\gamma_F}$ nearly a real number, and consequently again the fermionic quasinormal frequency $\omega_{\rm QNM} = \omega_* - i\Gamma$ lying closest to the Fermi surface is nearly real:

$$\frac{\Gamma}{\omega_*} = \tan 6\gamma_F \approx \frac{1}{13.2} \,, \tag{6.30}$$

for both $k_\perp > 0$ and $k_\perp < 0$. Again we find there are almost well-defined quasiparticles, in the sense that (6.30) indicates a small ratio of width to excitation energy. Unlike the four-dimensional case, we find a symmetry between particles and holes, which can be traced to the rational value of ν_{k_F} (6.29). Positive q again sees the same physics with particles and holes exchanged.

Moreover we find an unusual sixth-order dispersion relation,

$$\omega_* \propto (k_\perp)^{\frac{1}{2\nu_{k_F}}} = k_\perp^6 \,, \tag{6.31}$$

where the constant of proportionality involves h_2, as well as a rapidly vanishing residue,

$$Z \sim (k_\perp)^{\frac{1}{2\nu_{k_F}} - 1} = k_\perp^5 \,. \tag{6.32}$$

6.4 Field theory operators and charge density

All of the calculations so far have been done purely in gauged supergravity, without reference to the dual gauge theories. Of course, a primary motivation of studying the maximal gauged supergravities is that they are dual to the best understood field theory duals. In five dimensions, where the field theory dual is $\mathcal{N} = 4$ super-Yang-Mills theory, the operators dual to the three charge-5/2 fermion fields are $\mathcal{O}_j = \mathrm{tr}\, \lambda Z_j$ for $j = 1, 2, 3$, where λ is the charge 3/2 gaugino in the $\mathbf{4}$ of the R-symmetry group $SO(6)$, and $Z_j = X_{2j-1} + iX_{2j}$ where X_I are the six adjoint scalars. Thus the gaugino contributes $+3/2$ to the total charge of $\mathcal{O}_j$, while the scalars contribute $+1$.

A common view (perhaps the prevailing view) in the current literature is that the singularity in the two-point function of $\mathcal{O}_j$ at $\omega = 0$ and $k = k_F$ is a signal of a Fermi surface formed by color singlet bound states of λ and Z_j, which we will term mesinos: see for example [163, 164, 165]. An alternative view, suggested in [166], is that the singularity in the two-point function is due to a Fermi surface formed by adjoint fermions in the field theory—in short, gauginos, or gauginos dressed in some way by the strong gauge interactions. A Luttinger count of the charge density due to the charged fermions is

$$\begin{aligned} j_{\text{fermions}} &= \sum_{\text{Fermi surfaces}} q_{\text{f}} g_{\text{s}} \int_{|k|<|k_F|} \frac{d^3k}{(2\pi)^3} \\ &= \frac{q_{\text{f}}}{6\pi^2} \left(g_+ |k_{F,+}|^3 + g_- |k_{F,-}|^3 \right) , \end{aligned} \tag{6.33}$$

where q_{f} is the dimensionless charge of the gauge theory fermion involved and g_{s} is a degeneracy factor indicating the number of distinct fermions participating in the Fermi surface dynamics. In the second line of (6.33) we have specialized to the case of two Fermi surfaces with degeneracy factors g_+ and g_-. In the gaugino interpretation, clearly $q_{\text{f}} = 3/2$, and with $L = r_0 = 1$, the result (6.28) indicates that $|k_{F,\pm}| = 2 \pm 1/\sqrt{2}$. For the degeneracy factors, the most natural conjecture is that $g_+ = g_- = N^2$, which is simply the number of colors at leading order in N. There is no additional factor of 2 for the spin of the fermions because the gauginos are chiral. Plugging all the stated values into (6.33), we arrive at

$$j_{\text{fermions}} = \frac{11}{2\pi^2} N^2 \,. \tag{6.34}$$

This is an interesting result because it is numerically quite close to the total charge of the black brane. To compute the latter, we refer to [167] and find

$$j_{\text{total}} = \frac{9\sqrt{6}}{4\pi^2} N^2 \,, \tag{6.35}$$

with $L = r_0 = 1$ as before. The quantity j_{total} in (6.35) is related to the scaled quantities j_i of [167] by $j_{\text{total}} = N^2(j_1 + j_2 + j_3)$. Note also that our r_0 is denoted r_H in [167]. Comparing (6.34) and (6.35), we see that

$$\frac{j_{\text{fermions}}}{j_{\text{total}}} = \sqrt{\frac{242}{243}} \,. \tag{6.36}$$

See [168, 163, 165] for somewhat different approaches to the Luttinger theorem in holographic (non-) Fermi liquids.

Taking (6.36) at face value, we should conclude that most of the charge is indeed carried by the charge $+3/2$ gauginos. Let us bear in mind, however, that the choice $g_+ = g_- = N^2$ was conjectural. More conservatively, we could regard (6.36) as an upper limit on the amount of charge carried by these gauginos. There are other positively charged particles in the field theory, namely charge $+1/2$ gauginos and charge $+1$ scalars. If (6.36) is correct, one should ask why they carry such a small fraction of the charge. Possibly the charge $+1/2$ gauginos do not carry appreciable charge because there are tree-level interactions that convert pairs of them into charge $+1$ bosons, whereas no such interactions exist to convert two charge $+3/2$ gauginos into charge $+3$ bosons, simply because there are no charge $+3$ bosons.[4] But why do the scalars carry so little charge? This question is particularly sharp in light of the existence of flat directions for the scalars: it seems like they might naturally suck up all the charge into a Bose condensate.

We venture to suggest the following speculative interpretation. Perhaps the scalars do condense, but only a little; perhaps, as well, they condense in non-flat directions, which after all outnumber the flat directions by a factor of N. If they condense at all, they must do so in a manner that preserves the $U(1)$ gauge symmetry, since it is obviously unbroken in the RNAdS$_5$ solution. This is possible in the large N limit, since the N D3-branes can be distributed continuously over a $U(1)$-invariant configuration—perhaps even an $SO(6)$-invariant configuration. In fact, highly symmetric, continuous distributions of D3-branes have been previously derived as limits of spinning brane solutions [169, 170]. With a scalar condensate present at zero momentum, the operator $\mathcal{O}_j = \operatorname{tr} \lambda Z_j$ plausibly has a finite amplitude to create a zero momentum boson Z_j and to put all its momentum into the charge $+3/2$ gaugino λ. This is just what we need in order to explain why a Fermi surface for the gauginos would give rise to the singularity we observe in the two-point function of $\mathcal{O}_j$. Also, the overall $O(N^2)$ scaling of the two-point function of $\mathcal{O}_j$ is readily understood in terms of a sum over all possible gaugino colors.

[4] We thank D. Huse for suggesting this line of reasoning to us.

In the AdS_4 case, the field theory dual is more complicated than $\mathcal{N} = 4$ super-Yang-Mills [171, 172, 173, 174], and the overall scaling of Green's functions is $N^{3/2}$. In the theory of a single M2-brane, the operators dual to the charged fermions again have the form $X\lambda$. In the standard field theory presentation of $SO(8)$, X is a vector and λ is a spinor—let's say the $\mathbf{8}_c$, where an odd number of weights are negative. Under the $U(1)$ which is the diagonal sum of all four Cartan generators, the scalars and the fermions both have charge ± 1. With a little care one can see that 15 combinations $X\lambda$ have charge $+2$, another 15 have charge -2, and the rest are neutral. The $15 + 15$ charged combinations exactly match the 30 charged components of χ_{ijk}. While this bit of group theory indicates that all the fundamental fermions in the M2-brane theory are involved equally in the Fermi surface revealed by our AdS_4 gauged supergravity calculations, we do not know how to formulate a Luttinger count analogous to (6.33) and (6.34). However, in light of the recent progress [175, 176] in understanding the partition function of multiple M2-branes, it does not seem too far-fetched that one could find a field theory account of the same $N^{3/2}$ scaling in the Green's function in which the effective degrees of freedom participating in the Fermi surface dynamics are colored.

6.5 Discussion

Starting from maximal gauged supergravity, we have found Fermi surfaces for the spin-1/2 fermionic fluctuations around RNAdS black holes both in four and five dimensions. In four dimensions, the Fermi momentum is determined by a complicated transcendental equation, while in five dimensions the Fermi momenta appear to be simple multiples of the chemical potential leading to simple numbers like the dispersion relation exponent $z = 6$. Both cases are non-Fermi liquids but possess almost well-defined quasi-particles, in the sense that the width of low-energy excitations is more than ten times smaller that the excitation energy. The four-dimensional case manifests particle-hole asymmetry, while the five-dimensional case is symmetric, again due to the simple numbers.

In the five-dimensional case, an interpretation of the singularity in the Green's function as due to a Fermi surface of charge $+3/2$ gauginos in the dual field theory (as opposed to charge $+5/2$ color-singlet mesinos) leads to a Luttinger count of the charge carried by fermions that is surprisingly close to the total charge on the D3-branes. This count, together with the presence of massless charged scalars and the zero-point entropy of RNAdS black holes, clearly calls for a more precise field theory understanding. Evidently, the most interesting phenomena are all present in large N, strongly coupled $\mathcal{N} = 4$ super-Yang-Mills theory at zero temperature; so it may be enough to study this "simplest" of dual field theories.

Chapter 7

Concluding Comments

The ability to perform calculations in a strongly coupled field theory has been a central theme in this dissertation. What's more, the surprising discovery that this can be accomplished by considering a gravitational theory in a higher dimensional spacetime has encouraged connections between seemingly disparate physical systems. It is certainly remarkable that important properties of both interacting electrons at zero temperature and a nebulous partonic goo at very high temperatures might be revealed by a relatively simple geometric background with a handful of familiar fields inside.

With the dust now settling on many of the calculations contained in this work, it is interesting to reflect on the relevance of the results. For example, it is noteworthy if not a bit unfortunate, that in the years following the exploration of the robustness of sound speed and jet quenching detailed in chapter 2, the universal quantity η/s still presides as the most useful truly robust result to emerge from the duality. Evidently, such quantities are few and far between in applied AdS/CFT.

Presently, there is no direct experimental evidence for the location of the second order critical point addressed at length in chapters 3 and 4. That said, it remains an active area of interest for the experimental collaborations at the Relativistic Heavy Ion Collider, and accordingly these results remain relevant. The bulk theory we constructed has shown itself to be a useful proving ground for explorations of strongly coupled QCD-like gauge theories, as well at methods employed in "real" QCD. Specifically, numerical challenges associated with studying lattice QCD at finite chemical potential (the well known "sign problem") make lattice investigations of the QCD phase diagram problematic. In practice, several techniques have been employed to circumvent these issues, one of which is to Taylor expand thermodynamic quantities such as the pressure about zero chemical potential. In this approach, the location of the critical point is signaled by the radius of convergence of the Taylor series. By applying this method to the model developed in this thesis, where the location of the critical point is exactly known, we have been able to find preliminary evidence that the Taylor series method of Lattice QCD can predict the location of a critical point fairly well. More detailed explorations of these lattice techniques, a study of the robustness of the location of the critical point and its predictions, as well as the role of $1/N_c$ corrections still await further study.

The condensed matter applications described here have enjoyed mixed success. Computationally, the geometries dual to rotating non-relativistic conformal field theories were somewhat unwieldy, and investigating their phenomenology was quite complicated. Nonetheless, some calculations were performed by subsets of the original author list in [197] and [198]. The embedding of Fermi surfaces in maximal gauged supergravity, however, has continued to produce interesting surprises. An extension of the results presented in this dissertation to the so-called "two charge" black hole background of type IIB string theory is currently underway, with preliminary identification of a Fermi surface complete. This particular black hole is thermodynamically very interesting, as it allows the dual gauge theory to have the physically desirable trait of vanishing entropy at zero temperature. Certainly, many interesting questions related to non-Fermi liquidity can now hope to be answered in a consistent supergravity theory.

Globally, it seems very likely that the computational techniques afforded by gauge/gravity duality will continue to play an important role in elucidating the surprising secrets of strongly coupled systems. Despite the fact that the precise duals for QCD or other explicit theories may never be found, it is nevertheless obvious that the AdS/CFT correspondence is capable of describing and predicting an incredibly diverse collection of non-trivial phenomena. Whether these predictions will have the great fortune of coming under experimental scrutiny is an important question that eagerly awaits an answer.

Bibliography

[1] Juan Martin Maldacena. The Large N limit of superconformal field theories and supergravity. Adv.Theor.Math.Phys., 2:231–252, 1998.

[2] P. Kovtun, D. T. Son and A. O. Starinets, “Viscosity in strongly interacting quantum field theories from black hole physics,” Phys. Rev. Lett. **94**, 111601 (2005) [arXiv:hep-th/0405231].

[3] Y. Kats and P. Petrov, “Effect of curvature squared corrections in AdS on the viscosity of the dual gauge theory,” JHEP **0901**, 044 (2009) [arXiv:0712.0743 [hep-th]].

[4] M. Brigante, H. Liu, R. C. Myers, S. Shenker and S. Yaida, “Viscosity Bound Violation in Higher Derivative Gravity,” Phys. Rev. D **77**, 126006 (2008) [arXiv:0712.0805 [hep-th]].

[5] A. Adams, A. Maloney, A. Sinha and S. E. Vazquez, “1/N Effects in Non-Relativistic Gauge-Gravity Duality,” arXiv:0812.0166 [hep-th].

[6] A. Buchel, R. C. Myers and A. Sinha, “Beyond eta/s = 1/4pi,” arXiv:0812.2521 [hep-th].

[7] S. S. Gubser and A. Karch, “From gauge-string duality to strong interactions: a Pedestrian’s Guide,” arXiv:0901.0935 [hep-th].

[8] J. Erdmenger, N. Evans, I. Kirsch and E. Threlfall, “Mesons in Gauge/Gravity Duals - A Review,” Eur. Phys. J. A **35**, 81 (2008) [arXiv:0711.4467 [hep-th]].

[9] D. Mateos, “String Theory and Quantum Chromodynamics,” Class. Quant. Grav. **24**, S713 (2007) [arXiv:0709.1523 [hep-th]].

[10] A. Buchel, “N = 2* hydrodynamics,” Nucl. Phys. B **708**, 451 (2005) [arXiv:hep-th/0406200].

[11] A. Buchel and C. Pagnutti, “Bulk viscosity of N=2* plasma,” arXiv:0812.3623 [hep-th].

[12] A. Buchel, S. Deakin, P. Kerner and J. T. Liu, “Thermodynamics of the N = 2* strongly coupled plasma,” Nucl. Phys. B **784**, 72 (2007) [arXiv:hep-th/0701142].

[13] T. Sakai and S. Sugimoto, “Low energy hadron physics in holographic QCD,” Prog. Theor. Phys. **113**, 843 (2005) [arXiv:hep-th/0412141].

[14] T. Sakai and S. Sugimoto, “More on a holographic dual of QCD,” Prog. Theor. Phys. **114**, 1083 (2005) [arXiv:hep-th/0507073].

[15] O. Aharony, J. Sonnenschein and S. Yankielowicz, "A holographic model of deconfinement and chiral symmetry restoration," Annals Phys. **322**, 1420 (2007) [arXiv:hep-th/0604161].

[16] A. Parnachev and D. A. Sahakyan, "Chiral phase transition from string theory," Phys. Rev. Lett. **97**, 111601 (2006) [arXiv:hep-th/0604173].

[17] K. Kajantie, T. Tahkokallio and J. T. Yee, "Thermodynamics of AdS/QCD," JHEP **0701**, 019 (2007) [arXiv:hep-ph/0609254].

[18] H. Liu, K. Rajagopal and Y. Shi, "Robustness and Infrared Sensitivity of Various Observables in the Application of AdS/CFT to Heavy Ion Collisions," JHEP **0808**, 048 (2008) [arXiv:0803.3214 [hep-ph]].

[19] S. S. Gubser and A. Nellore, "Mimicking the QCD equation of state with a dual black hole," Phys. Rev. D **78**, 086007 (2008) [arXiv:0804.0434 [hep-th]].

[20] S. S. Gubser, S. S. Pufu and F. D. Rocha, "Bulk viscosity of strongly coupled plasmas with holographic duals," JHEP **0808**, 085 (2008) [arXiv:0806.0407 [hep-th]].

[21] S. S. Gubser, A. Nellore, S. S. Pufu and F. D. Rocha, "Thermodynamics and bulk viscosity of approximate black hole duals to finite temperature quantum chromodynamics," Phys. Rev. Lett. **101**, 131601 (2008) [arXiv:0804.1950 [hep-th]].

[22] U. Gursoy, E. Kiritsis, L. Mazzanti and F. Nitti, "Deconfinement and Gluon Plasma Dynamics in Improved Holographic QCD," Phys. Rev. Lett. **101**, 181601 (2008) [arXiv:0804.0899 [hep-th]].

[23] U. Gursoy, E. Kiritsis, L. Mazzanti and F. Nitti, "Holography and Thermodynamics of 5D Dilaton-gravity," arXiv:0812.0792 [hep-th].

[24] O. Andreev, "Some Thermodynamic Aspects of Pure Glue, Fuzzy Bags and Gauge/String Duality," Phys. Rev. D **76**, 087702 (2007) [arXiv:0706.3120 [hep-ph]].

[25] O. Andreev and V. I. Zakharov, "The Spatial String Tension, Thermal Phase Transition, and AdS/QCD," Phys. Lett. B **645**, 437 (2007) [arXiv:hep-ph/0607026].

[26] B. Muller and J. L. Nagle, "Results from the Relativistic Heavy Ion Collider," Ann. Rev. Nucl. Part. Sci. **56**, 93 (2006) [arXiv:nucl-th/0602029].

[27] P. Benincasa, A. Buchel and A. O. Starinets, "Sound waves in strongly coupled non-conformal gauge theory plasma," Nucl. Phys. B **733**, 160 (2006) [arXiv:hep-th/0507026].

[28] O. Aharony, A. Buchel and A. Yarom, "Holographic renormalization of cascading gauge theories," Phys. Rev. D **72**, 066003 (2005) [arXiv:hep-th/0506002].

[29] A. Buchel, "Transport properties of cascading gauge theories," Phys. Rev. D **72**, 106002 (2005) [arXiv:hep-th/0509083].

[30] P. Benincasa and A. Buchel, "Hydrodynamics of Sakai-Sugimoto model in the quenched approximation," Phys. Lett. B **640**, 108 (2006) [arXiv:hep-th/0605076].

[31] T. Springer, "Sound Mode Hydrodynamics from Bulk Scalar Fields," Phys. Rev. D **79**, 046003 (2009) [arXiv:0810.4354 [hep-th]].

[32] T. Springer, "Second order hydrodynamics for a special class of gravity duals," arXiv:0902.2566 [hep-th].

[33] H. Liu, K. Rajagopal and U. A. Wiedemann, "Calculating the jet quenching parameter from AdS/CFT," Phys. Rev. Lett. **97**, 182301 (2006) [arXiv:hep-ph/0605178].

[34] H. Liu, K. Rajagopal and U. A. Wiedemann, "Wilson loops in heavy ion collisions and their calculation in AdS/CFT," JHEP **0703**, 066 (2007) [arXiv:hep-ph/0612168].

[35] A. Buchel, "On jet quenching parameters in strongly coupled non-conformal gauge theories," Phys. Rev. D **74**, 046006 (2006) [arXiv:hep-th/0605178].

[36] N. Armesto, J. D. Edelstein and J. Mas, "Jet quenching at finite 't Hooft coupling and chemical potential from AdS/CFT," JHEP **0609**, 039 (2006) [arXiv:hep-ph/0606245].

[37] P. C. Argyres, M. Edalati and J. F. Vazquez-Poritz, "Lightlike Wilson loops from AdS/CFT," JHEP **0803**, 071 (2008) [arXiv:0801.4594 [hep-th]].

[38] S. A. Bass, C. Gale, A. Majumder, C. Nonaka, G. Y. Qin, T. Renk and J. Ruppert, "Systematic Comparison of Jet Energy-Loss Schemes in a realistic hydrodynamic medium," arXiv:0808.0908 [nucl-th].

[39] D. H. Rischke, "The quark-gluon plasma in equilibrium," Prog. Part. Nucl. Phys. **52** (2004) 197–296, [`nucl-th/0305030`].

[40] F. Karsch, "Recent lattice results on finite temperature and density QCD, part I," PoS **CPOD07** (2007) 026, [`arXiv:0711.0656`].

[41] A. Bazavov et. al., "Equation of state and QCD transition at finite temperature," Phys. Rev. **D80** (2009) 014504, [`arXiv:0903.4379`].

[42] S. Borsanyi et. al., "The QCD equation of state with dynamical quarks," `arXiv:1007.2580`.

[43] **STAR** Collaboration, M. M. Aggarwal et. al., "An Experimental Exploration of the QCD Phase Diagram: The Search for the Critical Point and the Onset of De- confinement," `arXiv:1007.2613`.

[44] **CBM** Collaboration, P. Staszel, "CBM experiment at FAIR," Acta Phys. Polon. **B41** (2010) 341–350.

[45] S. S. Gubser and A. Nellore, "Mimicking the QCD equation of state with a dual black hole," `arXiv:0804.0434`.

[46] S. S. Gubser, A. Nellore, S. S. Pufu, and F. D. Rocha, "Thermodynamics and bulk viscosity of approximate black hole duals to finite temperature quantum chromodynamics," `arXiv:0804.1950`.

[47] U. Gursoy, E. Kiritsis, L. Mazzanti, and F. Nitti, "Improved Holographic Yang-Mills at Finite Temperature: Comparison with Data," Nucl. Phys. **B820** (2009) 148–177, [`arXiv:0903.2859`].

[48] J. Noronha, “Connecting Polyakov Loops to the Thermodynamics of $SU(N_c)$ Gauge Theories Using the Gauge-String Duality,” Phys. Rev. **D81** (2010) 045011, [arXiv:0910.1261].

[49] C. Charmousis, B. Gouteraux, B. S. Kim, E. Kiritsis, and R. Meyer, “Effective Holographic Theories for low-temperature condensed matter systems,” JHEP **11** (2010) 151, [arXiv:1005.4690].

[50] U. Gursoy, E. Kiritsis, L. Mazzanti, G. Michalogiorgakis, and F. Nitti, “Improved Holographic QCD,” arXiv:1006.5461.

[51] J. B. Kogut and M. A. Stephanov, “The phases of quantum chromodynamics: From confinement to extreme environments,” Camb. Monogr. Part. Phys. Nucl. Phys. Cosmol. **21** (2004) 1–364.

[52] M. A. Stephanov, “QCD phase diagram: An overview,” PoS **LAT2006** (2006) 024, [hep-lat/0701002].

[53] M. G. Alford, A. Schmitt, K. Rajagopal, and T. Schafer, “Color superconductivity in dense quark matter,” Rev. Mod. Phys. **80** (2008) 1455–1515, [arXiv:0709.4635].

[54] M. A. Stephanov, K. Rajagopal, and E. V. Shuryak, “Signatures of the tricritical point in QCD,” Phys. Rev. Lett. **81** (1998) 4816–4819, [hep-ph/9806219].

[55] N. Goldenfeld, “Lectures on phase transitions and the renormalization group,” Addison-Wesley Frontiers in Physics **85** (1992) 1–394.

[56] M. Cheng et. al., “The transition temperature in QCD,” Phys. Rev. **D74** (2006) 054507, [hep-lat/0608013].

[57] Y. Aoki, Z. Fodor, S. D. Katz, and K. K. Szabo, “The QCD transition temperature: Results with physical masses in the continuum limit,” Phys. Lett. **B643** (2006) 46–54, [hep-lat/0609068].

[58] Y. Aoki et. al., “The QCD transition temperature: results with physical masses in the continuum limit II,” JHEP **06** (2009) 088, [arXiv:0903.4155].

[59] S. Borsanyi et. al., “QCD transition temperature: full staggered result,” arXiv:1011.4230.

[60] S. S. Gubser and I. Mitra, “Instability of charged black holes in anti-de Sitter space,” hep-th/0009126.

[61] S. S. Gubser and I. Mitra, “The evolution of unstable black holes in anti-de Sitter space,” JHEP **08** (2001) 018, [hep-th/0011127].

[62] R. Gregory and R. Laflamme, “Black strings and p-branes are unstable,” Phys. Rev. Lett. **70** (1993) 2837–2840, [hep-th/9301052].

[63] R. Gregory and R. Laflamme, “The Instability of charged black strings and p-branes,” Nucl. Phys. **B428** (1994) 399–434, [hep-th/9404071].

[64] M. A. Stephanov, “QCD phase diagram and the critical point,” Prog. Theor. Phys. Suppl. **153** (2004) 139–156, [hep-ph/0402115].

[65] S. S. Gubser, "Superconducting black holes," June, 2009. Talk delivererd at Strings 2009 in Rome, http://strings2009.roma2.infn.it/talks/Gubser_Strings09.pdf.

[66] S. S. Gubser, C. P. Herzog, S. S. Pufu, and T. Tesileanu, "Superconductors from Superstrings," Phys. Rev. Lett. **103** (2009) 141601, [arXiv:0907.3510].

[67] R. B. Griffiths and J. C. Wheeler, "Critical Points in Multicomponent Systems," Phys. Rev. **A2** (1970) 1047–1064.

[68] M. Stephanov, "QCD critical point and correlations," J. Phys. Conf. Ser. **27** (2005) 144–153.

[69] N. G. Antoniou and A. S. Kapoyannis, "Bootstraping the QCD critical point," Phys. Lett. **B563** (2003) 165–172, [hep-ph/0211392].

[70] S. Ejiri et. al., "Study of QCD thermodynamics at finite density by Taylor expansion," Prog. Theor. Phys. Suppl. **153** (2004) 118–126, [hep-lat/0312006].

[71] Z. Fodor and S. D. Katz, "Lattice determination of the critical point of QCD at finite T and mu," JHEP **03** (2002) 014, [hep-lat/0106002].

[72] Z. Fodor and S. D. Katz, "Critical point of QCD at finite T and mu, lattice results for physical quark masses," JHEP **04** (2004) 050, [hep-lat/0402006].

[73] A. M. Halasz, A. D. Jackson, R. E. Shrock, M. A. Stephanov, and J. J. M. Verbaarschot, "On the phase diagram of QCD," Phys. Rev. **D58** (1998) 096007, [hep-ph/9804290].

[74] M. Asakawa and K. Yazaki, "Chiral restoration at finite density and temperature," Nucl. Phys. **A504** (1989) 668–684.

[75] O. Scavenius, A. Mocsy, I. N. Mishustin, and D. H. Rischke, "Chiral phase transition within effective models with constituent quarks," Phys. Rev. **C64** (2001) 045202, [nucl-th/0007030].

[76] J. Berges and K. Rajagopal, "Color superconductivity and chiral symmetry restoration at nonzero baryon density and temperature," Nucl. Phys. **B538** (1999) 215–232, [hep-ph/9804233].

[77] Y. Hatta and T. Ikeda, "Universality, the QCD critical / tricritical point and the quark number susceptibility," Phys. Rev. **D67** (2003) 014028, [hep-ph/0210284].

[78] A. Barducci, R. Casalbuoni, S. De Curtis, R. Gatto, and G. Pettini, "Chiral symmetry breaking in QCD at finite temperature and density," Phys. Lett. **B231** (1989) 463.

[79] A. Barducci, R. Casalbuoni, G. Pettini, and R. Gatto, "Chiral phases of QCD at finite density and temperature," Phys. Rev. **D49** (1994) 426–436.

[80] P. Jacobs and X.-N. Wang, "Matter in extremis: Ultrarelativistic nuclear collisions at RHIC," Prog. Part. Nucl. Phys. **54** (2005) 443–534, [hep-ph/0405125].

[81] H. Liu, "Heavy ion collisions and AdS/CFT," J. Phys. **G34** (2007) S361–368, [hep-ph/0702210].

[82] J. Casalderrey-Solana, H. Liu, D. Mateos, K. Rajagopal, and U. A. Wiedemann, "Gauge/String Duality, Hot QCD and Heavy Ion Collisions," arXiv:1101.0618.

[83] G. Policastro, D. T. Son, and A. O. Starinets, "The shear viscosity of strongly coupled N = 4 supersymmetric Yang-Mills plasma," Phys. Rev. Lett. **87** (2001) 081601, [hep-th/0104066].

[84] A. Buchel and J. T. Liu, "Universality of the shear viscosity in supergravity," Phys. Rev. Lett. **93** (2004) 090602, [hep-th/0311175].

[85] P. Kovtun, D. T. Son, and A. O. Starinets, "Viscosity in strongly interacting quantum field theories from black hole physics," Phys. Rev. Lett. **94** (2005) 111601, [hep-th/0405231].

[86] J. B. Kogut and M. A. Stephanov, "The phases of quantum chromodynamics: From confinement to extreme environments," Camb. Monogr. Part. Phys. Nucl. Phys. Cosmol. **21** (2004) 1–364.

[87] M. A. Stephanov, "QCD phase diagram: An overview," PoS **LAT2006** (2006) 024, [hep-lat/0701002].

[88] M. G. Alford, A. Schmitt, K. Rajagopal, and T. Schafer, "Color superconductivity in dense quark matter," Rev. Mod. Phys. **80** (2008) 1455–1515, [arXiv:0709.4635].

[89] **STAR** Collaboration, M. M. Aggarwal et. al., "An Experimental Exploration of the QCD Phase Diagram: The Search for the Critical Point and the Onset of De- confinement," arXiv:1007.2613.

[90] Z. Fodor and S. D. Katz, "Lattice determination of the critical point of QCD at finite T and mu," JHEP **03** (2002) 014, [hep-lat/0106002].

[91] C. R. Allton et. al., "The QCD thermal phase transition in the presence of a small chemical potential," Phys. Rev. **D66** (2002) 074507, [hep-lat/0204010].

[92] P. de Forcrand and O. Philipsen, "The QCD phase diagram for small densities from imaginary chemical potential," Nucl. Phys. **B642** (2002) 290–306, [hep-lat/0205016].

[93] M. Asakawa and K. Yazaki, "Chiral restoration at finite density and temperature," Nucl. Phys. **A504** (1989) 668–684.

[94] O. Scavenius, A. Mocsy, I. N. Mishustin, and D. H. Rischke, "Chiral phase transition within effective models with constituent quarks," Phys. Rev. **C64** (2001) 045202, [nucl-th/0007030].

[95] J. Berges and K. Rajagopal, "Color superconductivity and chiral symmetry restoration at nonzero baryon density and temperature," Nucl. Phys. **B538** (1999) 215–232, [hep-ph/9804233].

[96] O. DeWolfe, S. S. Gubser, and C. Rosen, "A holographic critical point," Phys. Rev. **D83** (2011) 086005, [arXiv:1012.1864].

[97] S. S. Gubser, S. S. Pufu, and F. D. Rocha, "Bulk viscosity of strongly coupled plasmas with holographic duals," JHEP **08** (2008) 085, [arXiv:0806.0407].

[98] U. Gursoy, E. Kiritsis, G. Michalogiorgakis, and F. Nitti, "Thermal Transport and Drag Force in Improved Holographic QCD," JHEP **12** (2009) 056, [arXiv:0906.1890].

[99] P. Basu, F. Nogueira, M. Rozali, J. B. Stang, and M. Van Raamsdonk, "Towards A Holographic Model of Color Superconductivity," New J. Phys. **13** (2011) 055001, [arXiv:1101.4042].

[100] M. A. Stephanov, K. Rajagopal, and E. V. Shuryak, "Event-by-event fluctuations in heavy ion collisions and the QCD critical point," Phys. Rev. **D60** (1999) 114028, [hep-ph/9903292].

[101] B. Berdnikov and K. Rajagopal, "Slowing out of equilibrium near the QCD critical point," Phys. Rev. **D61** (2000) 105017, [hep-ph/9912274].

[102] P. C. Hohenberg and B. I. Halperin, "Theory of Dynamic Critical Phenomena," Rev. Mod. Phys. **49** (1977) 435–479.

[103] D. T. Son and M. A. Stephanov, "Dynamic universality class of the QCD critical point," Phys. Rev. **D70** (2004) 056001, [hep-ph/0401052].

[104] A. Onuki, "Dynamic equations and bulk viscosity near the gas-liquid critical point," Phys. Rev. **E55** (1997) 403.

[105] A. Buchel and C. Pagnutti, "Transport at criticality," Nucl. Phys. **B834** (2010) 222–236, [arXiv:0912.3212].

[106] K. Maeda, M. Natsuume, and T. Okamura, "Dynamic critical phenomena in the AdS/CFT duality," Phys. Rev. **D78** (2008) 106007, [arXiv:0809.4074].

[107] M. Natsuume and T. Okamura, "Dynamic universality class of large-N gauge theories," Phys. Rev. **D83** (2011) 046008, [arXiv:1012.0575].

[108] A. Buchel, "Critical phenomena in N=4 SYM plasma," Nucl. Phys. **B841** (2010) 59–99, [arXiv:1005.0819].

[109] A. Buchel, "Bulk viscosity of gauge theory plasma at strong coupling," Phys. Lett. **B663** (2008) 286–289, [arXiv:0708.3459].

[110] A. Buchel and C. Pagnutti, "Critical phenomena in N=2* plasma," Phys. Rev. **D83** (2011) 046004, [arXiv:1010.3359].

[111] R. C. Myers and O. Tafjord, "Superstars and giant gravitons," JHEP **11** (2001) 009, [hep-th/0109127].

[112] D. T. Son and A. O. Starinets, "Hydrodynamics of R-charged black holes," JHEP **03** (2006) 052, [hep-th/0601157].

[113] K. Behrndt, M. Cvetic, and W. A. Sabra, "Non-extreme black holes of five dimensional N = 2 AdS supergravity," Nucl. Phys. **B553** (1999) 317–332, [hep-th/9810227].

[114] S. S. Gubser, "Thermodynamics of spinning D3-branes," Nucl. Phys. **B551** (1999) 667–684, [hep-th/9810225].

[115] P. Kraus, F. Larsen, and S. P. Trivedi, “The Coulomb branch of gauge theory from rotating branes,” JHEP **03** (1999) 003, [hep-th/9811120].

[116] R.-G. Cai and K.-S. Soh, “Critical behavior in the rotating D-branes,” Mod. Phys. Lett. **A14** (1999) 1895–1908, [hep-th/9812121].

[117] M. Cvetic and S. S. Gubser, “Phases of R-charged black holes, spinning branes and strongly coupled gauge theories,” JHEP **04** (1999) 024, [hep-th/9902195].

[118] M. Cvetic and S. S. Gubser, “Thermodynamic Stability and Phases of General Spinning Branes,” JHEP **07** (1999) 010, [hep-th/9903132].

[119] S. A. Hartnoll, C. P. Herzog, and G. T. Horowitz, “Holographic Superconductors,” JHEP **12** (2008) 015, [arXiv:0810.1563].

[120] S. S. Gubser and I. Mitra, “Instability of charged black holes in anti-de Sitter space,” hep-th/0009126.

[121] S. S. Gubser and I. Mitra, “The evolution of unstable black holes in anti-de Sitter space,” JHEP **08** (2001) 018, [hep-th/0011127].

[122] S. Giorgini, L. P. Pitaevskii, S. Stringari, “Theory of ultracold Fermi gases,” [arXiv:0706.3360], to appear in *Rev. Mod. Phys.*; I. Bloch, J. Dalibard, W. Zwerger, “Many-Body Physics with Ultracold Gases,” [arXiv:0704.3011], to appear in *Rev. Mod. Phys.*

[123] Y. Nishida, D. T. Son, ”Nonrelativistic conformal field theories,” Phys. Rev. D **76**, 086004 (2007) [arXiv:0706.3746].

[124] D. T. Son, ”Toward and AdS/cold atoms correspondence: a geometric realization of the Schroedinger symmetry,” Phys. Rev. D **78**,046003 (2008) [arXiv:0804.3972].

[125] K. Balasubramanian, J. McGreevy, ”Gravity duals for non-relativistic CFTs,” Phys. Rev. Lett. 101:061601 (2008) [arXiv:0804.4053].

[126] A. Adams, K. Balasubramanian and J. McGreevy, “Hot Spacetimes for Cold Atoms,” JHEP **0811**, 059 (2008) [arXiv:0807.1111 [hep-th]].

[127] J. Maldacena, D. Martelli and Y. Tachikawa, “Comments on string theory backgrounds with non-relativistic conformal symmetry,” JHEP **0810**, 072 (2008) [arXiv:0807.1100 [hep-th]].

[128] C. P. Herzog, M. Rangamani and S. F. Ross, “Heating up Galilean holography,” JHEP **0811**, 080 (2008) [arXiv:0807.1099 [hep-th]].

[129] C. A. Fuertes, S. Moroz, “Correlation functions in the non-relativistic AdS/CFT correspondence,” Phys. Rev. D **79**, 106004 (2009) [arXiv:0903.1844].

[130] P. Kovtun, D. T. Son, A. O. Starinets, “Viscosity in Strongly Interacting Quantum Field Theories from Black Hole Physics,” Phys. Rev. Lett. **94** 111601 (2005) [arXiv:0405231].

[131] S. S. Gubser, “Breaking an Abelian gauge symmetry near a black hole horizon,” Phys. Rev. D **78**, 065034 (2008) [arXiv:0801.2977 [hep-th]].

[132] S. A. Hartnoll, C. P. Herzog and G. T. Horowitz, “Building a Holographic Superconductor,” Phys. Rev. Lett. **101**, 031601 (2008) [arXiv:0803.3295 [hep-th]];
S. A. Hartnoll, C. P. Herzog and G. T. Horowitz, “Holographic Superconductors,” JHEP **0812**, 015 (2008) [arXiv:0810.1563 [hep-th]].

[133] J. Sonner, “A Rotating Holographic Superconductor,” arXiv:0903.0627 [hep-th].

[134] H. Liu, J. McGreevy, D. Vegh, ”Non-Fermi liquids from holography,” [arXiv:0903.2477].

[135] M. Alishahiha and O. J. Ganor, “Twisted backgrounds, pp-waves and nonlocal field theories,” JHEP **0303**, 006 (2003) [arXiv:hep-th/0301080].

[136] E. G. Gimon, A. Hashimoto, V. E. Hubeny, O. Lunin and M. Rangamani, “Black strings in asymptotically plane wave geometries,” JHEP **0308**, 035 (2003) [arXiv:hep-th/0306131].

[137] A. Chamblin, R. Emparan, C. V. Johnson and R. C. Myers, “Charged AdS black holes and catastrophic holography,” Phys. Rev. D **60**, 064018 (1999) [arXiv:hep-th/9902170].

[138] M. Cvetic *et al.*, “Embedding AdS black holes in ten and eleven dimensions,” Nucl. Phys. B **558**, 96 (1999) [arXiv:hep-th/9903214].

[139] T. Faulkner, N. Iqbal, H. Liu and J. McGreevy to appear.

[140] S. W. Hawking, C. J. Hunter and M. Taylor, “Rotation and the AdS/CFT correspondence,” Phys. Rev. D **59**, 064005 (1999) [arXiv:hep-th/9811056].

[141] M. Cvetic, H. Lu and C. N. Pope, “Charged Kerr-de Sitter black holes in five dimensions,” Phys. Lett. B **598**, 273 (2004) [arXiv:hep-th/0406196].

[142] E. Imeroni, A. Sinha, “Nonrelativistic metrics with extremal limits” [arXiv:0907.1892 [hep-th]]

[143] P. Kovtun, D. Nickel, “Black holes and non-relativistic quantum systems”, Phys. Rev. Lett.102:011602 (2009) [arXiv:0809.2020].

[144] J. L. F. Barbon, C. A. Fuertes, “Ideal gas matching for thermal Galilean holography”, [arXiv:0903.4452].

[145] Sung-Sik Lee. A Non-Fermi Liquid from a Charged Black Hole: A Critical Fermi Ball. Phys.Rev., D79:086006, 2009.

[146] Hong Liu, John McGreevy, and David Vegh. Non-Fermi liquids from holography. Phys. Rev., D83:065029, 2011.

[147] Mihailo Cubrovic, Jan Zaanen, and Koenraad Schalm. String Theory, Quantum Phase Transitions and the Emergent Fermi-Liquid. Science, 325:439–444, 2009.

[148] S.S. Gubser, Igor R. Klebanov, and Alexander M. Polyakov. Gauge theory correlators from noncritical string theory. Phys.Lett., B428:105–114, 1998.

[149] Edward Witten. Anti-de Sitter space and holography. Adv.Theor.Math.Phys., 2:253–291, 1998.

[150] Thomas Faulkner, Hong Liu, John McGreevy, and David Vegh. Emergent quantum criticality, Fermi surfaces, and AdS2. Phys. Rev., D83:125002, 2011.

[151] Martin Ammon, Johanna Erdmenger, Matthias Kaminski, and Andy O'Bannon. Fermionic Operator Mixing in Holographic p-wave Superfluids. JHEP, 05:053, 2010.

[152] Kristan Jensen, Shamit Kachru, Andreas Karch, Joseph Polchinski, and Eva Silverstein. Towards a holographic marginal Fermi liquid. Phys.Rev., D84:126002, 2011.

[153] Jerome P. Gauntlett, Julian Sonner, and Daniel Waldram. Universal fermionic spectral functions from string theory. 2011.

[154] Raphael Belliard, Steven S. Gubser, and Amos Yarom. Absence of a Fermi surface in classical minimal four-dimensional gauged supergravity. JHEP, 1110:055, 2011.

[155] Jerome Gauntlett, Julian Sonner, and Daniel Waldram. Spectral function of the supersymmetry current (II). 2011.

[156] B. de Wit and H. Nicolai. N=8 Supergravity. Nucl.Phys., B208:323, 1982.

[157] M. J. Duff and James T. Liu. Anti-de Sitter black holes in gauged N = 8 supergravity. Nucl. Phys., B554:237–253, 1999.

[158] Nabil Iqbal and Hong Liu. Real-time response in AdS/CFT with application to spinors. Fortsch.Phys., 57:367–384, 2009.

[159] Thomas Hartman and Sean A. Hartnoll. Cooper pairing near charged black holes. JHEP, 06:005, 2010.

[160] M. Gunaydin, L.J. Romans, and N.P. Warner. Compact and Noncompact Gauged Supergravity Theories in Five-Dimensions. Nucl.Phys., B272:598, 1986.

[161] K. Behrndt, Mirjam Cvetic, and W.A. Sabra. Nonextreme black holes of five-dimensional N=2 AdS supergravity. Nucl.Phys., B553:317–332, 1999.

[162] Mohammad Edalati, Robert G. Leigh, Ka Wai Lo, and Philip W. Phillips. Dynamical Gap and Cuprate-like Physics from Holography. Phys.Rev., D83:046012, 2011.

[163] Liza Huijse and Subir Sachdev. Fermi surfaces and gauge-gravity duality. 2011.

[164] Nabil Iqbal, Hong Liu, and Mark Mezei. Lectures on holographic non-Fermi liquids and quantum phase transitions. 2011.

[165] Liza Huijse, Subir Sachdev, and Brian Swingle. Hidden Fermi surfaces in compressible states of gauge- gravity duality. 2011.

[166] Steven S. Gubser and Fabio D. Rocha. Peculiar properties of a charged dilatonic black hole in AdS5. Phys. Rev., D81:046001, 2010.

[167] Mirjam Cvetic and Steven S. Gubser. Thermodynamic Stability and Phases of General Spinning Branes. JHEP, 07:010, 1999.

[168] Sean A. Hartnoll, Diego M. Hofman, and Alireza Tavanfar. Holographically smeared Fermi surface: Quantum oscillations and Luttinger count in electron stars. Europhys.Lett., 95:31002, 2011.

[169] Per Kraus, Finn Larsen, and Sandip P. Trivedi. The Coulomb branch of gauge theory from rotating branes. JHEP, 03:003, 1999.

[170] D. Z. Freedman, S. S. Gubser, K. Pilch, and N. P. Warner. Continuous distributions of D3-branes and gauged supergravity. JHEP, 07:038, 2000.

[171] John H. Schwarz. Superconformal Chern-Simons theories. JHEP, 11:078, 2004.

[172] Jonathan Bagger and Neil Lambert. Gauge Symmetry and Supersymmetry of Multiple M2-Branes. Phys. Rev., D77:065008, 2008.

[173] Andreas Gustavsson. Algebraic structures on parallel M2-branes. Nucl. Phys., B811:66–76, 2009.

[174] Ofer Aharony, Oren Bergman, Daniel Louis Jafferis, and Juan Maldacena. N=6 superconformal Chern-Simons-matter theories, M2-branes and their gravity duals. JHEP, 10:091, 2008.

[175] Nadav Drukker, Marcos Marino, and Pavel Putrov. From weak to strong coupling in ABJM theory. Commun. Math. Phys., 306:511–563, 2011.

[176] Christopher P. Herzog, Igor R. Klebanov, Silviu S. Pufu, and Tiberiu Tesileanu. Multi-Matrix Models and Tri-Sasaki Einstein Spaces. Phys. Rev., D83:046001, 2011.

[177] Ofer Aharony, Steven S. Gubser, Juan Martin Maldacena, Hirosi Ooguri, and Yaron Oz. Large N field theories, string theory and gravity. Phys. Rept., 323:183–386, 2000.

[178] Ibrahima Bah, Alberto Faraggi, Juan I. Jottar, and Robert G. Leigh. Fermions and Type IIB Supergravity On Squashed Sasaki- Einstein Manifolds. JHEP, 01:100, 2011.

[179] Mirjam Cvetic and Steven S. Gubser. Phases of R charged black holes, spinning branes and strongly coupled gauge theories. JHEP, 9904:024, 1999.

[180] B. de Wit and H. Nicolai. N=8 Supergravity with Local SO(8) x SU(8) Invariance. Phys.Lett., B108:285, 1982.

[181] Bernard de Wit. Supergravity. 2002.

[182] Eric D'Hoker and Daniel Z. Freedman. Supersymmetric gauge theories and the AdS/CFT correspondence. 2002.

[183] Mohammad Edalati, Robert G. Leigh, and Philip W. Phillips. Dynamically Generated Mott Gap from Holography. Phys. Rev. Lett., 106:091602, 2011.

[184] Ryusuke Endo and Minoru Koseki. Gaugeon formalism for spin-3/2 Rarita-Schwinger gauge field. Prog. Theor. Phys., 103:685–696, 2000.

[185] Thomas Faulkner, Nabil Iqbal, Hong Liu, John McGreevy, and David Vegh. Holographic non-Fermi liquid fixed points. 2011.

[186] Daniel Z. Freedman and Ashok K. Das. Gauge Internal Symmetry in Extended Supergravity. Nucl.Phys., B120:221, 1977.

[187] Steven S. Gubser. Thermodynamics of spinning D3-branes. Nucl. Phys., B551:667–684, 1999.

[188] Steven S. Gubser and Igor R. Klebanov. Absorption by branes and Schwinger terms in the world volume theory. Phys. Lett., B413:41–48, 1997.

[189] Steven S. Gubser, Fabio D. Rocha, and Amos Yarom. Fermion correlators in non-abelian holographic superconductors. JHEP, 1011:085, 2010.

[190] Igor R. Klebanov. World-volume approach to absorption by non-dilatonic branes. Nucl. Phys., B496:231–242, 1997.

[191] Igor R. Klebanov and Giuseppe Torri. M2-branes and AdS/CFT. Int. J. Mod. Phys., A25:332–350, 2010.

[192] Giuseppe Policastro. Supersymmetric hydrodynamics from the AdS/CFT correspondence. JHEP, 0902:034, 2009.

[193] L.J. Romans. Supersymmetric, cold and lukewarm black holes in cosmological Einstein-Maxwell theory. Nucl.Phys., B383:395–415, 1992.

[194] Subir Sachdev. Condensed matter and AdS/CFT. 2010.

[195] Subir Sachdev. What can gauge-gravity duality teach us about condensed matter physics? 2011.

[196] Anastasia Volovich. Rarita-Schwinger field in the AdS / CFT correspondence. JHEP, 9809:022, 1998.

[197] C. M. Brown and O. DeWolfe, JHEP **1201**, 032 (2012) [arXiv:1110.3840 [hep-th]].

[198] A. Adams and J. Wang, New J. Phys. **13**, 115008 (2011) [arXiv:1103.3472 [hep-th]].

Appendix A

Two-charge $\mathcal{N} = 4$ black hole

Along with the one-charge $\mathcal{N} = 4$ black hole solution of section 4.4, another family of black holes coming from string theory is the so-called two-charge $\mathcal{N} = 4$ solution, which has equal charges for two $U(1)$ gauge fields inside the $SO(6)$ R-symmetry. Keeping only the diagonal gauge field, this geometry solves our ansatz with potential and gauge kinetic function,

$$V(\phi) = -\frac{1}{L^2}\left(8e^{\frac{\phi}{\sqrt{6}}} + 4e^{-\sqrt{\frac{2}{3}}\phi}\right), \qquad f(\phi) = e^{\sqrt{\frac{2}{3}}\phi}, \tag{A.1}$$

where the scalar potential matches that for the one-charge case, while the gauge kinetic function is slightly different. The solution takes the form

$$\begin{aligned} A(r) &= \log\frac{r}{L} + \frac{1}{3}\log\left(1 + \frac{Q^2}{r^2}\right), \quad B(r) = -\log\frac{r}{L} - \frac{2}{3}\log\left(1 + \frac{Q^2}{r^2}\right), \qquad \text{(A.2)} \\ h(r) &= 1 - \frac{\mu L^2}{(r^2+Q^2)^2}, \quad \phi(r) = \sqrt{\frac{2}{3}}\log\left(1 + \frac{Q^2}{r^2}\right), \quad \Phi(r) = \frac{\sqrt{2\mu}Q}{r^2+Q^2} - \frac{\sqrt{2\mu}Q}{r_H^2+Q^2}. \end{aligned}$$

This solution again is characterized by a charge Q, a mass parameter μ and the asymptotic AdS scale L. The solution has a horizon at

$$r_H = \sqrt{L\sqrt{\mu} - Q^2}, \tag{A.3}$$

For fixed Q and L, the mass parameter μ is bounded below by

$$\mu \geq \mu_{min} \equiv \frac{Q^4}{L^2}, \tag{A.4}$$

and at $\mu = \mu_{min}$ we have $r_H = T = 0$; extending $\mu < \mu_{min}$ results in a naked singularity.

It is more convenient to trade the parameter μ for r_H, which runs over all nonnegative values. The temperature and chemical potential are

$$T = \frac{r_H}{\pi L^2}\,, \qquad \Omega = \frac{\sqrt{2}Q}{L^2}\,, \tag{A.5}$$

giving a one-to-one relationship between the black hole parameters $(r_H,\, Q)$ and the thermodynamic parameters $(T,\, \Omega)$; a single black hole exists at each point in the phase diagram, and hence a single phase. The entropy and charge density are

$$\begin{aligned} s &= \tfrac{2\pi r_H}{\kappa^2 L^3}(Q^2 + r_H^2) = \tfrac{N_c^2 T}{4}(2\pi^2 T^2 + \Omega^2)\,, \\ \rho &= \tfrac{\sqrt{2}}{\kappa^2 L^3} Q(Q^2 + r_H^2) = \tfrac{N_c^2 \Omega}{8\pi^2}(2\pi^2 T^2 + \Omega^2)\,, \end{aligned} \tag{A.6}$$

which can be obtained as derivatives of the pressure

$$p = \frac{N_c^2}{32\pi^2}(2\pi^2 T^2 + \Omega^2)^2\,. \tag{A.7}$$

The $U(1)$ susceptibility is

$$\chi \equiv \left(\frac{\partial \rho}{\partial \Omega}\right)_T = \frac{N_c^2}{8\pi^2}(2\pi^2 T^2 + 3\Omega^2)\,, \tag{A.8}$$

and it along with other derivatives of s and ρ such as as the specific heat are everywhere well-behaved; this example has no phase transitions.

We can consider the conductivity and related diffusion coefficient for this model. Proceeding analogously to the one-charge case, we find the $\omega = 0$ solutions

$$a(r) = C_1 \frac{r^2}{Q^2 + r^2} + C_2\, a_2(r)\,, \tag{A.9}$$

where, as for the one-charge case, $a_2(r)$ is a more complicated expression including $\log(r - r_H)$. Matching to the near-horizon solution

$$a(r) = (r - r_H)^\alpha\,, \tag{A.10}$$

with the exponent α imposing infalling boundary conditions given as 4.29

$$\alpha = -\frac{i\omega L^2}{4 r_H}\,, \tag{A.11}$$

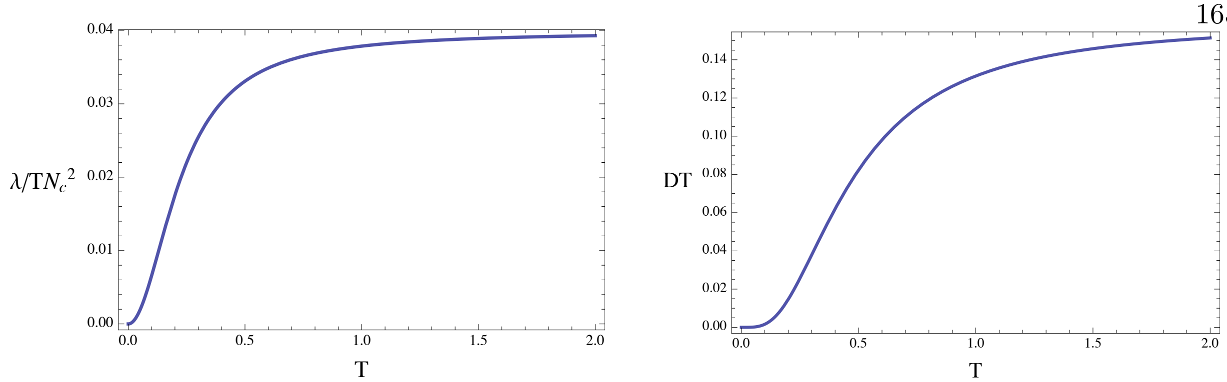

Figure A.1: The conductivity over temperature and diffusion times temperature for the two-charge black hole with $\Omega = 1$.

we determine C_1 and C_2 and solve for the conductivity 4.44. For small ω we find the result

$$\sigma(\omega) = \frac{iQ^2}{\omega\kappa^2 L} + \frac{r_H^3 L}{2\kappa^2(Q^2 + r_H^2)} + \mathcal{O}(\omega)\,. \tag{A.12}$$

It is straightforward to convert this to dependence on the thermodynamic quantities T, Ω, and one finds

$$\frac{\sigma}{T} = \frac{N_c^2}{4\pi^2}\left(\frac{i\tilde{\Omega}^2}{2\tilde{\omega}} + \frac{\pi^3}{2\pi^2 + \tilde{\Omega}^2} + \mathcal{O}(\omega)\right)\,, \tag{A.13}$$

where again $\tilde{\Omega} = \Omega/T$, $\tilde{\omega} = \omega/T$. As in the one-charge case we find a $1/\omega$ pole in the imaginary part, indicating a delta function in the real part, and the remaining zero-frequency conductivity

$$\lambda = \frac{N_c^2 \pi T^3}{4(2\pi^2 T^2 + \Omega^2)} = \frac{N_c^2 \pi T}{4(2\pi^2 + \tilde{\Omega}^2)}\,, \tag{A.14}$$

which using the susceptibility A.8 gives the diffusion constant

$$D = \frac{1}{2\pi T}\left(\frac{1}{1 + 2\tilde{\Omega}^2/\pi^2 + 3\tilde{\Omega}^4/4\pi^4}\right)\,. \tag{A.15}$$

We plot λ/TN_c^2 and DT in figure A.1.

Appendix B

Details of NRCFT Duals

B.1 Coordinates on S^3 and S^5

In our examples, we employ a Hopf parameterization of the coordinates on the compact S^5 and, in the cases built on global AdS, the S^3. The metrics may be elegantly expressed in terms of the left-invariant one-forms of SU(2),

$$\sigma_1 = \frac{1}{2}(\cos\psi d\theta + \sin\psi \sin\theta d\phi) \ , \quad \sigma_2 = \frac{1}{2}(\sin\psi d\theta - \cos\psi \sin\theta d\phi) \ , \quad \sigma_3 = \frac{1}{2}(d\psi + \cos\theta d\phi) \, . \tag{B.1}$$

The hopf-fibration $S^1 \to S^3 \to \mathbb{P}^1$ enjoys the round metric,

$$ds^2_{S^3} = \sigma_1^2 + \sigma_2^2 + \sigma_3^2 = ds^2_{\mathbb{P}^1} + (\eta^{(3)})^2 \, , \tag{B.2}$$

where the metric on $\mathbb{P}^1$ is

$$ds^2_{\mathbb{P}^1} = \sigma_1^2 + \sigma_2^2 = \frac{1}{4}\left(d\theta^2 + \sin^2\theta d\phi^2\right) \ , \tag{B.3}$$

and the Hopf fiber is

$$\eta^{(3)} \equiv \sigma_3 = \frac{1}{2}(d\psi + \cos\theta d\phi) \ , \tag{B.4}$$

with Hopf coordinate ψ; thus the metric may be written

$$ds^2_{S^3} = \frac{1}{4}\left[d\theta^2 + \sin^2\theta d\phi^2 + (d\psi + \cos\theta d\phi)^2\right] \, . \tag{B.5}$$

Meanwhile the Hopf-fibration $S^1 \to S^5 \to \mathbb{P}^2$ has the metric

$$ds^2_{S^5} = ds^2_{\mathbb{P}^2} + (\eta^{(5)})^2 \, , \tag{B.6}$$

where the metric on $\mathbb{P}^2$ is

$$ds^2_{\mathbb{P}^2} = d\mu^2 + \sin^2\mu \left(\sigma_1^2 + \sigma_2^2 + \cos^2\mu\, \sigma_3^2\right) \,, \tag{B.7}$$

and the Hopf fiber $\eta^{(5)}$ is

$$\eta^{(5)} \equiv d\chi + \mathcal{A} \equiv d\chi + \sin^2\mu\, \sigma^3 \,, \tag{B.8}$$

where the Hopf coordinate is χ.

In the literature on five-dimensional black holes in global AdS, the S^3 is typically written in Boyer-Lindquist coordinates θ_B, ψ_B, ϕ_B rather than the Hopf coordinates θ, ψ, ϕ given above. These are related by

$$\theta = 2\theta_B \qquad \psi = \psi_B + \phi_B \qquad \phi = \psi_B - \phi_B \,, \tag{B.9}$$

which leads to the BL metric on S^3,

$$ds^2_{S^3} = d\theta_B^2 + \sin^2\theta_B d\phi_B^2 + \cos^2\theta_B d\psi_B^2 \,.$$

B.2 T-duality conventions

We can express the T-duality rules as follows. Let y be the isometry direction along which T-duality is taken and x^α the remaining coordinates. Any 10D string metric, B-field and RR fields with a y isometry can be written as

$$\begin{aligned} ds^2 &= g_{yy}(dy + g_{(y)})^2 + \mathcal{G}_{\alpha\beta}\, dx^\alpha dx^\beta \,, & \text{(B.10)} \\ B_2 &= \left(dy + \frac{1}{2} g_{(y)}\right) \wedge B_{(y)} + \frac{1}{2}\mathcal{B}_{\alpha\beta}\, dx^\alpha \wedge dx^\beta \,, & \text{(B.11)} \\ F_p &= (dy + g_{(y)}) \wedge F_{p(y)} + F_{p(\not y)} \,, & \text{(B.12)} \end{aligned}$$

where the one-forms $g_{(y)}$ and $B_{(y)}$ capture the off-diagonal terms between y and the other directions:

$$g_{(y)} \equiv \frac{g_{y\alpha}}{g_{yy}} dx^\alpha \,, \qquad B_{(y)} \equiv B_{y\alpha} dx^\alpha \,, \tag{B.13}$$

and $F_{p(y)}$ and $F_{p(\not y)}$ are $(p-1)$- and p-forms polarized along the x^α directions, respectively. T-duality along the y-direction gives a result that may also be written in the form of (B.10)-(B.12),

$$\begin{aligned} ds^{2\prime} &= g'_{yy}(dy + g'_{(y)})^2 + \mathcal{G}_{\alpha\beta}\, dx^\alpha dx^\beta\,, && \text{(B.14)}\\ B'_2 &= \left(dy + \frac{1}{2}g'_{(y)}\right) \wedge B'_{(y)} + \frac{1}{2}\mathcal{B}_{\alpha\beta}\, dx^\alpha \wedge dx^\beta\,, && \text{(B.15)}\\ F'_p &= (dy + g'_{(y)}) \wedge F'_{p(y)} + F'_{p(\not y)}\,, && \text{(B.16)} \end{aligned}$$

with

$$\begin{aligned} g'_{yy} &\equiv \frac{1}{g_{yy}}\,, \qquad g'_{(y)} \equiv -B_{(y)}\,, \qquad B'_{(y)} \equiv -g_{(y)}\,, \qquad e^{2\Phi'} = \frac{e^{2\Phi}}{g_{yy}}\,, && \text{(B.17)}\\ F'_{p(y)} &= F_{(p-1)(\not y)}\,, \qquad F'_{p(\not y)} = F_{(p+1)(y)}\,. && \text{(B.18)} \end{aligned}$$

Note that $\mathcal{G}_{\alpha\beta}$ and $\mathcal{B}_{\alpha\beta}$ are invariant.

B.3 Dimensional reduction

B.3.1 Hodge dual conventions

We use conventions for the Hodge dual where, acting on a noncoordinate basis $\hat\theta^a$,

$$*(\hat\theta^{a_1} \wedge \ldots \wedge \hat\theta^{a_p}) = \frac{1}{(D-p)!}\epsilon^{a_1\ldots a_p}{}_{a_{p+1}\ldots a_D}\hat\theta^{a_{p+1}} \wedge \ldots \wedge \hat\theta^{a_D}\,, \tag{B.19}$$

which implies

$$F_p \wedge *F_p = \frac{1}{p!}F_{a_1 a_2\ldots a_p}F^{a_1 a_2 \ldots a_p}\,\mathrm{vol}\,, \tag{B.20}$$

with vol the D-dimensional volume form.

For a 10D metric of the Kaluza-Klein form (5.21), we can split the 10D Hodge star into Hodge stars acting on the 5D $ds_5^2(M)$, the 4D $ds^2(X)$, and the 1D $e^{2V}(\eta^{(5)} + A_q)^2$ parts. Conventionally ordering forms as 5D, then 1D, then 4D parts, we find

$$*_{10} = (-1)^\delta *_5 *_1 *_4\,, \tag{B.21}$$

where $\delta = 1$ if the form being acted on has (even, odd, even) or (odd, even, odd) numbers of indices in the (5D, 1D, 4D) parts, and $\delta = 0$ otherwise, **i.e.** $\delta = n_5 n_4 + n_1(1 + n_5 + n_4)$. We then have the useful expressions

$$*_5 1 \equiv \mathrm{vol}_M \,, \qquad *_1 1 = e^V(\eta^{(5)} + A_q)\,, \qquad *_4 1 = \frac{1}{8} d\mathcal{A} \wedge d\mathcal{A}\,, \qquad *_4 d\mathcal{A} = d\mathcal{A}\,, \tag{B.22}$$

where $J \equiv d\mathcal{A}/2$ is the Kähler form on X, implying

$$*_{10} 1 = e^V \mathrm{vol}_M \wedge \eta^{(5)} \wedge \frac{1}{8} d\mathcal{A} \wedge d\mathcal{A}\,. \tag{B.23}$$

The volume form on Y is then $(*_1 1)(*_4 1)$ with $V = A_q = 0$:

$$\mathrm{vol}(Y) = \int \eta^{(5)} \wedge \frac{1}{8} d\mathcal{A} \wedge d\mathcal{A}\,. \tag{B.24}$$

B.3.2 Non-coordinate basis

We would like to determine the effective five-dimensional action for which the fields of Section (2.3) provide solutions. To do so, it is useful to write the pre- and post-Melvinized 5D metrics in a non-coordinate basis, in which the map simplifies even further. Reexpress the original metric (5.22) as the t-ξ version of (5.48),

$$ds_5^2(M) = \mathcal{G}_{tt} e^t e^t + \mathcal{G}_{\xi\xi}\Big(e^\xi + \frac{G_{t\xi}}{G_{\xi\xi}} e^t\Big)^2 + G_{mn} dx^m dx^n\,, \tag{B.25}$$

$$\mathcal{G}_{tt} \equiv \frac{G_{tt}G_{\xi\xi} - G_{t\xi}^2}{G_{\xi\xi}}\,, \qquad \mathcal{G}_{\xi\xi} \equiv G_{\xi\xi}\,, \tag{B.26}$$

so we can define non-coordinate basis 1-forms,

$$\hat\theta^t \equiv \sqrt{\mathcal{G}_{tt}} e^t\,, \qquad \hat\theta^\xi \equiv \sqrt{\mathcal{G}_{\xi\xi}}\Big(e^\xi + \frac{G_{t\xi}}{G_{\xi\xi}} e^t\Big)\,. \tag{B.27}$$

One may then show that $\mathcal{G}_{tt}$ is unchanged by Melvinization due to the cancelation of $1/K$ and the new term, generalizing (5.38), so that $\hat\theta^t$ is fixed. Meanwhile $\hat\theta^\xi$ changes only by an overall factor of $K^{-1/2}$. Thus the entire Melvin map boils down to the transformation

$$\hat\theta^\xi \to (\hat\theta^\xi)' \equiv \frac{1}{K^{1/2}} \hat\theta^\xi = \frac{1}{\sqrt{1 + \mathcal{G}_{\xi\xi}}} \hat\theta^\xi\,. \tag{B.28}$$

One can also see that A_M is a 1-form proportional to $(\hat{\theta}^\xi)'$:

$$A_M = -\sqrt{G'_{\xi\xi}}(\hat{\theta}^\xi)' \,. \tag{B.29}$$

This presentation allows us to understand the relationship between the 5D Hodge duals $*_5$ and $*'_5$. When acting on a form that contains $\hat{\theta}^\xi$, they differ by e^V:

$$e^V *'_5 (\ldots \wedge \hat{\theta}^\xi \wedge \ldots) = *_5(\ldots \wedge \hat{\theta}^\xi \wedge \ldots) \,, \tag{B.30}$$

while the converse is true when acting on a form that does not contain $\hat{\theta}^\xi$:

$$e^{-V} *'_5 (\ldots \wedge \not{\hat{\theta}}^\xi \wedge \ldots) = *_5(\ldots \wedge \not{\hat{\theta}}^\xi \wedge \ldots) \,. \tag{B.31}$$

These relations are useful in understanding the presentation of the tensor F_5^0 (5.24) after Melvinization. This object is not changed, but it contains the pre-Melvin Hodge star $*_5$, and it is useful for the dimensional reduction we are about to carry out to write it in terms of the post-Melvin metric. We can easily see

$$\mathrm{vol}_M \equiv *_5(1) = e^{-V} *'_5 (1) = e^{-V} \mathrm{vol}_{M'} \,, \tag{B.32}$$

since the Hodge stars act on a 0-form. The $*_5 F_q$ term is not so simple, since in general F_q contains both terms with and without $\hat{\theta}^\xi$. However, we can use the fact that while F_5^0 is self-dual with respect to the unMelvinized 10D metric, only $F_5 \equiv F_5^0 + B'_2 \wedge F'_3$ is self-dual with respect to the Melvin metric; one can think of the additional $B'_2 \wedge F'_3$ term as being what is needed to ensure the tensor is still self-dual after the metric changes. Given that

$$B'_2 \wedge F'_3 = f \wedge A_M \wedge (\eta + A_q) \wedge d\mathcal{A} \,, \tag{B.33}$$

we must have that $*_5 F_q$ becomes in the new metric,

$$*_5 F_q = e^{-V} *'_5 (F_q - 2f \wedge A_M) \,, \tag{B.34}$$

and the five-forms can be written,

$$\begin{aligned} F_5^0 &= -4e^{-V}\mathrm{vol}_{M'} + \frac{1}{2}(\eta + A_q) \wedge d\mathcal{A} \wedge d\mathcal{A} \\ &\quad + \frac{1}{2} e^{-V} *'_5 (F_q - 2f \wedge A_M) \wedge d\mathcal{A} - \frac{1}{2} F_q \wedge (\eta + A_q) \wedge d\mathcal{A} \,, \end{aligned} \tag{B.35}$$

and

$$F_5' = -4e^{-V}\mathrm{vol}_{M'} + \frac{1}{2}(\eta + A_q)\wedge d\mathcal{A}\wedge d\mathcal{A} + \frac{1}{2} *_5' (F_q - 2f\wedge A_M)\wedge d\mathcal{A} - \frac{1}{2}(F_q - 2f\wedge A_M)\wedge(\eta + A_q)\wedge d\mathcal{A}\,. \tag{B.36}$$

The Bianchi identity $dF_5' = H_3' \wedge F_3'$ implies

$$de^{-V} *_5' (F_q - 2f\wedge A_M) = F_q \wedge F_q\,, \tag{B.37}$$

consistent with (5.25) and (B.34).

B.3.3 Reduction of IIB action

The IIB action in string frame with $C_0 = 0$ is

$$2\kappa_{10}^2 S = \int \Big[(*1)e^{-2\Phi}\Big(R + 4(\partial\Phi)^2\Big) - \frac{1}{2}e^{-2\Phi}H_3\wedge *H_3 - \frac{1}{2}F_3\wedge *F_3 - \frac{1}{4}F_5\wedge *F_5 - \frac{1}{2}C_4\wedge H_3\wedge F_3\Big]\,. \tag{B.38}$$

Here $F_5 \equiv dC_4 - C_2\wedge H_3$ is the gauge-invariant field strength. As usual the IIB action gives the correct equations of motion, but $F_5 = *F_5$ must be imposed only after deriving the equations. Using the expressions (5.29) and (5.30) for F_3 and H_3 and dropping primes for convenience, we find

$$*F_3 = e^V *_5 df\wedge(\eta^{(5)} + A_q)\wedge d\mathcal{A} + e^V *_5 df_2\wedge(\eta^{(5)} + A_q)\wedge\frac{1}{8}d\mathcal{A}\wedge d\mathcal{A}\,, \tag{B.39}$$

$$*H_3 = -e^{-V} *_5 F_M \wedge \frac{1}{8}d\mathcal{A}\wedge d\mathcal{A} - e^V *_5 A_M\wedge(\eta^{(5)} + A_q)\wedge d\mathcal{A} - e^V *_5 (A_M\wedge F_q)\wedge(\eta^{(5)} + A_q)\wedge\frac{1}{8}d\mathcal{A}\wedge d\mathcal{A}\,, \tag{B.40}$$

The Ricci scalar is

$$R = R^{(5)} - 2\partial_\mu V\partial^\mu V - 2\nabla^2 V + 24 - 4e^{2V} - \frac{1}{4}e^{2V}(F_q)_{\mu\nu}(F_q)^{\mu\nu}\,. \tag{B.41}$$

Using integration by parts and the fact that $d(B_2\wedge C_2)\wedge B_2\wedge F_3 = \frac{1}{2}d(B_2\wedge B_2\wedge C_2\wedge F_3)$ is a total derivative, the Chern-Simons term can be reexpressed as,

$$-\frac{1}{2}\int C_4\wedge H_3\wedge F_3 \to \frac{1}{2}\int F_5^0\wedge B_2\wedge F_3\,, \tag{B.42}$$

Using the above relations, and the ansatz (5.27)-(5.31) and (B.35) and (B.36) for the RR 5-form, we perform the dimensional reduction leading to (5.40). Because of the subtlety arising from the self-duality of the RR 5-form, the coefficients were checked using the mode decomposition of the F_3 and H_3 equations of motion.